# Integratie van elektronische systemen op draagbare textielantenneplatformen

# Integration of Electronic Systems on Wearable Textile Antenna Platforms

Peter Vanveerdeghem

Promotoren: prof. dr. ir. H. Rogier, prof. dr. ing. J. Knockaert, dr. ing. P. Van Torre
Proefschrift ingediend tot het behalen van de graad van
Doctor in de Ingenieurswetenschappen: Elektrotechniek

Vakgroep Informatietechnologie
Voorzitter: prof. dr. ir. D. De Zutter

Vakgroep Industrieel Systeem- en Productontwerp
Voorzitter: prof. dr. ing. K. Stockman

Vakgroep Industriële Technologie en Constructie
Voorzitter: prof. dr. M. Vanhaelst

Faculteit Ingenieurswetenschappen en Architectuur
Academiejaar 2014 - 2015

UNIVERSITEIT GENT

ISBN 978-90-8578-770-9
NUR 959
Wettelijk depot: D/2015/10.500/14

# Integration of Electronic Systems on Wearable Textile Antenna Platforms

Peter Vanveerdeghem

Dissertation submitted to obtain the academic degree of
Doctor of Electrical Engineering

Publicly defended at Ghent University on Feb 17th, 2015

**Supervisor:**

prof. dr. ir. H. Rogier
dr. ing. P. Van Torre
Electromagnetics group
Dept. of Information Technology
Faculty of Engineering and Architecture
Ghent University
St.-Pietersnieuwstraat 41
B-9000 Ghent, Belgium
http://emweb.intec.ugent.be

**Co-Supervisor:**

prof. dr. ing. J. Knockaert
Lemcko
Dept. of Industrial System
and Product Design
Faculty of Engineering and Architecture
Ghent University
Graaf Karel de Goedelaan 5
B-8500 Kortrijk, Belgium
http://isp.ugent.be

**Members of the examining board:**

| | |
|---|---|
| prof. dr. ir. Luc Taerwe (chairman) | Ghent University, Belgium |
| prof. ir. C. Stevens (secretary) | Ghent University, Belgium |
| prof. dr. ir. H. Rogier (supervisor) | Ghent University, Belgium |
| prof. dr. ing. J. Knockaert (co-supervisor) | Ghent University, Belgium |
| dr. ing. P. Van Torre (co-supervisor) | Ghent University, Belgium |
| prof. dr. ir. M. Bozzi | University of Pavia, Italy |
| dr. ir. A. Georgiadis | Centre Tecnològic de Telecomunicacions de Catalunya, Spain |
| prof. dr. ir. J. Doutreloigne | Ghent University, Belgium |
| prof. dr. ir. W. Joseph | Ghent University, Belgium |



# Acknowledgment

After four years of doctoral research, I am pleased to write this dissertation. The past four years have been a very interesting period in which I independently but with expert supervision was able to do research at the University of Ghent. Furthermore, it was a very interesting period at the University College West-Flanders, providing me a comprehensive teaching assignment at the training program of industrial engineering, which was in 2014 integrated in the University of Ghent. During the past four years, I was able to meet several people, who are listed below.

First of all I would like to thank my supervisor prof. Hendrik Rogier, for accepting and guiding me as a PhD-student at the electromagnetics group of the department of Information Technology (INTEC). He was always ready to provide essential feedback on many levels or to analyze problems and providing interesting solutions. Moreover, his constructive remarks and instructions were always very helpful during the writing process of papers. Also I would like to thank my co-supervisors, prof. Jos Knockaert for guiding me as a PhD-student of the department of Industrial System and Product Design (ISP), always ready for providing critical comments and providing solutions when needed. Dr. Patrick Van Torre was always prepared for providing aid during measurement campaigns, providing critical comments, writing papers, etc. All these elements certainly helped to bring this dissertation to a successful result. Also, thank you for the interesting non-research related conversations.

I would also like to thank the other members of the examination board, for evaluating my dissertation and providing valuable comments: prof. Maurizio Bozzi, dr. Apostolos Georgiadis, prof. Wout Joseph, prof. Jan Doutreloigne and prof. Chris Stevens.

Furthermore, I wish to thank prof. Dries Vande Ginste as well as prof. Daniël De Zutter, as head of the Department of Information Technology, for providing me the opportunity to perform research at the electromagnetics research group.

Special thanks to Isabelle Van der Elstraeten, for the support with all the administrative matters.

During my stay at the electromagnetics research group, I met lots of interesting people. Therefore thank you to all the people of the INTEC -T floor. I would like to announce especially the colleagues of the office where I spent four years during my research: Celina, Marina S., Luca, Marina M., Zdravko, Giorgos, Gert-Jan, Karel and Olivier.

Furthermore, I would also like to thank the colleagues of Ghent University campus Kortrijk, especially the colleagues from the ELIT research group. In particular I would like to mention three colleagues. Prof. Chris Stevens for his support during my PhD research, as well as ing. Wesley Cottegnie and dr. Frederick Declercq as great colleagues at the office B2.13, who were always providing support when needed.

I also wish to thank my family, especially my parents, who always have fully supported me during my study- and PhD period. And last but not least, I would like to thank my girlfriend Nathalie, who always supported me in the past years. Together we enjoyed many wonderful moments, and I look forward to the beautiful moments that lie ahead.

*Ghent, February 2015*
*Peter Vanveerdeghem*

*The important thing is not to stop questioning.*
*Curiosity has its own reason for existing.*

ALBERT EINSTEIN

# Contents

# Samenvatting

Slimme textielsystemen die discreet geïntegreerd zijn in kleding bieden interessante mogelijkheden. Ze maken ondermeer gebruikers beter bewust van hun omgevings- en fysieke toestand. Deze systemen integreren sensoren, actuatoren alsook rekenkracht in alledaagse kledij. Door de integratie van draadloze communicatie in de kleding, worden de mogelijkheden verder uitgebreid, zoals bewaking in ware tijd van de activiteiten van de gebruiker alsmede het controleren van zijn of haar fysieke toestand en omgevingsfactoren. Deze toepassingen zijn zeer interessant, enerzijds in de gezondheidszorg, voor het verbeteren van het comfort van de patiënten, en anderzijds voor het monitoren van reddingswerkers. In het kader van deze laatste toepassing maken slimme textielsystemen het mogelijk om de interventie door reddingswerkers efficiënter te laten verlopen zonder dat zij specifieke aandacht moeten besteden aan het opvolgen van de sensordata betreffende hun fysieke toestand en de omgevingsfactoren. Op deze manier kunnen ze hun belangrijkste taak tijdens reddingsoperaties verbeteren en dit is uiteraard het redden van mensenlevens.

De integratie van intelligente textielsystemen moet voldoen aan bepaalde voorwaarden. Deze systemen moeten discreet geïntegreerd worden in kleding zonder de gebruiker te hinderen in het uitvoeren van zijn/haar taken. Dit houdt in dat het systeem licht, luchtdoorlatend en flexibel dient te zijn om de integratie in kleding toe te laten. Deze slimme textielsystemen worden ook blootgesteld aan zware omstandigheden, zoals hoge temperaturen, vochtigheid en extreme mechanische belastingen. Deze extreme omstandigheden verbieden het gebruik van rigide en niet-robuuste materialen.

Slimme textielsystemen worden opgesplitst in verschillende onderdelen, verspreid over het totale oppervlak van de kleding onderling en verbonden door middel van breekbare draadverbindingen. Deze fragiele verbindingen kunnen de werking van het systeem verstoren. Dit is absoluut niet verantwoord in toepassingen waarvan het leven van mensen afhankelijk is. Het vermijden van deze kwetsbare onderdelen verbetert de robuustheid van het systeem en creëert slimme textielsystemen die een toegevoegde waarde bieden voor reddingswerkers.

In Hoofdstuk 1 wordt een overzicht gegeven van slimme textielsystemen en hun toepassingen, alsmede het verband van dit doctoraatsonderzoek met deze slimme textielsystemen.

Hoofdstuk 2, gaat in op het gebruik van antennes in draagbare toepassingen. Het gebruik van efficiënte textiel patchantennes in kledij voor reddingswerkers werd experimenteel geëvalueerd om het zendvermogen in een draadloos sensor netwerk te

verminderen. Er werd aangetoond dat het gebruik van textiel patchantennes op het lichaam ervoor kan zorgen dat het ontvangen signaalvermogen stijgt op de verschillende nodes van het draadloos sensor netwerk en dat hierdoor eveneens het pakketverlies vermindert in vergelijking met niet-flexibele printplaat antennes met eenzelfde zendvermogen. Het energieverbruik van de verschillende nodes kan verminderd worden door het extra ontvangen signaalvermogen te benutten om het zendvermogen te verminderen.

In Hoofdstuk 3, wordt een nieuwe flexibele draadloze textiel sensornode voorgesteld. Deze node bestaat uit een draagbare textielantenne met een geïntegreerde zendontvanger en een sensor circuit. Op het voedingsvlak van deze antenne is een zendontvanger met ontvangstdiversiteit geïntegreerd samen met een microcontroller, geheugen en een sensor. De antenne is opgebouwd uit textielmateriaal dat voornamelijk gebruikt wordt in kledij voor reddingswerkers. Dit laat de naadloze integratie van het systeem toe in deze kleding. De draadloze node is zodanig opgebouwd dat breekbare en verlieshebbende verbindingen vermeden worden door deze te vervangen door zeer korte RF signaalpaden in het voedingsvlak van de antenne. Hierbij vermindert de kans op mogelijke problemen op het vlak van elektromagnetische compatibiliteit en signaalintegriteit. De toepassing van deze flexibele draadloze node is tweeledig. Ten eerste is de node ontworpen voor de integratie in kledij voor brandweerlieden met als doel om het gevaar dat gekoppeld is aan hun werk te verminderen. Ten tweede wordt de draadloze node gebruikt als een on-body en off-body persoonsgericht meetinstrument. Conventionele persoonsgerichte metingen worden vaak uitgevoerd met complexe en dure meetinstrumenten, welke verbonden zijn met op het lichaam gedragen antennes door middel van breekbare coaxiale kabels, die dan op hun beurt het gebruik verhinderen om vrij te bewegen. Deze draadloze node is gevalideerd in de anechoïsche kamer, zowel in een vlakke als gebogen toestand om de kenmerken van het systeem te karakteriseren in de vrij ruimte. De performantie van het systeem is eveneens gevalideerd in verschillende werkelijke situaties, met name geïntegreerd in brandweerkledij als een autonoom persoonsgericht meetinstrument.

Dankzij de comfortabele draagbare integratie in textiel kan deze module gebruikt worden voor valdetectie bij de bewaking van zowel patiënten als reddingswerkers monitoring. Een dergelijk systeem werd geïmplementeerd in Hoofdstuk 4. Daarom werden er vier nodes geïntegreerd in de beschermende kledij als een draadloos sensor netwerk. Hierbij voert elke node samenwerkende synchrone acquisitie en gedistribueerde gebeurtenisdetectie uit. Efficiënte automatische detectie-algoritmes zijn rechtstreeks geïmplementeerd op de microcontroller zelf. Zowel de gedetecteerde gebeurtenissen als de sensorgegevens worden betrouwbaar draadloos verzonden naar een basisstation, rechtstreeks of doorgestuurd via andere nodes op het lichaam. Het basisstation laat toe om de ontvangen sensorgegevens te visualiseren en voorziet de interventie coördinatoren van de reddingsoperatie van levensreddende informatie. De experimenten in werkelijke omstandigheden demonstreren dat dit autonoom draadloos sensor-

netwerk de verschillende situaties correct detecteert. Verder is het draadloze sensor netwerk gebruikt als autonoom ”body-centric”meetinstrument, welke statistische analyse toelaat van zowel de gemeten on-body node-naar-node als de off-body persoon-naar-persoon kanalen. De metingen bevestigen de kwaliteit van het draadloze kanaal.

In Hoofdstuk 5 wordt een compacte draagbare persoonlijke gedistribueerde exposimeter voorgesteld. De persoonlijke gedistribueerde exposimeter is opgebouwd uit verschillende nieuwe afzonderlijke RF exposimeter modules. Iedere exposimeter module is afzonderlijk geïntegreerd op het voedingsvlak van een draagbare textiel antenne, wat de comfortabele integratie in kledij toelaat. De persoonlijke gedistribueerde exposimeter is specifiek ontworpen voor epidemiologische studies naar de invloed van elektromagnetische golven op het lichaam, door middel van het meten van de invallende vermogensdichtheid. Iedere exposimeter module werd gevalideerd en gekalibreerd in de anechoïsche kamer en eveneens vergeleken met een commercieel verkrijgbare exposimeter. Bovendien werden realistische metingen uitgevoerd in het centrum van Gent voor de GSM-900 downlink band. Dezelfde metingen werden terzelfdertijd eveneens uitgevoerd met een commerciële exposimeter. Daaruit blijkt duidelijk dat de persoonlijke gedistribueerde exposimeter een meer nauwkeurigere schatting geeft van de vermogensdichtheid rondom het menselijk lichaam. De commerciële niet-gekalibreerde exposimeter wordt beïnvloed door het schaduweffect veroorzaakt door het lichaam, wat aanleiding geeft tot het onderschatten van de vermogensdichtheid op dit lichaam.

# Summary

Smart textile systems, which are unobtrusively integrated into clothing, offer exciting new possibilities for improving the user's awareness of his environmental or physical conditions. These systems integrate sensing, actuating as well as computing power into everyday garments. By integrating wireless communication into clothing, the possibilities are even more extended, by including real-time monitoring of the user's activities, physical and environmental conditions. These applications are very interesting in health-care for improving the comfort of patients and for monitoring rescue workers. In the context of the latter, smart textile systems allow the rescue workers to optimize their interventions without having to pay special attention to sensor data to be aware of their personal health and the status of their environment. In this way, they can improve their main task during rescue operations, being saving human lives.

The integration of smart textiles must comply with certain requirements. These systems need to be unobtrusively integrated into clothing, not hindering the user performing his or her tasks, which also implies that the system needs to be light-weight, breathable and flexible to allow wearable garment integration. In rescue-worker applications, these smart textile systems are exposed to harsh environments, such as high temperatures, humidity and extreme mechanical stresses. These extreme conditions, prohibit the use of non-robust materials.

Smart textile systems are currently split into several parts, distributed over the total area of the garment, using fragile wired interconnections in between them. These interconnections may cause malfunctions of the system, which are not tolerated in life-threatening applications. Avoiding these fragile components, improves the robustness of the system, creating Smart textile systems which provide added value and life-saving functionality for rescue workers.

In Chapter 1, an overview is given of smart textile systems and their applications, as well as the relation of this work to the reseach domain of smart textile systems.

Chapter 2, focuses on the use of antennas in wearable applications. The deployment of efficient textile patch antennas in fire fighter garments is experimentally evaluated, in order to reduce the transmit power in a wireless sensor node network. The ability of on-body textile patch antennas to increase the power received at the nodes of a wireless sensor network and reduce the packet loss in the network is demonstrated, compared to rigid integrated PCB antennas with the same transmit power. Energy consumption can be reduced by exploiting the additional received power, while maintaining the same link quality.

In Chapter 3, an novel flexible wireless textile sensor node is presented. This node is composed of a wearable textile antenna with an integrated transceiver and sensor circuit. Onto the feed plane of this antenna, a transceiver with receive diversity is integrated together with a microcontroller, memory and sensor. The textile antenna is composed of textile material generally used in rescue worker garments, which allows unobtrusive integration of the wireless sensor node into the garment. The wireless node is designed in such a way that fragile and lossy interconnections are eliminated, by replacing them by very short radio-frequency signal paths in the antenna feed plane, reducing electromagnetic compatibility as well as signal integrity problems. The application of the flexible wireless sensor node is twofold. First, the node is designed for integration into fire fighter garments, with the aim to reduce the risk associated to firefighting operations. Second, the wireless node is used as an on- and off-body body-centric measurement device. Conventional body-centric channel measurements are generally performed with complex and expensive measurement devices, which are connected to body-worn external antennas by means of fragile coaxial cables, hindering the test person to move freely. This textile wireless node was validated in the anechoic chamber, in several states such as under a bent conditions, assessing the characteristics of the integrated system in free-space. The performance is also verified in various real-world conditions, integrated into a firefighter garment, and used as an autonomous body-centric measurement device.

Thanks to its functionality integrated in a textile node that is comfortable to wear, the unit can serve for fall detection as well as for patient or rescue-worker monitoring, an application which is implemented in Chapter 4. Therefore, four nodes are integrated into the protective garment, deployed in a wireless sensor network, where each flexible textile node performs cooperative synchronous acquisition and distributed event detection. Computationally efficient situational-awareness algorithms are implemented directly on the microcontroller. The detected events as well as the sensor data are reliably wireless transferred to a base station, by making use of both a direct wireless connection and forwarding by other on-body nodes. The base station allows to visualize the received sensor data in a more detailed and comprehensive way. This information provides intervention coordinators and commanders with life-saving situational awareness of the entire rescue operation. The experiments in realistic conditions demonstrated that this autonomous, body-centric, wireless sensor network is able to correctly detect different operating conditions of a firefighter during an intervention. Furthermore, the wireless sensor network is deployed as an autonomous body-centric measurement device, providing statistical analysis of measured on-body node-to-node, and off-body person-to-person channels. These channel measurements confirm the reliability of the communication system.

In Chapter 5, a compact wearable Personal Distributed Exposimeter is proposed. The Personal Distributed Exposimeter is composed of several newly designed compact personal wearable RF exposimeter modules. Each exposimeter module is individually

integrated onto the feedplane of a wearable textile patch antenna, allowing unobtrusive garment integration, leading to user-friendly operation. The Personal Distributed Exposimeter is specifically designed to enable epidemiological studies, by measuring the incident power density on the person wearing the Personal Distributed Exposimeter. The system is validated and calibrated in the anechoic chamber, and compared to a commercially available single-unit exposimeter. Furthermore, a real world exposure measurement was carried out for the GSM-900 downlink band, performed in the city center of Ghent. The measurement was also carried out employing a commercial exposimeter, clearly illustrating that the PDE provides a more accurate estimation of the power density levels on the human body. The commercial, non-calibrated exposimeter deployed on the body, influences the measurement results due to shadowing by proximity of the body, leading to an underestimation of the power density levels on the human body.

# List of Abbreviations

| | |
|---|---|
| ADC | Analog to digital converter |
| BER | bit error rate |
| BSN | Body Sensor Network |
| DAC | Digital to analog converter |
| DPU | Data Processing Unit |
| EIRP | effective isotopic radiated power |
| FFT | fast Fourier transform |
| FPGA | Field-programmable gate array |
| FSK | Frequency-shift keying |
| GFSK | Gaussian frequency-shift keying |
| GMSK | Gaussian minimum-shift keying |
| GPS | Global Positioning System |
| GSM | Global System for Mobile Communications |
| ISM | industrial, scientific and medical |
| LNA | Low-Noise Amplifier |
| LoS | Non-Line-of-sight |
| MCU | Microcontroller |
| MRC | Maximum Ratio Combining |
| MSK | minimum-shift keying |
| NLoS | Non-Line-of-sight |
| PC | Personal computer |
| PCB | Printed Circuit Board |
| PDE | Personal Distributed Exposimeter |
| PPS | Personal Protective System |
| PS | Power Supply |
| RF | Radio Frequency |
| RSSI | Received signal strength indication |
| SAR | Specific Absorption Rate |
| SC | Selection Combining |
| SFIT | Smart Fabric Interactive Textile |
| SNR | Signal-to-Noise Ratio |
| TPU | Thermoplastic PolyUrethane |

| | |
|---|---|
| USB | Universal Serial Bus |
| WBAN | Wireless Body Area Networks |
| WPAN | Wireless Personal Area Network |
| WSN | Wireless Sensor Network |
| XPD | Cross-Polar Discrimination |

# List of Publications

## Articles in International Journals

- P. Vanveerdeghem, P. Van Torre, C. Stevens, J. Knockaert, and H. Rogier, "Flexible dual-diversity wearable wireless node integrated on a dual-polarised textile patch antenna", Published in *IET Science, Measurement and Technology*, vol. 8, no. 6, pp. 452-458, 2014.
- P. Vanveerdeghem, P. Van Torre, C. Stevens, J. Knockaert, and H. Rogier, "Synchronous Wearable Wireless Body Sensor Network Composed of Autonomous Textile Nodes", Published in *Sensors*, vol. 14, no. 10, pp. 18583-18610, 2014.
- A. Thielens, P. Vanveerdeghem, S. Agneessens, P. Van Torre, G. Vermeeren, H. Rogier, L. Martens, and W. Joseph, "Whole-Body Averaged Specific Absorption Rate Estimation using a Personal, Distributed Exposimeter", Accepted for publication in *Antennas and Wireless Propagation Letters, IEEE*, October 2014.
- P. Vanveerdeghem, P. Van Torre, A. Thielens, J. Knockaert, W. Joseph, and H. Rogier, "Compact Personal Distributed Wearable Exposimeter", Submitted to *IEEE Sensors*.

## Articles in Conference Proceedings

- P. Vanveerdeghem, B. Jooris, P. Becue, P. Van Torre, H. Rogier, I. Moerman, and J. Knockaert, "Reducing power consumption in body-centric ZigBee communication links by means of wearable textile antennas", presented in *2nd International Workshop on Measurement-based Experimental Research, Methodology and Tools*, 2013.
- P. Van Torre, P. Vanveerdeghem, H. Rogier, and I. Moerman, "Energy-efficient Off-body Communication Nodes with Receive Diversity", in *Proceedings of the 20 th IEEE Symposium on Communications and Vehicular Technology in the Benelux*, 2013.

- P. Van Torre, P. Vanveerdeghem, and H. Rogier, "Correlated Shadowing and Fading Characterization of MIMO Off-body Channels by Means of Multiple Autonomous On-body Nodes", in *Proceedings of the* 8 *th European Conference on Antennas and Propagation*, 844848, 2013.

- H. Rogier, S. Agneessens, T. Castel, S. Lemey, F. Declercq, P. Vanveerdeghem, P. Van Torre, L. Vallozzi, and W. Joseph "Novel wearable antenna systems for high datarate mobile communication in healthcare", in 4 *th International Conference on Wireless Mobile Communication and Healthcare*, 2014.

- A. Thielens, P. Vanveerdeghem, S. Agneessens, P. Van Torre, G. Vermeeren, H. Rogier, L. Martens, and W. Joseph "Whole-body Averaged SAR Assessment Using a Personal, Distributed Exposimeter", in *BioEM2014 Joint Meeting of The Bioelectromagnetics Society (BEMS) and the European BioElectromagnetics Association (EBEA)*, 2014.

# Integration of Electronic Systems on Wearable Textile Antenna Platforms

CHAPTER 1

# Introduction

## 1.1 Wearable textile systems and its applications

Today, wearable electronics are developed for consumer as well as professional purposes. These systems need to be easy to use, unobtrusively integrated into clothing and must provide the required connectivity with other devices. Such products are called *wearable textile systems*. This is one of the fastest developing interdisciplinary research fields, where information technology and micro-systems meet textile sciences, with the ultimate goal of embedding electronics into clothing, creating intelligent systems which are seamlessly integrated into garment.

The first research prototypes were called *Smart Textiles*, which are special textiles that are woven into clothing. Besides the traditional use of personal protective clothing, being a layer to protect the body from the elements of nature as well as from hazardous situations, these textiles are used for adding sensing and/or actuating functionalities into clothing. The sensing functionality is realized by integrating sensors into the clothing, measuring vital signs such as heart rate, body temperature, blood pressure, humidity, etc. The actuator functionality is enabled by integrating actuators into the clothing, such as alarms, notifying the wearer in case of an emergency situation regarding his/her vital signs or environment.

One of the first wearable textile systems is described in [1], ”The Wearable Motherboard: The first generation of adaptive and responsive textile structures (ARTS) for medical applications”. In this project, a smart shirt is presented, developed by the Georgia Institute of Technology for medical as well as battlefield management. The name *Wearable Motherboard* is chosen, because just like a regular Personal Computer (PC) motherboard, the various components are plugged into the *wearable* board.

These wearable systems can be deployed in numerous applications in various market segments, where monitoring of persons is important. In the health-care segment, for example, various monitoring situations can readily be envisaged, starting from monitoring vital signs of patients after surgery to monitoring geriatric patients and

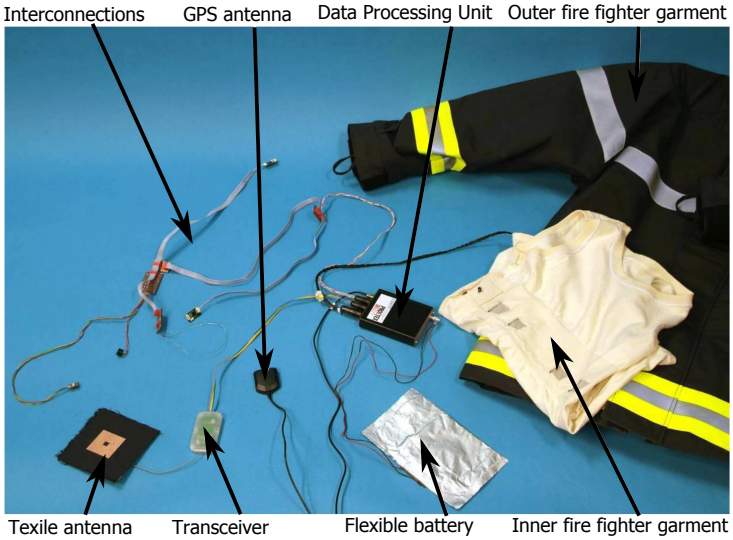


**Figure 1.1:** Prototype of the wearable textile system for firefighters, developed by the partners of the European ProeTex project

small children, preventing Sudden Infant Death Syndrome (SIDS). By continuously monitoring patients, health-care workers are capable of improving the quality of their service. Furthermore, wearable textile systems can be used by athletes for monitoring vital signs, such as breathing rate and heart,beat. In scientific environments, such as space applications, unobtrusively monitoring the astronauts medical status will gain insight in understanding the influence of space onto the human body. In critical and dangerous environments, such as mining excavations, nuclear plants, etc, special sensing devices can be applied to the wearable textile systems, detecting the presence of hazardous gasses, materials, radiation or other life-threatening conditions for the people working in those environments. In military applications, the wearable textile systems enable monitoring of the soldiers medical conditions during combat and alert the military staff. Together with this alert, the condition of the soldier can be transmitted to the medical unit, providing the necessary information to provide first aid. For public safety, wearable textile systems can be employed on fire fighters and law enforcement. Monitoring the health-, physical conditions and/or location of public regulatory services, will enhance their ability of performing operations in dangerous conditions or in remote areas. In this manuscript, we will discus this segment in particular, where the wearable system is employed onto fire fighters. Earlier, Ghent University participated in the European FP6 *ProeTex* Integrated Project, in which a wearable textile system was developed for fire fighters. A picture showing the prototype developed by the partners is shown in Fig. 1.1

A overview of these applications was summarized in Table. 1.1

| Segment | Application type | Target audience |
|---|---|---|
| Military | Combat casualty care | Soldiers and support personnel in battlefield |
| Civilian | Medical monitoring | Patients: surgical recovery, psychiatric care<br>Senior citizens: geriatric care, nursing homes<br>Infants: SIDS prevention<br>Teaching in hospitals and medical research institutions |
| | Sports | Athletes, individuals, scuba diving |
| | Performance monitoring | Mountaineering, hiking |
| Space | Space experiments | Astronauts |
| Specialized | Missions critical<br>Hazardous applications | Mining, Mass transportation |
| Public safety | Fire fighting<br>Law enforcement | Firefighters<br>Police |
| Universal | Wearable mobile information infrastructure | All information processing applications |

**Table 1.1:** Potential applications of wearable textile systems (From [1])

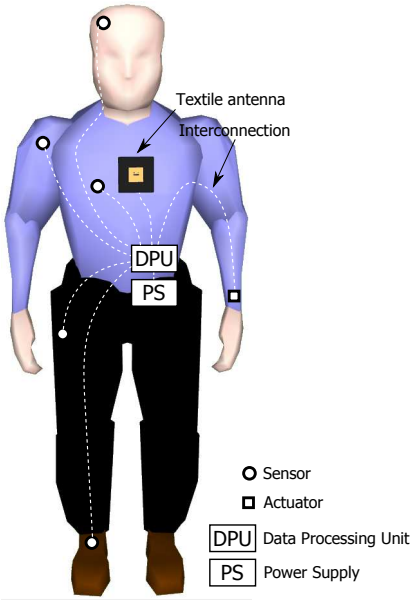


**Figure 1.2:** Wearable system integrated on-body

### 1.1.1 Typical Smart Textile system building blocks

Smart textile systems consist of a wearable garment, composed of several building blocks. These blocks extend the functionalities of the classic garment to enhance the quality of life of the person wearing the garment. A schematic drawing of a typical Smart Textile system is shown in Fig. 1.2, with its six fundamental building blocks. These blocks are the sensors, the Data Processing Unit (DPU), actuators, Power Supply (PS), communication device and interconnections.

Here, a brief overview of these fundamental building blocks is listed.

- The first building blocks of the smart textile systems are the **sensors**. Sensors can be integrated into garment, allowing to assess the vital functions of the person wearing the system, such as heart rate, blood pressure, respiration rate and body temperature. Besides monitoring the vital functions, the sensors can measure the environmental conditions of the person wearing the Smart Textile system, such as outside temperature, the presence of explosive or hazardous gasses, oxygen level, and many other parameters

- The second building block is the **Data Processing Unit (DPU)**, which is responsible for the management of the full Smart Textile system. The *intelligence* that is introduced by the data processing unit, allows the smart textile system to take autonomous decisions, such as detecting dangerous sensors levels and

alarming the user.

- Furthermore, the third building block of the system are the **actuators**. These devices generate a mechanical action, based on an electrical input signal. This allows the user to be alarmed when a dangerous condition occurs, such as a high level of toxic gas in the environment, high external temperature or a low oxygen levels and so on.

- The **Power Supply** (PS) of the system is the fourth essential building block of the smart textile system. The power supply is facing some concerns regarding implementation in a Smart Textile system. Integration of bulky batteries is not an ideal solution for providing the necessary power to the electronic system, as this limits the user in his/her movements. Small, light weight and flexible batteries are proposed in [2], to resolve the problem of rigid batteries. Furthermore, researchers are working on other methods of powering electronic devices, such as energy scavenging from human body sources, such as respiration, movements (walking, vibrations, ...) and body heat. The mechanical energy generated by the body can be converted into electrical energy by means of piezoelectric systems. Besides energy scavenging from the human body, the energy needed for powering the system can be extracted from the user's environment. A proven example of such a system is solar energy [3, 4]. A small solar panel can provide sufficient energy for powering the Smart textile System. Besides directly powering the system, several scavenging systems can be combined to provide charge to flexible light-weight batteries, buffering energy and providing the necessary power when no energy can be scavenged (for example, no sunlight or movement of the user).

- The fifth building block of the smart textile system is the **communication unit**. This unit will provide the necessary wireless connection between the smart textile system and the external devices. By making the system capable of communicating with the outside world, valuable services are added to enhance the performance of the smart textile system, such as the capability of establishing an wireless network. This allows the system to communicate, for example, with a base-station, allowing real-time monitoring of the sensor data provided by the smart-textile system. The unit is composed of an antenna connected to a transceiver unit, mostly integrated onto the data processing unit. The communication unit has the same design requirements as the other building blocks. It needs to be light weight and flexible for unobtrusive integration in the garment, resulting in a system that is comfortable to wear. Numerous textile antenna designs have proven to fulfill this requirements.

- Finally, the last building block, consists of the **interconnections**. All other critical building blocks of the smart textile system mentioned above, are obviously

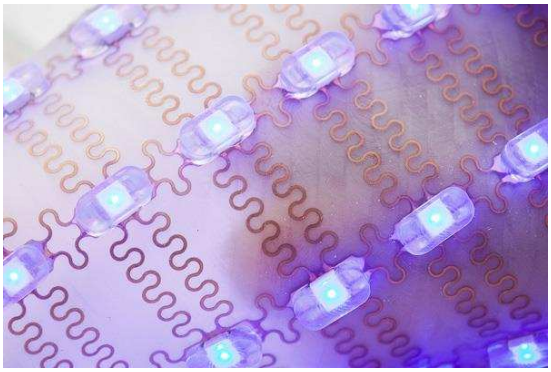

**Figure 1.3:** Prototype of stretchable interconnections for integration into clothing, from cmst.be

distributed over the body of the users. The distribution of the different blocks is chosen for optimal flexibility and on-body performance of the Smart Textile system. Therefore, the different units need to be connected to each other, by means of reliable and robust electrical connections, which still maintain the overall flexibility and performance of the system. To achieve these interconnections, different technologies are available. A first approach of connecting the different blocks, is by making use of conductive yarn, woven into the garment [5, 6]. Another solution for connecting electronic components, developed at Ghent University, is by making use of stretchable interconnections. By using a meandered structure for these interconnections, flexible properties are obtained [7]. This technique is also available for high frequency interconnections, as described in [8]. This high frequency interconnection makes use of a coplanar waveguide topology, also in a meandered structure. A picture of these stretchable interconnections is shown in Fig. 1.3 Furthermore, a wireless connection can be provided, avoiding fragile interconnections which are woven into the garments. This technique of connection is called *wireless on-body communication* [9–11]. Several independent nodes mounted onto the body have there own communication unit, communication to each other, sharing data. This approach is further studies in this work.

## 1.2 From wearable antenna to smart textile system

### 1.2.1 Wearable antennas

Conventional antennas are made of rigid materials such as copper. For wireless applications, these antennas can be integrated onto the system by means of Printed Circuit Board (PCB) antennas. When these systems are worn onto the body, the antennas are influenced by the body, making the antennas less performant. A way to improve the antenna performance is by replacing it by an antenna that is less affected by the nearby body. Excellent performance is obtained deploying patch antennas. The patch antenna is consists of a metallic ”patch”, mounted on top of larger metallic sheet or ”ground plane”. Both patch and groundplane are separated by a non-conductive material, called the ”substrate”. The Patch and ground plane form a resonator with a length of approximately half a wavelength of the radio signal. These patch antennas are typically constructed using rigid materials, such as Duroid®, as a substrate material and copper for the ground plane and patch of the antenna.

In [12], a quarter-wavelength wearable planar inverted F-antenna is proposed for operation in the GSM-900 band, suitable for off-body communication thanks to the radiation which is directed away from the body. Furthermore, thanks to this antenna topology, a higher antenna gain is obtained.

Today, these wearable antennas are commercial available. For example Flextenna® flexible antenna technology [1] patented by Pharad, provides wearable textile antennas for military purposes as well as for law enforcement applications. As stated by the manufacturer, these antennas are waterproof, flexible, lightweight and unobtrusively integrable in garments.

From the research on textile electronics, the research expanded into the research into the field of textile patch antennas. These textile patch antennas are partially or completely constructed based on textile materials, for the substrate as well as the conductive parts of the antenna. The need for textile antennas arises from the need of wearable applications, in which antennas need to be integrated into clothing as a part of a Smart Textile system. These textile antennas are thoroughly developed and investigated by our research group [3, 4, 13–23] as well as by other research groups [24, 25].

In this work, one of the proposed antennas, is a dual-polarized textile antenna [13]. The substrate material of the textile antenna being a flexible, closed-cell, water-repellent, expanded-rubber protective foam (permittivity $\epsilon_r = 1.53$ and tan $\delta = 0.0012$, density = 187.3 kg/m$^3$, thickness = 5 mm) is commonly used in protective garments for rescue workers. The antenna ground plane and radiating patch are constructed using a low-cost, conductive, electro-textile material called FlecTron, with a thickness less than 0.25 mm and a surface resistivity less than $0.1\ \Omega/\text{sq}$. The patch of the textile antenna consists of a rectangular patch with a slot, and two antenna feed points

[1] http://www.pharad.com/wearable-antennas.html

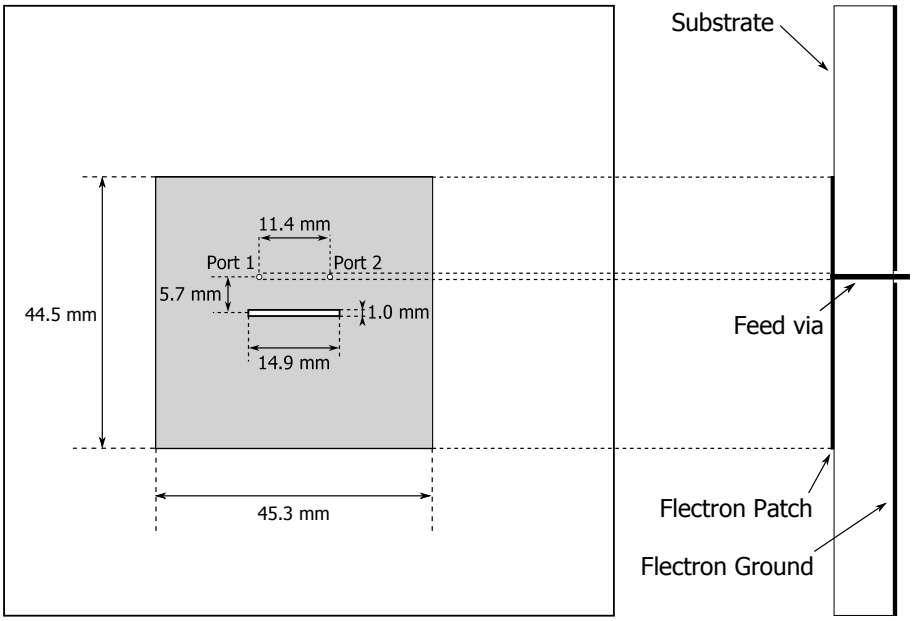


**Figure 1.4:** Detailed geometry of the dual-polarized antenna

symmetrical along the y-axis, each point corresponding to an antenna port. The topology of this antenna allows to excite two orthogonal linearly-polarized waves, enabling $2^{nd}$-order diversity on a single antenna. The antenna has an antenna gain of $6$ dBi along the boresight at a centerfrequency of f = $2.45$ GHz, and an isolation between the two feed-ports, better than $15$ dB. Fig. 1.4 and Fig. 1.5 show the detailed geometry with the antenna dimensions and a picture of the antenna, respectively.

Deploying of these wearable textile antennas, the total flexibility of the smart textile system and its overall performance should be taken into consideration. These wearable textile antennas cannot operate on their own, they always need to be connected to a wireless transceiver system. To connect the transceiver unit of the wearable textile system to the textile antenna, an RF-coaxial cable is needed. These cables will limit the movements of the person wearing the textile system, due to the non-flexibility of the coaxial cables and total size of the system. Moreover, the use of long coaxial cables that connect the transceiver unit to the antenna introduces RF losses, reducing, the sensitivity of the receiver unit. Besides the losses when receiving a signal, the power of the transmitted signal generated by the transmitter will be reduced at the antenna feed, reducing the total power transmitted by the antenna. The use of coaxial cables requires interconnections between the antenna port and the cable, these fragile interconnections need to be avoided in wearable applications where severe operative conditions occur.

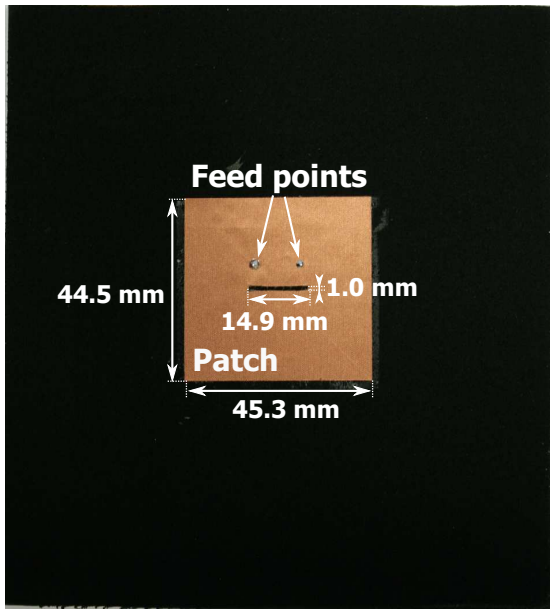


**Figure 1.5:** The dual-polarized antenna, with two antenna feeds

In order to solve some of the problems mentioned above, researchers have proposed some solutions. In current literature, the number of wearable systems that integrate *flexible* electronic circuits with textile antennas is very limited. In [14], the first wearable active receive textile antenna for use in personal area networks in the $2.45$ GHz ISM band is proposed. The integrated Low-Noise Amplifier (LNA), which is realized on a hybrid textile substrate is integrated on the backside of the wearable patch antenna. Thanks to the integration process, this antenna has an active gain of about $12$ dB, added to the passive antenna gain of approximately $5$ dBi. After deploying the newly designed active antenna into a fire fighter garment, the on-body performance was evaluated. Experiments show that only the gain performance of the antenna is mainly affected by the body, in contrast to the active circuitry, which is less influenced by the nearby human body. In [15], an active circularly polarized textile antenna is developed for use in the Global Positioning System (GPS) and Iridium satellite phone applications. On the feed substrate, a compact LNA chip is directly integrated underneath the antenna patch, with a gain higher than $28$ dBi and a $3$ dB axial ratio bandwidth in free-space of $183$ MHz. Furthermore, in [16, 26] an active textile receive antenna is deployed in a wearable through-wall Doppler radar system and integrated into clothing.

By integrating an LNA, its noise characteristic can be optimized, eliminating the influence of the coaxial cables that connect the antenna with the receiving unit of the

wearable textile system. Furthermore, other active components can be integrated onto the textile patch antenna. In [3], a wearable aperture-coupled shorted patch antenna combined with flexible solar cells covering the $902-928$ MHz ISM band, is presented. The antennas are constructed using textile materials and flexible foam, allowing convenient integration into garments.

The antennas proposed above, only integrate a Low Noise Amplifier, forming an active antenna which is highly useable in low noise applications, however still requiring a coaxial cable to be connected to transceiver or receiver units. Due to the size and rigidity of coaxial cables, the total system is bulky and vulnerable to defects. Eliminating these problems is the next step in the development of wearable textile systems.

### 1.2.2 Body-centric communication

Three main communication classes can be distinguished, depending on the application. Together, these communication classes implement body-centric communication [9, 27].

- **On-body communication** [28–32] focuses on the communication between different components on the body. This communication class is typically used in Wireless Body Area Networks (WBAN), where the goal is to eliminate the wired connections between the different components of the network. The most common example of on-body communication is the wearable Wireless Sensor Network (WSN), where several wireless sensors communicate and work together.

- **Off-body communication** identifies the communication between the human body and any external device, such as a wireless command post or satellite. In a Wireless Personal Area network (WPAN), this includes short-wave radio communication, such as Bluetooth®, ZigBee®, WiMax, WiFi and Ultra-Wideband (UWB) protocols. This category also includes in long range communication, such as Global Positioning Systems (GPS) and the Global System for Mobile Communications (GSM).

- **In-body communication** focuses on the communication between different devices, which are implanted into or placed onto the body. Antennas for these applications need to be constructed using bio-compatible materials. [27, 33–37]

In the context of rescue-worker applications, two communication classes are commonly used, being on-body as well as off-body communication.

Today, measurement campaigns on body-centric communications are generally performed by means of complex or expensive measurement devices [38–40], connected to antennas mounted onto the body of the human test person by means of fragile coaxial cables. The connections hinder the test person to move freely.

During the last years, several measurement campaigns on body-centric communications for rescue workers were performed at our research group [41–53].

The human body provides a large area for deploying off-body communication platforms with multi-antenna systems. When these antennas are sufficiently distributed over the available body area, they provide spatial diversity. By implementing these antennas by means of flexible textile fabrics into a garment, a convenient integrated system is obtained.

### Off-body communication

Typical off-body communication systems for rescue workers are commonly deployed in indoor environments. In these environments, the radio signal is influenced by varying path loss, shadowing and fading as well as a variable Doppler shift for a walking person according to his or her walking speed.

In general, these effects are described separately in radio wave propagation theory. However, these three effects are difficult to distinguish, as they appear superimposed. Fading causes fast signal fluctuations that occur over sub-wavelengths, due to destructive and constructive interference of the signals following different paths, arriving at the receiver with different phases and amplitudes. The multiple signals paths are caused by multiple reflections and scattering at different objects such as the ground, large buildings and objects in the near environment of the receiver. Shadowing or large-scale fading is observed when displacements of the wireless system exceeds several wavelengths. This effect is present in the signal when the signal paths are blocked by different obstacles. The last effect, path loss is dependent on the distance between the receiver and transmitter as well as the propagation environment.

The influence of the fading and shadowing on the signal in the indoor environment is hard to predict. Hence, these effects are mostly treated in a statistical way, due to unknown details of the indoor environment influencing the radio propagation. The distribution of the measured signals are commonly fitted to known statistical distributions, allowing further analysis of the propagation environment.

### On-body communication

Together with off-body communication systems for rescue workers, on-body communication links are also commonly deployed in indoor environments. The on-body communication channel can include different propagation mechanisms. Direct communication between the different wireless nodes onto the body is sometimes possible, but often the link is realized by scattering of the RF signal in the environment, causing significant fading [9, 10]. Even in static positions of the body, the propagation is not constant, because the body is still subjected to various small movements. The on-body communication channel can be statistically characterized according to the wireless link between the different positions of the wireless nodes onto the body.

### Diversity

The signal impinging on the antenna of the receiver exhibits fast fluctuations and deep fades in signal level, where the signal powers drop down over orders of magnitude compared to the median signal level. This effect is caused by the multipath environment and is very dependent on the position of the receiving antenna as well as on the particular time instant. These effects cannot be changed by the design of the system, as the multipath effect is entirely caused by the propagation environment. Therefore the system needs to be able to deal with these fluctuations. A powerful technique to improve the quality of the signals is diversity. A summary of some of diversity techniques is listed below

- **Space diversity** uses multiple antennas, which are deployed such that the diversity branches experience uncorrelated fading. Separation of the antennas by about a half-wavelength will be sufficient.
- **Pattern diversity** is obtained by deploying a number of directional antennas, pointing in different directions, each receiving uncorrelated signals.
- **Polarization diversity** exploits the scattering property of the environment, which tends to depolarize a signal. To obtain diversity, the receive antenna must have antenna ports with different polarizations, or the diversity system can be constructed using multiple antennas with different polarizations. In this work, a dual-polarized antenna is used, to construct a wireless node with polarization diversity.

By using several antennas, receive diversity is obtained. The uncorrelated signals received by the antenna system need to be further processed in order to enable the system to deal with the effects of the multipath environment. Two of these techniques are listed below.

- **Selection Combining** (SC) is the simplest technique to implement receive diversity, by selecting the received signals that have the strongest signal level in comparison to the signals received by the other antennas. Only the selected signal is processed by the receiver unit. Practically, the signal can be selected by a low-cost logarithmic detector, generating an output voltage that is linear to the input signal strength in dBm. As only one receiving unit is required, a low-cost diversity solution is obtained.
- **Maximum Ratio Combining** (MRC) is a diversity technique that achieves a signal with a highest possible signal-to-noise ratio (SNR). In theory, the SNR of the resulting signal, is the sum of the SNRs of each of the signals of the receiving channels. This technique has a better performance than SC. Yet, this diversity technique requires full receiving chain for each separate channel. Furthermore,

accurate channel estimation is needed to combine of the signals with a correct phase relationship and correct gain, making it a less cost-efficient solution.

#### Typical measurement setup for body-centric measurements

Measurement campaigns that evaluate off-body communication are generally performed by means of complex or expensive measurement devices. The antennas, which are integrated into the garment, are connected by means of fragile coaxial cables to these measurement devices. The RF connections can be integrated into the garment, minimizing the installation time onto the body. However, coaxial cables and their connectors are fragile, and stress and strain can damage the antenna system.

### 1.2.3 Body sensor networks

In the last decade, a rapidly increasing interest in sensing and monitoring devices was observed, evolving in the research on Body Sensor Networks (BSN) [54–57], which are networks of wearable computing and sensing devices. These BSNs are deployed in different domains, from healthcare to law enforcement as well as daily use for individuals.

Body Sensor Networks perform monitoring, of vital signs such as being respiration rate, body temperature, heart rate, etc. As well as monitoring of motion of the user, enabling to identify the position of the user, being the absolute location (for example by means of GPS localization) as well as his/her posture determined by means of accelerometers, compass or gyroscope. Moreover, sensing the environment is enabled by adding sensors for sensing gas, temperature, etc. Furthermore, the BSN is equipped with a communication unit, to transmit the sensor data to the staff monitoring the user.

The BSN is can be deployed on different ways. First, the BSN can be deployed by integrating the sensor into clothing as well as surface-mounted onto the body of the user. Second, the BSN can be deployed by means of sensors nodes, that are implanted into the body or swallowed by the user, these network nodes need to be constructed using bio-compatible materials.

#### Rescue-worker applications

One of the most important fields to deploy wearable systems, is in rescue workers interventions. During major disasters, rescue workers are exposed to hostile and harsh environments. At our research group, research has been carried out on the integration of wearable textile systems into garments of rescue workers, in the context of the European project ProeTex. The work at Ghent University was mainly focused on the development and prototyping of textile antennas for integration into rescue worker garments. This project was the first step into the current project, the Smart@Fire Seventh Framework Programme (FP7) project (2012-2015) [58].

As stated on the website of the Smart@Fire FP7, every year, more than 100 firefighters of the European union lose their lives whilst saving others. They lose their way in smoke, become surrounded by a sea of flames, get cut off by suddenly rising water, and continually find themselves in perilous situations. The aim of the Smart@Fire FP7 [58] project is to reduce the risk associated with firefighting, by the development of innovative ICT-solutions, which need to be integrated in a smart Personal Protective System (PPS). Current ICT-solutions available on the market do not provide full satisfaction. Based on large scale survey of 961 fire brigades, the main needs have been identified. To increase the safety of the fire fighters, three main innovative technologies need to be studied. First, *sensors* to measure vital body functions of the fire fighters and environmental parameters. Second, *localization* systems to determine the position of the fire fighters. Third, *data transfer* and visualization systems to better assess situations. These innovative technologies need to be integrated in the PPS of fire fighters

### RF signal level sensing

Besides deploying Body sensor networks for rescue worker applications or health care applications, these networks can be deployed in research related domains. For example epidemiological studies on the influence of the absorption of Radio Frequency (RF) electromagnetic fields by the human body.

In the last three decades, the number of devices emitting RF radiation is dramatically increased. These devices such as microwave ovens, smart-phones, military and civilian radar systems, radio transmitters, base stations for the Global System for Mobile Communications (GSM), satellite communications systems (Global Positioning System or GPS, Iridium, etc.) and other are widely used in daily environment of the general public [59]. The increasing development of devices, increased the concerns about the influence on the human body, which is still an important research topic today.

The absorption of radio frequency (RF) radiation is presented in terms of the specific absorption rate (SAR) in watts per kilogram. The SAR was suggested by the National Council on Radiation Protection and Measurement, and generally accepted by engineers and scientists. The most commonly studied SAR is the whole-body averaged SAR (SARwb) [60], which only can be evaluated using numerical simulations. To accommodate this, reference levels have been defined on the incident power density, which can be measured. The measured level can be compared to the international guidelines issued by organizations such as INCIRP [65]. Personal exposimeters or dosimeters are developed to measure exposure levels of a subject [60–64]. These devices are used to measure the electromagnetic fields incident on the human body.

## 1.3 Goal of the thesis

The research in this work focuses on the **integration of electronic systems onto textile antenna platforms**. By integrating the electronic systems onto the textile antennas, several improvements are achieved in comparison with previous non-integrated designs. The design requires to be integratable into clothing. By integrating electronic systems onto the antennas, fragile and lossy coaxial RF interconnections are avoided, making it convenient to integrate. Several specific applications are developed to validate the potential of the integrated textile antenna systems.

First, A wireless sensor node is developed, which is integratable in rescue workers garments. The wireless node enables the potential to be deployed as an Personal Protective System for fire fighters, as requested by the Smart@Fire project. Wireless systems that integrate several sensors can be used to monitor the fire fighters conditions and environment. Furthermore, the wireless node needs to be deployed in the research domain of body-centric communication, which requires to evaluate body-centric wireless communication in terms of signal levels and data packet loss. This enables convenient measurement procedures in comparison with the traditional techniques, that use separate antennas onto the body which are connected by means of long RF coaxial cables to large and expensive measurement equipment, which is very difficult to handle and requires lost of time to deploy the system.

The second integrated textile antenna system that is designed, is a wireless senor node network for RF exposure measurements. Current RF exposure measurements are compromised by large measurement uncertainties, caused by the influence of the nearby body. Moreover, the uncertainties are also caused by out-of-band detection as well as the dependence of the polarization of the detected RF signals. Besides the required improvement on the measurement results, the flexibility of the system is crucial, to enable unobtrusive garment integration. Therefore, textile antennas with integrated electronic systems are an excellent solution in comparison with the traditional exposure measurements on the human body.

## 1.4 Overview of the manuscript and own contributions

### 1.4.1 Reducing Power Consumption by means of Textile Antennas

Employing textile antennas has several advantages in comparison with regular PCB antennas on electronics systems. By replacing the integrated PCB antenna by a textile patch antenna, the quality of the off-body wireless communication link is improved both in receive and transmit mode. In Chapter 2 the advantage of making use of textile antennas instead of regular PCB antennas is experimentally validated. Furthermore,

this may be be exploited in reducing transmit power at the mobile nodes while guaranteeing the same link quality. enabling to reduce the to further reduce the power consumption.

### 1.4.2 Flexible Dual-Diversity Wearable Wireless Node Design

In Chapter 3 the first autonomous textile wireless sensor node, fully integrated onto the feedplane of a flexible dual-polarized textile patch antenna, is presented. The wireless node is particularity designed for two purposes. First, as an autonomous body-centric channel measurement device with all the equipment integrated into clothing. Second, as an wireless network node for rescue worker applications. The wearable node is equipped with a dual-polarized textile patch antenna with integrated microcontroller, sensor, memory, and transceiver with receive diversity. The performance of the wearable wireless node is enhanced by implementing $2^{nd}$-order receive diversity, by means of selection combining. By integrating the node onto a flexible substrate directly below the antenna patch and the ground plane, fragile and lossy interconnections are avoided, allowing to be unobtrusively integrated into rescue worker garments, which was not possible earlier for body-centric communication measurements The compact and flexible module combines sensing and wireless channel monitoring functionality with reliable and energy-efficient off-body wireless communication capability, by fully exploiting dual polarization diversity. This novel textile wireless node is validated, both in flat and bent state, in the anechoic chamber, assessing the characteristics of the integrated system in free-space conditions. Moreover, the wireless performance is verified in various real-world conditions, integrated into a firefighter garment, used as an autonomous body-centric measurement device.

### 1.4.3 Wearable Wireless Body Sensor Network for Fire Fighters

In Chapter 4 a fully-autonomous, wearable, wireless sensor network is presented, where each flexible textile node, which is presented in Chapter 3 performs cooperative synchronous acquisition and distributed event detection. Onto each microcontroller of the wireless nodes, a computationally efficient situational-awareness algorithm is implemented, performing event detecting at the user. The detected events are wirelessly transmitted to a base station, directly, as well as forwarded by other on-body nodes. Thanks to the integrated polarization diversity, the reliability and energy-efficiency of the wireless transmission is improved. The body centric communication is further statistically analyzed for on-body node-to-node, as well as off-body person-to-person communication. On-body node-to-node communication is exploited to synchronize measurements on multiple autonomous nodes, at different body locations, and to share sensor data between these nodes. $N^{th}$ order transmit diversity performance is approached, by repeating the sensor data from the other on-body nodes, drastically

enhancing communication reliability by eliminating packet loss. The signal levels received at the receiver are at least $15$ dB above the transceiver's specified receiving threshold of $-95$ dBm for 98% of the received packets. Off-body person-to-person communication has the same functional purpose as the on-body node-to-node communication, synchronizing measurements and sharing/forwarding sensor data. The signal levels received at the receiver for off-body person-to-person communication is at least $20$ dB above the transceiver's specified receiving threshold of $-95$ dBm for 98% of the received packets. The development of the integratable sensor network for rescue workers is a first step in the development of a smart PPS for the Smart@Fire project.

### 1.4.4 Compact Personal Distributed Wearable Exposimeter

Integrating electronic systems onto textile antennas is an ideal solution for body sensor networks. Exposure measurements currently performed with commercially available personal exposimeters, are compromised by large measurement uncertainties, due to the influence of the body of the test person, as well as dependence on polarization and out-of-band detection. Moreover, conventional personal exposimeters do not allow unobtrusive integration onto the human body, making them uncomfortable to wear. In Chapter $5$ the hardware to construct a compact wearable Personal Distributed Exposimeter (PDE) is proposed for measuring the power density on the human body. A fully integrated wearable on-body personal exposimeter enables continuously monitoring of the long-term RF exposure, without hindering the users daily activities. The on-body PDE, is composed out of several newly designed RF exposimeter sensor modules, increasing the measurement accuracy. Each exposimeter sensor module is integrated onto the feedplane of a wearable textile patch antenna, enabling unobtrusive garment integration. The sensor modules are employed with an RF detector and necessary memory for data logging. The proposed system is validated and calibrated in the anechoic chamber, as well as compared to a commercially available single-unit exposimeter. Further validation of the PDE is performed in a real-environment, determining the average power density on a human during a walk in an urban city.

### 1.4.5 Conclusions and further work

The conclusions and further work in Chapter $6$ evaluate the benefits of integrating electronic systems onto textile antenna platforms. Further research that needs to be performed in the near further for developing the wearable technology on a large scale is outlined.

### 1.4.6 Schematics of the wearable integrated electronic designs

In the appendix of this work, the schematics of the developed systems are included, together with the composite drawing of the top- and bottom- layer of PCB layout.

# Bibliography


[1] C. Gopalsamy, S. Park, R. Rajamanickam, and S. Jayaraman, "The wearable motherboard: The first generation of adaptive and responsive textile structures (arts) for medical applications", *Virtual Reality*, vol. 4, no. 3, pp. 152–168, 1999.

[2] D.P. Roller and S. Slane, "Wearable lithium-ion polymer batteries for military applications", in *Battery Conference on Applications and Advances, 1998., The Thirteenth Annual*, Jan 1998, pp. 71–74.

[3] Frederick Declercq, A Georgiadis, and Hendrik Rogier, "Wearable aperture-coupled shorted solar patch antenna for remote tracking and monitoring applications (invited)", in *Proceedings of the 5th European conference on Antennas and propagation EUCAP*. 2011, pp. 2992–2996, IEEE.

[4] Sam Lemey, Frederick Declercq, and Hendrik Rogier, "Dual-band substrate integrated waveguide textile antenna with integrated solar harvester", *IEEE ANTENNAS AND WIRELESS PROPAGATION LETTERS*, vol. 13, pp. 269–272, 2014.

[5] I. Locher and G. Troster, "Fundamental building blocks for circuits on textiles", *Advanced Packaging, IEEE Transactions on*, vol. 30, no. 3, pp. 541–550, Aug 2007.

[6] D. Cottet, J. Grzyb, T. Kirstein, and G. Troster, "Electrical characterization of textile transmission lines", *Advanced Packaging, IEEE Transactions on*, vol. 26, no. 2, pp. 182–190, May 2003.

[7] Dominique Brosteaux, Fabrice Axisa, M GONZALEZ, and Jan Vanfleteren, "Design and fabrication of elastic interconnections for stretchable electronic circuits", *IEEE ELECTRON DEVICE LETTERS*, vol. 28, no. 7, pp. 552–554, 2007.

[8] Benoît Huyghe, Hendrik Rogier, Jan Vanfleteren, and Fabrice Axisa, "Design and manufacturing of stretchable high-frequency interconnects", *IEEE TRANSACTIONS ON ADVANCED PACKAGING*, vol. 31, no. 4, pp. 802–808, 2008.

[9] P. S. Hall and Y. Hao, "Antennas and propagation for body centric communications", in *Antennas and Propagation, 2006. EuCAP 2006. First European Conference on*, 2006, pp. 1–7.

[10] P.S. Hall, Yang Hao, Y.I. Nechayev, A. Alomainy, C.C. Constantinou, C. Parini, M.R. Kamarudin, T.Z. Salim, D.T.M. Hee, R. Dubrovka, A.S. Owadally, Wei Song, A. Serra, P. Nepa, M. Gallo, and M. Bozzetti, "Antennas and propagation for on-body communication systems", *Antennas and Propagation Magazine, IEEE*, vol. 49, no. 3, pp. 41–58, June 2007.

[11] E. Reusens, W. Joseph, B. Latre, B. Braem, G. Vermeeren, E. Tanghe, L. Martens, I. Moerman, and C. Blondia, "Characterization of on-body communication channel and energy efficient topology design for wireless body area networks", *Information Technology in Biomedicine, IEEE Transactions on*, vol. 13, no. 6, pp. 933–945, Nov 2009.

[12] P. Salonen, L. Sydanheimo, M. Keskilammi, and M. Kivikoski, "A small planar inverted-f antenna for wearable applications", in *Wearable Computers, 1999. Digest of Papers. The Third International Symposium on*, Oct 1999, pp. 95–100.

[13] L. Vallozzi, H. Rogier, and C. Hertleer, "Dual polarized textile patch antenna for integration into protective garments", *Antennas and Wireless Propagation Letters, IEEE*, vol. 7, pp. 440–443, 2008.

[14] Frederick Declercq and Hendrik Rogier, "Active integrated wearable textile antenna with optimized noise characteristics", *IEEE TRANSACTIONS ON ANTENNAS AND PROPAGATION*, vol. 58, no. 9, pp. 3050–3054, 2010.

[15] A. Dierck, H. Rogier, and F. Declercq, "A wearable active antenna for global positioning system and satellite phone", *Antennas and Propagation, IEEE Transactions on*, vol. 61, no. 2, pp. 532–538, Feb 2013.

[16] Arnaut Dierck, Sam Agneessens, Frederick Declercq, Bart Spinnewyn, Gert-Jan Stockman, Patrick Van Torre, Luigi Vallozzi, Dries Vande Ginste, Thomas Vervust, Jan Vanfleteren, and Hendrik Rogier, "Active textile antennas in professional garments for sensing, localisation and communication", *INTERNATIONAL JOURNAL OF MICROWAVE AND WIRELESS TECHNOLOGIES*, vol. 6, no. 3-4, pp. 331–341, 2014.

[17] Sam Agneessens and Hendrik Rogier, "Compact half diamond dual-band textile hmsiw on-body antenna", *IEEE TRANSACTIONS ON ANTENNAS AND PROPAGATION*, vol. 62, no. 5, pp. 2374–2381, 2014.

[18] Maria Lucia Scarpello, Luigi Vallozzi, Hendrik Rogier, and Dries Vande Ginste, "High-gain textile antenna array system for off-body communication", *INTERNATIONAL JOURNAL OF ANTENNAS AND PROPAGATION*, p. 12, 2012.

[19] Maria Lucia Scarpello, Dries Vande Ginste, and Hendrik Rogier, "Design of a low-cost steerable textile antenna array operating in varying relative humidity conditions", *MICROWAVE AND OPTICAL TECHNOLOGY LETTERS*, vol. 54, no. 1, pp. 40–44, 2012.

[20] Freek Boeykens, Luigi Vallozzi, and Hendrik Rogier, "Cylindrical bending of deformable textile rectangular patch antennas", *International Journal of Antennas and Propagation*, p. 11, 2012.

[21] Carla Hertleer, Annelien Van Laere, Hendrik Rogier, and Lieva Van Langenhove, "Influence of relative humidity on textile antenna performance", *TEXTILE RESEARCH JOURNAL*, vol. 80, no. 2, pp. 177–183, 2010.

[22] Luigi Vallozzi, W Vandendriessche, Hendrik Rogier, Carla Hertleer, and Maria Lucia Scarpello, "Design of a protective garment gps antenna", *MICROWAVE AND OPTICAL TECHNOLOGY LETTERS*, vol. 51, no. 6, pp. 1504–1508, 2009.

[23] Carla Hertleer, Hendrik Rogier, Luigi Vallozzi, and Lieva Van Langenhove, "A textile antenna for off-body communication integrated into protective clothing for firefighters", *IEEE TRANSACTIONS ON ANTENNAS AND PROPAGATION*, vol. 57, no. 4, pp. 919–925, 2009.

[24] J. Lilja, P. Salonen, T. Kaija, and P. de Maagt, "Design and manufacturing of robust textile antennas for harsh environments", *Antennas and Propagation, IEEE Transactions on*, vol. 60, no. 9, pp. 4130–4140, Sept 2012.

[25] P. Salonen and Y. Rahmat-Samii, "Textile antennas: Effects of antenna bending on input matching and impedance bandwidth", *Aerospace and Electronic Systems Magazine, IEEE*, vol. 22, no. 12, pp. 18–22, Dec 2007.

[26] Sam Agneessens, Patrick Van Torre, Frederick Declercq, Bart Spinnewyn, Gert-Jan Stockman, Hendrik Rogier, and Dries Vande Ginste, "A through wall doppler radar system: active textile antenna design, prototyping and experiment", in *2013 IEEE TOPICAL CONFERENCE ON WIRELESS SENSORS AND SENSOR NETWORKS (WISNET)*. 2013, pp. 16–18, IEEE.

[27] R. Chavez-Santiago, K. Sayrafian-Pour, A. Khaleghi, K. Takizawa, Jianqing Wang, I. Balasingham, and Huan-Bang Li, "Propagation models for ieee 802.15.6 standardization of implant communication in body area networks", *Communications Magazine, IEEE*, vol. 51, no. 8, pp. 80–87, August 2013.

[28] G.A. Conway, W.G. Scanlon, and D. Linton, "Low-profile microstrip patch antenna for over-body surface communication at 2.45 ghz", in *Vehicular Technology Conference, 2007. VTC2007-Spring. IEEE 65th*, April 2007, pp. 392–396.

[29] K.Y. Yazdandoost, "Antenna for over body surface communication", in *Microwave Conference Proceedings (APMC), 2011 Asia-Pacific*, Dec 2011, pp. 578–581.

[30] G.A. Conway and W.G. Scanlon, "Antennas for over-body-surface communication at 2.45 ghz", *Antennas and Propagation, IEEE Transactions on*, vol. 57, no. 4, pp. 844–855, April 2009.

[31] Shih-Chung Tuan, Hsi-Tseng Chou, Ching-Hui Chen, et al., "Creeping wave antenna design and application for on-body surface communication", *Session 3A5 Microstrip and Printed Antenna, Antenna Theory*, p. 456, 2013.

[32] L. Petrillo, T. Mavridis, J. Sarrazin, D. Lautru, A. Benlarbi-Delai, and P. De Doncker, "Analytical creeping waves model at 60 ghz for on-body communications", in *Antennas and Propagation (EuCAP), 2013 7th European Conference on*, April 2013, pp. 570–573.

[33] Maria Lucia Scarpello, Divya Kurup, Hendrik Rogier, Dries Vande Ginste, Fabrice Axisa, Jan Vanfleteren, Wout Joseph, Luc Martens, and Günter Vermeeren, "Design of an implantable slot dipole conformal flexible antenna for biomedical applications", *IEEE TRANSACTIONS ON ANTENNAS AND PROPAGATION*, vol. 59, no. 10, pp. 3556–3564, 2011.

[34] Maria Lucia Scarpello, *Implantable and wearable antennas for body-centric communication*, PhD thesis, Ghent University, 2012.

[35] Sam Agneessens, Patrick Van Torre, Emmeric Tanghe, Günter Vermeeren, Wout Joseph, and Hendrik Rogier, "On-body wearable repeater as a data link relay for in-body wireless implants", *IEEE ANTENNAS AND WIRELESS PROPAGATION LETTERS*, vol. 11, pp. 1714–1717, 2012.

[36] Thijs Castel, Patrick Van Torre, Emmeric Tanghe, Sam Agneessens, Günter Vermeeren, Wout Joseph, and Hendrik Rogier, "Improved reception of in-body signals by means of a wearable multi-antenna system", *INTERNATIONAL JOURNAL OF ANTENNAS AND PROPAGATION*, p. 9, 2013.

[37] Wout Joseph, Emmeric Tanghe, Patrick Van Torre, Günter Vermeeren, Sam Agneessens, Hendrik Rogier, and Luc Martens, "Power delay profiles for a wireless endoscopy link", in *International Conference on Electromagnetics in Advanced Applications*, 2013, pp. 239–242.

[38] A. Alomainy, A. Sani, A. Rahman, J.G. Santas, and Yang Hao, "Transient characteristics of wearable antennas and radio propagation channels for ultra-wideband body-centric wireless communications", *Antennas and Propagation, IEEE Transactions on*, vol. 57, no. 4, pp. 875–884, 2009.

[39] P.A. Catherwood and W.G. Scanlon, "Body-centric ultra-wideband multi-channel characterisation and spatial diversity in the indoor environment", *Microwaves, Antennas Propagation, IET*, vol. 7, no. 1, pp. 61–70, 2013.

[40] Q.H. Abbasi, A. Sani, A. Alomainy, and Yang Hao, "On-body radio channel characterization and system-level modeling for multiband OFDM ultra-wideband body-centric wireless network", *Microwave Theory and Techniques, IEEE Transactions on*, vol. 58, no. 12, pp. 3485–3492, 2010.

[41] Patrick Van Torre, Luigi Vallozzi, Carla Hertleer, Hendrik Rogier, Marc Moeneclaey, and Jo Verhaevert, "Dynamic link performance analysis of a rescue worker's off-body communication system using integrated textile antennas", *IET SCIENCE MEASUREMENT & TECHNOLOG*, vol. 4, no. 2, pp. 41–52, 2010.

[42] Patrick Van Torre, Luigi Vallozzi, Hendrik Rogier, and Jo Verhaevert, "Diversity textile antenna systems for firefighters", in *Proceedings of the fourth European Conference on Antennas and Propagation*. 2010, p. 5, IEEE.

[43] L. Vallozzi, P. Van Torre, C. Hertleer, H. Rogier, M. Moeneclaey, and J. Verhaevert, "Wireless communication for firefighters using dual-polarized textile antennas integrated in their garment", *Antennas and Propagation, IEEE Transactions on*, vol. 58, no. 4, pp. 1357–1368, 2010.

[44] Patrick Van Torre, Luigi Vallozzi, Hendrik Rogier, Marc Moeneclaey, and Jo Verhaevert, "Channel characterization and robust tracking for diversity reception over time-variant off-body wireless communication channels", *EURASIP Journal on Advances in Signal Ppocessing*, p. 14, 2010.

[45] P. Van Torre, L. Vallozzi, C. Hertleer, H. Rogier, M. Moeneclaey, and J. Verhaevert, "Indoor off-body wireless MIMO communication with dual polarized textile antennas", *Antennas and Propagation, IEEE Transactions on*, vol. 59, no. 2, pp. 631 –642, feb. 2011.

[46] Patrick Van Torre, Maria Lucia Scarpello, Luigi Vallozzi, Hendrik Rogier, Marc Moeneclaey, Dries Vande Ginste, and Jo Verhaevert, "Indoor off-body wireless communication: static beamforming versus space-time coding", *International Journal of Antennas and Propagation*, 2012.

[47] Patrick Van Torre, Luigi Vallozzi, Lennert Jacobs, Hendrik Rogier, Marc Moeneclaey, and Jo Verhaevert, "Characterization of measured indoor off-body MIMO channels with correlated fading, correlated shadowing and constant path loss", *Wireless Communications, IEEE Transactions on*, vol. 11, no. 2, pp. 712–721, 2012.

[48] Patrick Van Torre, Luigi Vallozzi, Arnaut Dierck, Hendrik Rogier, and Marc Moeneclaey, "Power-efficient body-centric communications", in *URSI Benelux Forum 2012, Proceedings*, 2012, pp. 8–10.

[49] Patrick Van Torre, Luigi Vallozzi, Hendrik Rogier, Marc Moeneclaey, and Jo Verhaevert, "Energy-efficient off-body data transmission by means of antenna diversity and tracking of the time-variant wireless channel state", in *6th European Conference on Antennas and Propagation, Proceedings*, 2012, pp. 3459–3463.

[50] Patrick Van Torre, Luigi Vallozzi, Hendrik Rogier, and Jo Verhaevert, "Indoor off-body wireless communication using static zero-elevation beamforming on front and back textile antenna arrays", in *6th European Conference on Antennas and Propagation, Proceedings*, 2012, pp. 732–736.

[51] Patrick Van Torre, Luigi Vallozzi, Hendrik Rogier, Marc Moeneclaey, and Jo Verhaevert, "Reliable mimo communication between firefighters equipped with wearable antennas and a base station using space-time codes", in *Proceedings of the 5th European conference on Antennas and propagation EUCAP*. 2011, pp. 2690–2694, IEEE.

[52] Patrick Van Torre, Hendrik Rogier, Luigi Vallozzi, Carla Hertleer, and Marc Moeneclaey, "Application of channel models to indoor off-body wireless mimo communication with textile antennas", in *COST 2100 MCM, 9th*. 2009, p. 19, COST 2100.

[53] Patrick Van Torre, Luigi Vallozzi, Carla Hertleer, Frederick Declercq, Hendrik Rogier, Marc Moeneclaey, and Jo Verhaevert, "Off-body communication in a multipath environment over time-variant channels using multiple textile antennas for the 2.45 ghz band", in *Communications and Vehicular Technology, 16th Annual symposium of the IEEE Benelux Chapter, Proceedings*. 2009, p. 6, IEEE/CVT Benelux Chapter.

[54] B. Lo and G. Z. Yang, "Key technical challenges and current implementations of body sensor networks", in *Wearable and Implantable Body Sensor Networks*, 2005.

[55] Wang Lei, Yang Guang-Zhong, Huang Jin, Zhang Jinyong, Yu Li, Nie Zedong, and D.R.S. Cumming, "A wireless biomedical signal interface system-on-chip for body sensor networks", *Biomedical Circuits and Systems, IEEE Transactions on*, vol. 4, no. 2, pp. 112–117, April 2010.

[56] Xiaochen Lai, Quanli Liu, Xin Wei, Wei Wang, Guoqiao Zhou, and Guangyi Han, "A survey of body sensor networks", *Sensors*, vol. 13, no. 5, pp. 5406–5447, 2013.

[57] Saim Kim, Christian Brendle, Hyun-Young Lee, Marian Walter, Sigrid Gloeggler, Stefan Krueger, and Steffen Leonhardt, "Evaluation of a 433 mhz band body sensor network for biomedical applications", *Sensors*, vol. 13, no. 1, pp. 898–917, 2013.

[58] IWT Belgium, the Flemish government agency for Innovation by Science and Technology, "Smart@Fire, a groundbreaking european project (FP7) to encourage companies and researchers and provide them with financial means to develop innovative ICT solutions that better protect firefighters and help prevent accidents, and to integrate them into smart Personal Protective Equipment (PPE).", June 2013.

[59] Carl H. Durney, Habib Massoudi, and Magdy F. lskander, *Radiofrequency radiation dosimetry handbook*, Electrical Engineering Department, University of Utah, 50 Central Campus Dr, Salt Lake City, UT 84112, USA, 2002.

[60] Wout Joseph, Günter Vermeeren, Leen Verloock, and Luc Martens, "Estimation of whole-body SAR from electromagnetic fields using personal exposure meters", *Bioelectromagnetics*, vol. 31, no. 4, pp. 286–295, 2010.

[61] Damiano Urbinello, Anke Huss, Johan Beekhuizen, Roel Vermeulen, and Martin Röösli, "Use of portable exposure meters for comparing mobile phone base station radiation in different types of areas in the cities of Basel and Amsterdam", *Science of The Total Environment*, vol. 468469, no. 0, pp. 1028 – 1033, 2014.

[62] György Thurczy, Ferenc Molnr, Gbor Jnossy, Nomi Nagy, Györgyi Kubinyi, Jzsef Bakos, and Judit Szab , "Personal RF exposimetry in urban area", *annals of telecommunications - annales des télécommunications*, vol. 63, no. 1-2, pp. 87–96, 2008.

[63] Wout Joseph, Günter Vermeeren, Leen Verloock, Mauricio Masache Heredia, and Luc Martens, "Characterization of personal RF electromagnetic field exposure and actual absorption for the general public", *HEALTH PHYSICS*, vol. 95, no. 3, pp. 317–330, 2008.

[64] Arno Thielens, Sam Agneessens, Leen Verloock, Emmeric Tanghe, Hendrik Rogier, Luc Martens, and Wout Joseph, "On-body calibration and processing for a combination of two radio-frequency personal exposimeters", *Radiation Protection Dosimetry*, 2014.

[65] International Commission on Non-Ionizing Radiation Protection, "Guidelines for limiting exposure to time-varying electric, magnetic, and eletromagnetic fields (up to 300GHz)", *Health Physics*, vol. 74, pp. 494–552, 1998.

CHAPTER 2

# Reducing Power Consumption in Body-centric Zigbee Communication Links by means of Wearable Textile Antennas

**Peter Vanveerdeghem, Bart Jooris, Pieter Becue, Patrick Van Torre, Hendrik Rogier, Ingrid Moerman, Jos Knockaert**

based on “Reducing power consumption in body-centric ZigBee communication links by means of wearable textile antennas”, presented in 2 *nd International Workshop on Measurement-based Experimental Research, Methodology and Tools, 2013.*

★★★

*Smart-fabric interactive textile systems have been studied intensively during the last decades and are ready to penetrate the market. Such systems are being tested in different application domains, such as health monitoring, coordination of military and emergency operations monitoring, sports and gaming. To make such systems attractive to consumers, they need to be low cost, low weight, flexible and primarily energy-efficient. We experimentally evaluate the deployment of efficient textile patch antennas in fire fighter garments to reduce the transmit power in a wireless sensor node network. The measurements performed in an advanced testbed setup, demonstrate the potential of on-body textile patch antennas to increase the power received at the nodes of a wireless sensor network and reduce the packet loss in the network, compared to using a rigid integrated PCB antenna with the same transmit power. The additional margin in received power may be exploited to reduce the transmit power while maintaining the same packet, resulting in a reduced energy consumption, paving the way towards smaller, lower-weight and less expensive consumer products.*

## 2.1 Introduction

Wireless body-centric sensor networks received increasing interest in the last decade. At first, these systems were very complex, high-cost and dedicated to professional applications such as monitoring of military, law enforcement officers and rescue workers by means of, for example, the intelligent fire fighter suit developed in the FP6 Proetex Integrated Project. Nowadays, such systems are ready to penetrate the market for all kinds of consumer applications, given their potential in personal communications, gaming, sports and healthcare. In order to be successful and to achieve high market penetration, besides offering the required performance, these systems must be low-cost, light-weight, comfortable to wear and highly energy-efficient, as, especially in wearable applications, heavy batteries and frequent recharging should be avoided.

In this chapter, we demonstrate how the power required for off-body wireless communication may be reduced by making use of more efficient antennas. The key idea consists of exploiting the large area available in a garment to deploy a flexible textile antenna that provides high gain and large radiation efficiency while being seamlessly integrated in the garment. In particular, we make use of the RM090 transceiver module [1] to study the potential reduction in transmit power while maintaining the wireless link quality by replacing a simple printed PCB antenna by a wearable textile antenna. In addition, we study the effect of antenna polarization on link quality.

In current literature, the experimental characterization of textile patch antennas for different applications is mainly performed in terms of Signal-to-noise ratio (SNR) and bit error rate (BER) for uncoded data transmission relying on basic modulation schemes [2–5]. In this chapter, measurements are performed following the IEEE

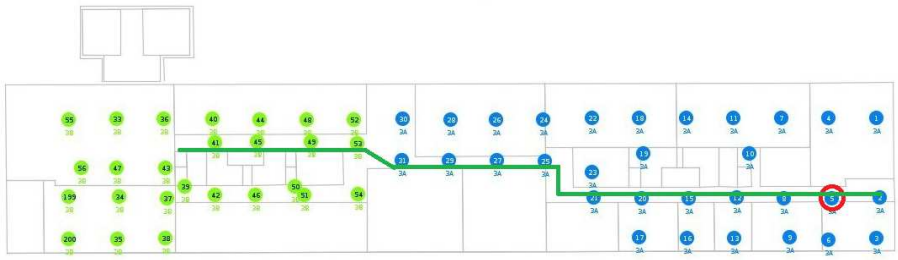

**Figure 2.1:** The w-ilab.t testbed, 3th floor

802.15.4 standard. In particular, we experimentally evaluate a wireless cooperative network, where a mobile node deployed on the human body serves as a hop, relaying data between the fixed nodes of the sensor network.

The chapter is organized as follows: Section 2.2 provides a complete description of the measurement setup, whereas Section 2.3 discusses the measurement results.

## 2.2 Measurement setup

### 2.2.1 w-iLab.t testbed setup

To assess the potential in terms of transmit power reduction when deploying textile patch antennas, instead of simply using small printed PCB monopole antennas for off-body communication, we integrated different types of textile antennas into a professional fire fighter jacket and connected them to the RM090 transceiver modules. We then compare link quality obtained when using these wearable antennas connected as external antenna to the transceiver with the link quality provided by the internal transceiver antenna. Therefore, a fire fighter equipped with the wireless modules walks at normal walking speed along a fixed path, shown in green (walked from right to left) on Fig. 2.1, in the w-iLab.t testbed [6] indoor office environment. The testbed is deployed in an office building of 18 x 90 m and spreads out over three floors. It consists of 200 node locations at fixed locations at the iMinds office premises, including meeting rooms, classrooms, offices and corridors. For this setup, only the nodes on the third floor are used, as shown in Fig. 2.1.

While the fire fighter is walking along the fixed path, in the first time slot of the frame, one fixed node (marked by the red circle Fig. 2.1) broadcasts to all fixed nodes as well as to the two RM090 mobile nodes. The two latter nodes are mounted together with their antennas in the shoulder sections of a professional fire fighter jacket, as shown in Fig. 2.2. In the two subsequent time slots of the frame, the two mobile nodes modify the packet received at time slot 1 by inserting their own specific node ID and RSSI-value into the packet, while maintaining the packet length. The two mobile

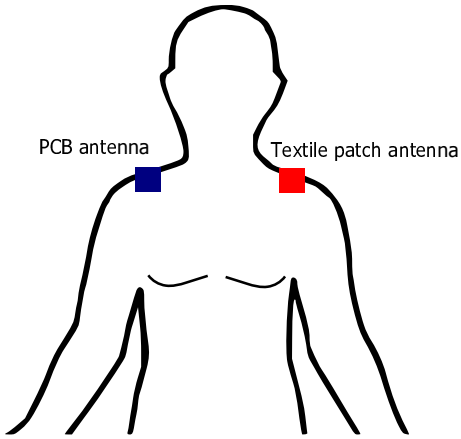


**Figure 2.2:** Mobile node setup on the fire fighter jacket

**Table 2.1:** Textile patch antenna parameters

| | | |
|---|---|---|
| **Antenna dimensions [mm]** | W | 44.46 |
| | Ls | 14.88 |
| | Ws | 1 |
| | Fx | 5.7 |
| | Fy | 11.4 |
| | Substrate Height h | 3.94 |
| **Substrate parameters** | Permittivity $\mu$r | 1.53 |
| | tan $\delta$ | 0.0012 |

nodes alternately broadcast their adapted packets to all fixed nodes in the w-iLab.t testbed. Both mobile nodes apply the same transmit power.

### 2.2.2 Textile patch antenna

By means of the experiment described above, textile antennas exhibiting different kinds of polarization are studied. One of these textile antennas is a dual polarized textile patch antenna [7], as shown in Fig. 2.3. The two ports of this antenna transmit and receive two signals along orthogonal linear polarizations. The antenna is implemented on a flexible protective foam substrate commonly found in protective garments for rescue workers. The foam protects vulnerable body parts such as elbows, shoulders and knees. The flexible closed-cell foam is fire-resistant, water-repellent, and regains its original form after deformation. The patch and ground plane were realized in the low-cost e-textiles FlecTron and ShieldIt, respectively. The rectangular slot in the antenna patch ensures impedance matching and provides the bandwidth required to cover the 2.45 GHz ISM band.

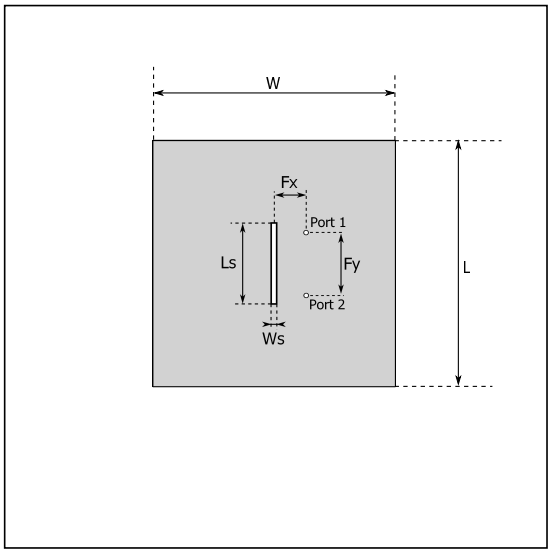


**Figure 2.3:** Dual polarized patch antenna

In the experiments we also consider circularly polarized textile patch antennas implemented on an Aramid substrate. These textile antennas were developed within the FP6 Proetex Integrated Project [8, 9].

## 2.3 Measurement results

Table 2.2 presents the total packet loss on each of the $51$ receive nodes, when the fire fighter walks along the fixed path shown in Fig. 2.1. In this measurement, node $5$, indicated by the red circle in Fig. 2.1, is the fixed transmitter node. The first row shows the packet loss of the complete dual-hop link (transmit node-mobile node-receive node), where the packets are forwarded by the mobile node with a wearable circularly polarized textile antenna. The second row of the table shows the total packet loss from the transmit node $5$ to all receive nodes, along the dual-hop link (transmit node-mobile node-receive node), where packets are forwarded by the mobile node with the small printed PCB antenna. The last row shows the packet loss for the direct link from the transmit node to the receive nodes, without forwarding the packets by a mobile node on the fire fighter jacket. The small distance between some of the fixed receive nodes in the testbed and the fixed transmitter node $5$, explains the low values of the packet loss for these fixed nodes.

Table 2.2 demonstrates that relaying data by means of the mobile node with the textile patch antenna reduces the total packet loss observed at the majority of the receive nodes, compared to the rigid PCB antenna. This result is consistent with

**Table 2.2:** Packet loss measurement 1

| **Node:** | **1** | **4** | **5** | **6** | **7** |
|---|---|---|---|---|---|
| **Patch** | 20.27% | 20.27% | 16.28% | 29.24% | 16.94% |
| **PCB** | 25.91% | 24.92% | 24.92% | 34.88% | 21.59% |
| **TX** | 0.66% | 20.60% | | 0.33% | 13.95% |
| **8** | **9** | **10** | **11** | **12** | **13** |
| 17.28% | 23.92% | 26.58% | 18.60% | 17.61% | 23.59% |
| 25.25% | 29.90% | 36.54% | 23.26% | 24.58% | 29.24% |
| 1.33% | 1.33% | 15.95% | 3.65% | 1.99% | 0.33% |
| **14** | **15** | **16** | **17** | **19** | **20** |
| 17.94% | 17.94% | 17.61% | 17.28% | 21.93% | 15.61% |
| 21.59% | 21.59% | 26.58% | 22.59% | 28.24% | 21.93% |
| 0.33% | 0.33% | 0.33% | 1.33% | 0.33% | 0.33% |
| **21** | **22** | **23** | **25** | **26** | **27** |
| 15.61% | 18.60% | 15.28% | 19.27% | 20.60% | 16.61% |
| 21.26% | 19.60% | 20.60% | 21.26% | 20.60% | 22.26% |
| 10.30% | 0.66% | 1.33% | 1.66% | 12.29% | 0.33% |
| **28** | **29** | **30** | **31** | **33** | **34** |
| 21.93% | 22.59% | 25.58% | 23.26% | 58.47% | 40.86% |
| 22.92% | 24.92% | 24.92% | 24.58% | 48.17% | 38.87% |
| 2.66% | 9.97% | 13.29% | 10.63% | 98.67% | 25.25% |
| **35** | **36** | **37** | **39** | **40** | **41** |
| 49.17% | 51.50% | 35.22% | 58.14% | 45.18% | 37.87% |
| 40.20% | 42.19% | 31.56% | 46.51% | 39.53% | 37.87% |
| 54.15% | 99.67% | 22.59% | 28.24% | 54.82% | 46.84% |
| **43** | **44** | **45** | **46** | **47** | **48** |
| 57.81% | 50.17% | 35.22% | 28.57% | 62.13% | 35.55% |
| 45.85% | 42.52% | 34.55% | 27.24% | 46.84% | 36.88% |
| 87.04% | 95.68% | 57.48% | 23.92% | 100.0% | 63.12% |
| **49** | **50** | **51** | **52** | **53** | **54** |
| 34.22% | 47.84% | 27.91% | 32.89% | 26.25% | 23.26% |
| 37.21% | 36.88% | 30.56% | 35.22% | 27.24% | 37.87% |
| 51.50% | 25.58% | 7.97% | 19.27% | 30.56% | 29.24% |
| **55** | **56** | **199** | **200** | | |
| 59.14% | 59.47% | 32.89% | 46.84% | | |
| 46.84% | 46.18% | 30.90% | 37.21% | | |
| 55.48% | 100.0% | 17.28% | 62.79% | | |

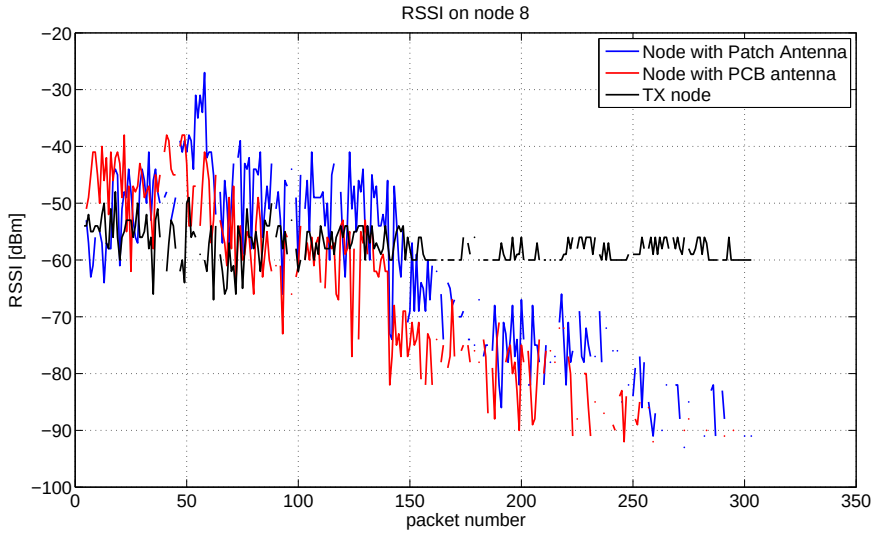


**Figure 2.4:** RSSI levels at fixed node 8

Fig. 2.4 - 2.4, showing the RSSI levels at fixed nodes 8 and 9. For most of the packets, the mobile node with the textile patch antenna provides a larger RSSI value compared to the mobile node with the printed PCB antenna.

The received power on the mobile nodes was also recorded. The node equipped with the textile patch antenna exhibits significantly larger RSSI levels than the node with the printed PCB antenna, as shown in Fig. 2.6.

The same results are obtained when using the *dual polarized textile patch antenna*. During the experiment with this antenna, one of the two ports is terminated with a load impedance, to ensure impedance matching over the required bandwidth at the port connected to the transceiver node.

Although the straightforward experimental approach of attaching textile antennas to the RM090 transceiver modules external antenna input by means of a small flexible coaxial cable provides some indication about the potential benefits of textile antennas over integrated PCB antennas, this measurement setup does not provide an entirely fair comparison between both types of antennas, as the integrated PCB antennas is attached directly to the transceiver's RF port, thereby avoiding the cable losses encountered by the external textile patch antenna. Therefore, the straightforward measurement protocol was refined to ensure that both antennas encounter the same amount of losses in the RF patch between the antenna and transceiver. This new measurement protocols corrects for the additional insertion loss introduced by the coaxial cable, which was measured to be 1.57 dB. In addition, it also includes the extra losses in the lossy RF signal path on the transceiver PCB, connecting the RF pin of the transceiver

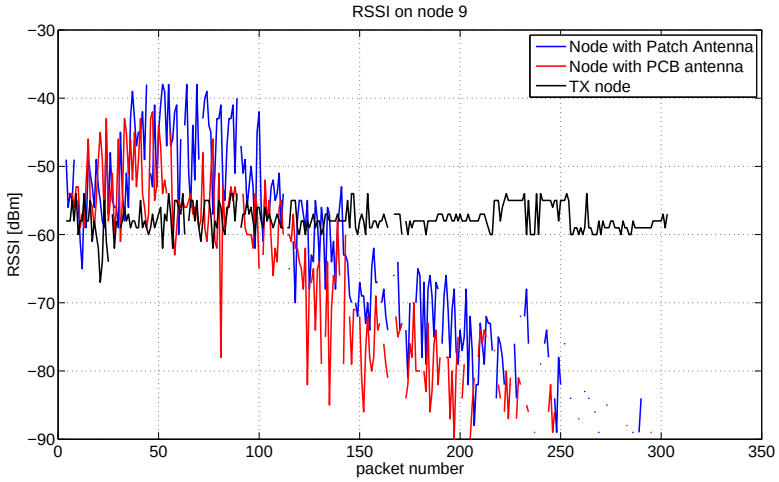


**Figure 2.5:** RSSI levels at fixed node 9

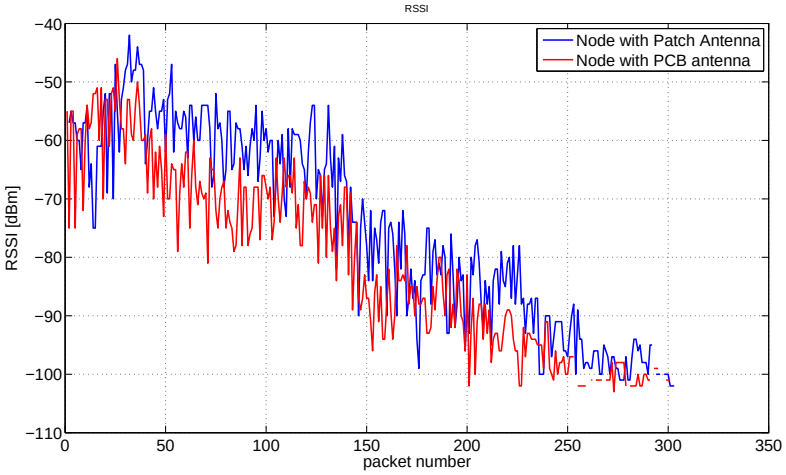


**Figure 2.6:** RSSI levels at mobile nodes

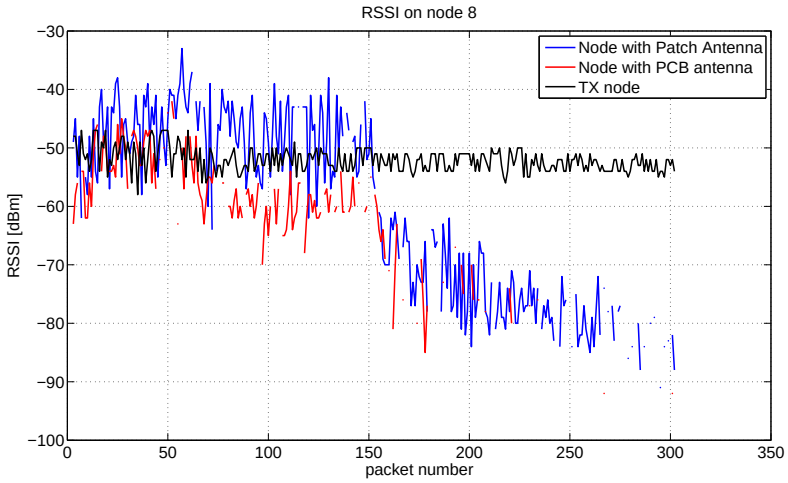


**Figure 2.7:** RSSI levels at fixed node 8

to the connection point for the external antenna.

To calibrate out these losses, a printed PCB antenna, identical to the one found on the RM090 wireless sensor node, is isolated on a separate printed circuit board, having the same size and shape of the mobile node, including the same ground plane size. This printed PCB antenna is then connected to the external antenna output of the wireless sensor node by means of the same type of coaxial cable as used for the textile patch antenna.

Applying this new measurement protocol, Table 2.3 represents the total packet loss on each of the 51 fixed receive nodes, when the fire fighter walks along the same fixed path as the previous measurement setup. Node 5 again serves as the fixed transmitter node. The figures of merit shown in Table 2.3 are the same as in the previous measurement (Table 2.2).

The results in Table 2.3 demonstrate clearly an additional improvement in terms of total packet loss for the textile patch antenna, compared to the PCB antenna. Now, the total packet loss for the link where the node with the textile patch antenna acts as relay is less than the packet loss along the link where the node with the PCB antenna acts as relay, for almost all fixed nodes. This result is consistent with Fig. 2.7 - 2.8, showing the RSSI levels at fixed nodes 8 and 9.

The power received by the mobile nodes is shown in Fig. 2.9. In this graph, it is clearly visible that the received power is larger for the node with the textile patch antenna. Even when the node with the printed PCB antenna is unable to decode the packets, the wireless node with the textile patch antenna still receives the packets at a reasonable RSSI level.

**Table 2.3:** Packet loss measurement 2

| **Node:** | **1** | **4** | **5** | **6** | **7** |
|---|---|---|---|---|---|
| **Patch** | 40.20% | 17.94% | 28.57% | 23.92% | 32.56% |
| **PCB** | 47.51% | 47.84% | 43.19% | 48.84% | 47.84% |
| **TX** | 19.60% | 0.33% | | 0.33% | 0.66% |
| **8** | **9** | **10** | **11** | **12** | **13** |
| 13.29% | 19.27% | 37.87% | 60.47% | 12.62% | 53.49% |
| 48.84% | 44.85% | 56.15% | 45.18% | 43.85% | 46.18% |
| 0.33% | 3.99% | 0.66% | 2.33% | 0.33% | 12.62% |
| **14** | **15** | **16** | **17** | **19** | **20** |
| 17.94% | 28.90% | 14.29% | 13.95% | 24.25% | 14.29% |
| 44.85% | 44.52% | 44.52% | 44.85% | 51.16% | 42.86% |
| 3.65% | 1.00% | 0.66% | 1.33% | 29.90% | 0.33% |
| **21** | **22** | **23** | **25** | **26** | **27** |
| 53.82% | 49.83% | 13.62% | 15.95% | 19.27% | 13.95% |
| 42.86% | 47.18% | 42.19% | 43.19% | 47.18% | 42.52% |
| 0.33% | 3.32% | 6.98% | 0.33% | 11.96% | 2.99% |
| **28** | **29** | **30** | **31** | **33** | **34** |
| 17.94% | 16.94% | 25.58% | 22.26% | 56.15% | 23.92% |
| 44.52% | 44.19% | 48.17% | 45.51% | 78.07% | 47.51% |
| 12.29% | 1.00% | 11.96% | 11.30% | 80.07% | 13.62% |
| **35** | **36** | **37** | **39** | **40** | **41** |
| 43.52% | 57.14% | 23.26% | 58.47% | 47.51% | 37.21% |
| 58.14% | 71.76% | 48.50% | 52.49% | 71.76% | 57.14% |
| 41.53% | 46.18% | 9.97% | 46.51% | 63.12% | 49.50% |
| **43** | **44** | **45** | **46** | **47** | **48** |
| 46.51% | 44.19% | 32.89% | 19.27% | 57.48% | 27.24% |
| 56.81% | 62.46% | 58.14% | 45.51% | 60.47% | 51.50% |
| 26.25% | 46.51% | 70.76% | 1.66% | 95.68% | 64.45% |
| **49** | **50** | **51** | **52** | **53** | **54** |
| 27.24% | 61.46% | 16.94% | 21.59% | 21.26% | 18.27% |
| 54.15% | 57.14% | 45.85% | 56.15% | 48.84% | 46.51% |
| 14.62% | 11.63% | 2.33% | 22.92% | 16.61% | 7.31% |
| **55** | **56** | **199** | **200** | | |
| 57.48% | 59.80% | 30.56% | 40.53% | | |
| 75.75% | 69.10% | 54.49% | 58.47% | | |
| 100% | 88,04% | 12.96% | 16.94% | | |

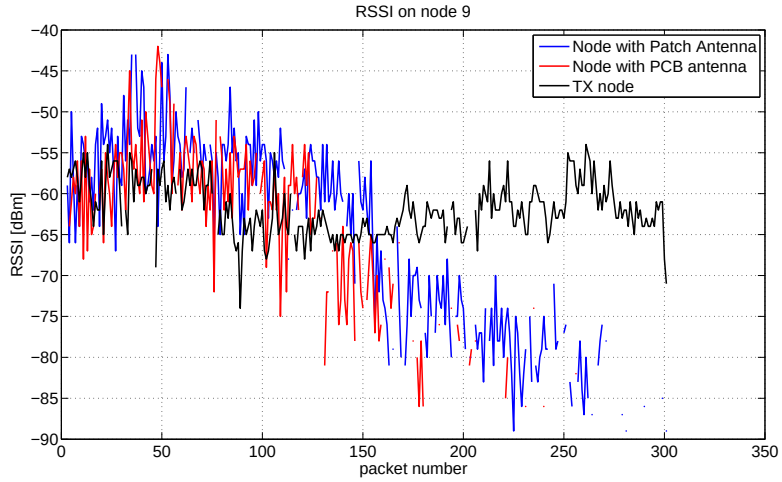


**Figure 2.8:** RSSI levels at fixed node 9

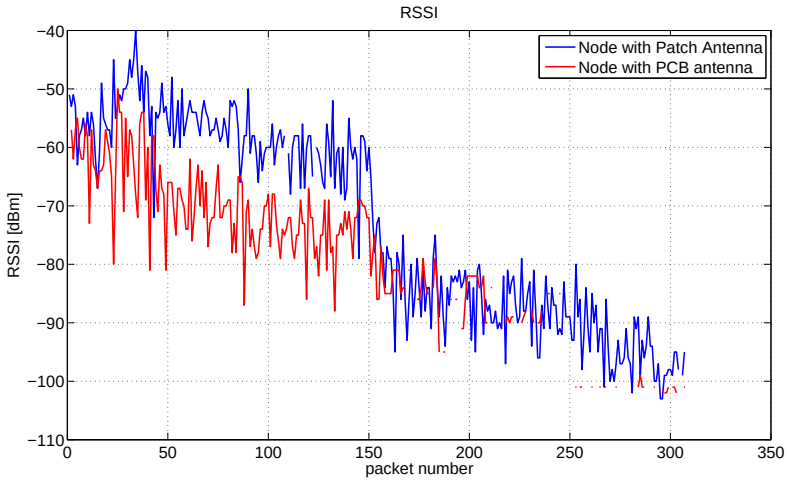


**Figure 2.9:** RSSI levels at mobile nodes

**Table 2.4:** Packet loss overview

| | Circ. Pol. Patch antenna | | Dual Pol. Patch antenna | |
|---|---|---|---|---|
| | **Avg. loss Patch** | **Avg. loss PCB** | **Avg. loss Patch** | **Avg. loss PCB** |
| **Meas. 1** | 30.8%<br>26.2% | 31.2%<br>28.4% | 27.4%<br>27.2% | 31.4%<br>31.4% |
| **Meas. 2** | 31.0%<br>29.1% | 52.0%<br>33.6% | 24.5%<br>34.9% | 31.8%<br>51.0% |

**Table 2.5:** Packet loss improvement

| | Circ. Pol. Patch antenna | |
|---|---|---|
| | **Circ. Pol. Patch antenna** | **Dual Pol. Patch antenna** |
| **Meas. 1** | 31 (60%)<br>36 (71%) | 27 (53%)<br>40 (78%) |
| **Meas. 2** | 45 (88%)<br>41 (80%) | 48 (94%)<br>44 (86%) |

Next, the new measurement protocol was repeated with all other textile patch antennas, leading to similar results. A small overview of the packet loss obtained during these measurements is given in Table 2.4 and Table 2.5.

## 2.4 Conclusion

A way to reduce the power required for off-body wireless communication by making use of more efficient antennas is experimentally validated. By replacing the integrated PCB antenna by a textile patch antenna, the quality of the wireless link may be improved both in receive and transmit mode. This may be exploited to reduce transmit power at the mobile nodes while guaranteeing the same amount packet loss. To further reduce the power consumption, we need to improve the transceiver design such that cable and interconnect losses are avoided in the RF circuitry. This may be implemented by directly integrating the transceiver onto the textile patch antenna, following the design methodology outlined in [10]. A second path for future research consists in integrating two or more textile patch antennas into the professional fire fighter jacket and combining their signals by means of a power combiner. An optimal position for two antennas could be on opposite sides of the fire fighter jacket (for example, one antenna integrated in the back-section and one in the front-section of the jacket). This setup may be further extended to one or more dual polarized textile patch antennas, where each of the antenna ports is connected to two wireless nodes. This allows two wireless nodes to transmit and receive along orthogonal linear polarizations on a single antenna.

# Bibliography


[1] iMinds, "Sensornode: Rm090", April 2013.

[2] Patrick Van Torre, Luigi Vallozzi, Hendrik Rogier, and Jo Verhaevert, "Diversity textile antenna systems for firefighters", in *Proceedings of the fourth European Conference on Antennas and Propagation*. 2010, p. 5, IEEE.

[3] Sang-Hun Han and Sang Kyu Park, "Performance analysis of wireless body area network in indoor off-body communication", *Consumer Electronics, IEEE Transactions on*, vol. 57, no. 2, pp. 335–338, May 2011.

[4] L. Vallozzi, P. Van Torre, C. Hertleer, H. Rogier, M. Moeneclaey, and J. Verhaevert, "Wireless communication for firefighters using dual-polarized textile antennas integrated in their garment", *Antennas and Propagation, IEEE Transactions on*, vol. 58, no. 4, pp. 1357–1368, 2010.

[5] P. Van Torre, L. Vallozzi, C. Hertleer, H. Rogier, M. Moeneclaey, and J. Verhaevert, "Indoor off-body wireless mimo communication with dual polarized textile antennas", *Antennas and Propagation, IEEE Transactions on*, vol. 59, no. 2, pp. 631–642, Feb 2011.

[6] iMinds, "w-ilab.t", April 2013.

[7] L. Vallozzi, H. Rogier, and C. Hertleer, "Dual polarized textile patch antenna for integration into protective garments", *Antennas and Wireless Propagation Letters, IEEE*, vol. 7, pp. 440–443, 2008.

[8] Carla Hertleer, Lieva Van Langenhove, Hendrik Rogier, and Luigi Vallozzi, "A textile antenna for fire fighter garments", in *AUTEX 2007 Conference (Association of Universities for Textiles): From Emerging Innovations to Global Business*, 2007.

[9] ProeTEX, "Advanced e-textiles for firefighters and civilian victims", April 2013.

[10] F. Declercq and H. Rogier, "Active integrated wearable textile antenna with optimized noise characteristics", *Antennas and Propagation, IEEE Transactions on*, vol. 58, no. 9, pp. 3050–3054, Sept 2010.

CHAPTER 3

# Flexible Dual-Diversity Wearable Wireless Node Integrated on a Dual-Polarized Textile Patch Antenna

**Peter Vanveerdeghem, Patrick Van Torre, Christiaan Stevens, Jos Knockaert, and Hendrik Rogier**

Based on the article published in *IET Science, Measurement & Technology*, vol. 8, no. 6, pp. 452-458, 2014.

★★★

*A new textile wearable wireless node, for operation in the 2.45GHz industrial, scientific and medical band, is proposed. It consists of a dual-polarized textile patch antenna with integrated microcontroller, sensor, memory, and transceiver with receive diversity. Integrated into a garment, the flexible unit may serve for fall detection, as well as for patient or rescue-worker monitoring. Fragile and lossy interconnections are eliminated. They are replaced by very short radio-frequency signal paths in the antenna feed plane, reducing electromagnetic compatibility and signal integrity problems. The compact and flexible module combines sensing and wireless channel monitoring functionality with reliable and energy-efficient off-body wireless communication capability, by fully exploiting dual polarization diversity. By integrating a battery, a fully autonomous and flexible system is obtained. This novel textile wireless node was validated, both in flat and bent state, in the anechoic chamber, assessing the characteristics of the integrated system in free-space conditions. Moreover, its performance was verified in various real-world conditions, integrated into a firefighter garment, and used as an autonomous body-centric measurement device.*

## 3.1 Introduction

Smart Fabric Interactive Textile (SFIT) systems add life-saving functionality to professional garments, as they monitor rescue workers during interventions [1], sense their environment and movements during an operation, and also establish critical communication links with other firefighters and a command post. However, further improvements, in terms of efficiency, autonomy, reliability and safety, are still needed to guarantee their market penetration and to develop the next generation of Smart Personal Protective Systems [2]. Indeed, conventional wearable body-centric wireless sensing and communication systems, for real-time tracking and monitoring of persons, rely on sensor, processor, transceiver and antenna hardware components that are often very complicated, non-flexible or bulky [3]. This makes these systems generally costly and difficult to unobtrusively integrate into garments for firefighters. Also for other applications, such as in patient and elderly monitoring [4, 5], comfort and washability may still be improved.

The indoor environments, in which these systems typically operate, suffer from severe multipath radio propagation, resulting in decreased data throughput caused by fading. In addition, body shadowing plays an important role in wearable communication systems [6]. Reducing the effects of multipath fading is achieved on a single node by exploiting antenna polarization diversity [7]. The cooperation of multiple nodes provides higher-order combined polarization, spatial and pattern diversity, allowing to effectively counter fading as well as body shadowing [8]. Reliable body-centric communication requires accurate knowledge of the wireless channel characteristics

in proximity of the human body [9]. This results in complex transceiver hardware that was until recently only implemented on *rigid* planar circuit boards and, therefore, difficult to comfortably integrate into SFIT systems.

In this chapter, a novel, fully-flexible, low-cost, compact, and autonomous wearable $2.45$ GHz wireless sensor node is introduced, with all its functionality fully integrated onto a dual-polarized textile patch antenna [7, 10]. The electronic circuitry, implemented on a compact, very thin, and flexible polyimide substrate, includes a microcontroller, an ADF7242 diversity transceiver, a non-volatile memory, battery and power management unit, combined with sensors. All RF interconnects are integrated onto the feed plane of the textile antenna, fully eliminating coaxial cables. Such a *textile* wireless node, realized as one compact *flexible* unit, enabling true non-obtrusive and comfortable integration into garments, was not documented in literature before. The efficient textile patch antenna, which serves as a platform for the active electronics, provides high antenna gain, reduces the required transmit power [11] and contributes to an energy-efficient wireless system. The textile ground plane of the wearable antenna limits the interaction with the human body, providing a wireless platform with stable characteristics and very limited radiation exposure for the user. Embedded software on the microcontroller provides wireless ad-hoc network functionality, allowing the nodes to actively forward data packets, to cooperate, share data, and synchronize over the wireless links. These properties enable the nodes to operate in a wide range of practical applications, including patient, rescue-worker or law-enforcement officer monitoring networks. The compact, autonomous, and wearable wireless node may be applied as a key building block for the construction of a modular, low-power, body-worn system with receive diversity, by means of multiple cooperating nodes. The network topology of multiple wirelessly interconnected nodes, unobtrusively integrated in a single garment, allows us to add or remove nodes, depending on the required functionality. In addition, each node can be made washable by encapsulating the textile antenna together with the integrated electronics by a breathable Thermoplastic PolyUrethane coating (TPU) [12].

For research purposes, this autonomous unit can also be deployed as a channel measurement device, synchronously logging signal levels received on different autonomous nodes that are not interconnected by any wires. Conventional off-body channel measurements are generally performed with complex or expensive measurement devices [13–15], connected to body-worn external antennas by means of fragile coaxial cables, which hinder the test person to move freely. Truly wireless measurement nodes open new opportunities for more realistic multi-node body-centric measurement campaigns. Existing *rigid* wireless wearable nodes [3–5], used as a channel measurement device or as people-monitoring systems, are non-flexible and do not implement receive diversity.

In current literature, the number of wearable systems that integrate *flexible* electronic circuits with textile antennas is very limited. In [16], only a Low-Noise Ampli-

fier (LNA) is integrated, forming an active antenna that still requires a coaxial cable to be connected to transceiver units. Although in [17], the antenna and electronic system of the sensor node are integrated on the flexible substrate, the system only operates in Gaussian frequency-shift keying (GFSK) modulation without diversity.

The chapter is organized as follows. Section 3.2 provides a complete description of the wearable node. In section 3.3, the measurement results validating the performance of the system are presented, ending with the conclusions presented in section 3.4.

## 3.2 Wearable node design

### 3.2.1 Requirements/specifications

During rescue operations and hazardous interventions, reliable wireless communication is critical for the safe operation of firefighters. Therefore, a textile wireless node, specifically designed for comfortable integration into firefighter garments, must implement reliable and energy-efficient wireless communication. Hence, the performance of the antenna, with the system integrated onto the antenna feedplane, should not be significantly affected by the presence of the human body. The $2.45$ GHz license-exempt industrial, scientific and medical (ISM) band is selected to set up highly energy-efficient wireless links, via one of the many standards that operate in this band. Moreover, for wearable applications or for integration into a firefighter garment, the textile wireless node needs to be flexible and resistant against extreme conditions, such as high temperatures, moisture, and bending. Besides the technical specifications, the wireless node must be non-obtrusive for the user, as well as light-weight, low-cost, and energy efficient. To be useful in emergency situations, the intelligent textile system is required to be user friendly, by allowing fast and easy activation and deployment. Finally, easy replacement of certain textile nodes in the system is preferred, without the need of making wired connections between separate sub-systems.

Besides being suitable for wireless off-body communication, the wearable node should provide functionality that enables the wearable system to operate as an autonomous channel-measurement device, monitoring parameters such as Bit-Error-Rate (BER) and signal strength. For the node to be useful as a measurement device for body-centric channel characterization, sufficient memory is required to store large sets of data, obtained during the measurements. Depending on the selected modulation scheme and data rate, the node should be able to store at least a few minutes of data obtained by channel measurements. The sample period for these measurements needs to be shorter than $21.2$ ms [18], the coherence time of the $2.45$ GHz indoor channel for a walking person. Therefore, the sampling frequency is at least $50$ Hz on each polarization of the antenna system. Assuming $2$ bytes for each data sample, providing signal strength and packet-number information, $4$ MB of memory can store more than $5$ hours of continuous measurements.

### 3.2.2 Topology/system overview

The key components of the newly designed wearable node are presented in the block diagram shown in Fig. 3.1. A top view of the circuit is given in Fig. 3.2. The selection of these components is motivated as follows.

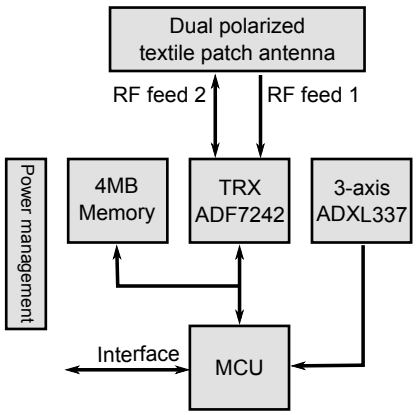


**Figure 3.1:** Simplified block diagram of the system.

The dual-polarized textile antenna, described in detail in [7], is fully integrable into protective garments and was designed to operate in the $2.4 - 2.4835$ GHz ISM band, with a high (being better than 10 dB) return loss, as well as excellent isolation between the antenna ports. The textile antenna, which receives two orthogonal linearly-polarized signals, is an excellent solution to reduce the undesired effect of multipath fading in wireless communications, by exploiting polarization diversity. The human body behind the ground plane of the antenna only slightly affects the performance of the antenna [7].

The heart of the transceiver system is formed by the ADF7242 integrated circuit from Analog Devices. The transceiver supports the IEEE 802.15.4-2006 $2.4$ GHz PHY requirements, as well as proprietary Gaussian frequency-shift keying / frequency-shift keying / Gaussian minimum-shift keying / minimum-shift keying (GFSK / FSK / GMSK / MSK) modulation schemes. Depending on the desired application and/or data rate, one of these transmission schemes will be selected. The IEEE 802.15.4-2006 standard provides reliable data packet communication for low data-rate, wireless sensor networks. Moreover, channel measurements can also be performed with the proprietary modulation schemes, at data rates up to $2$ Mbps, by measuring Bit-Error-Rate and Signal strength. The device features a dual-port radio-frequency (RF) interface, directly connected to the textile antenna's orthogonally-polarized feeds that generate quasi-linearly polarized signals along the $\pm 45^{\circ}$ diagonals of the patch [7]. This architecture enables second-order receive polarization diversity by means of selection combining, improving the reliability of the wireless communication. A compact low-

power C8051F921 microcontroller (MCU), by Silicon Laboratories, is used to process the received data and to characterize the wireless links. After processing, the signal parameters are stored in a $4$ MB flash memory, integrated into the system, providing sufficient non-volatile storage space for several hours of channel measurement data. The actions of the fire-fighter are monitored by an on-board 3-axis accelerometer. A serial port provides system access to retrieve the measurement data, or real-time data transmission to the PC at the base-station node.

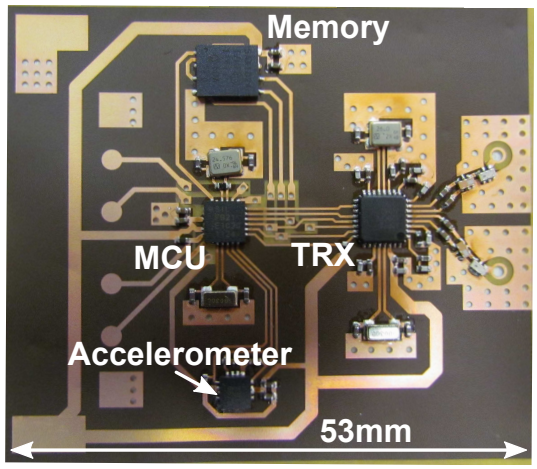


**Figure 3.2:** Top view of the flexible wireless node circuit.

The energy-efficient, wearable node is powered by a small battery ($3.6$ V, $660$ mAh), ensuring the autonomy of the textile wireless node, when integrated into the garment during the course of a full rescue operation without recharging. With a power consumption lower than 90mW, the system can be used continuously for many hours.

### 3.2.3 Material/fabrication

The dual-polarized textile patch antenna [7], which serves as the node's platform, is constructed using FlecTron, a low-cost, conductive, electro-textile material with a thickness less than $0.25$ mm and surface resistivity less than $0.1$ $\Omega$/sq. This material implements the antenna patch and ground plane. Flexible, closed-cell, expanded-rubber protective foam (density $187.3$ kg/m$^3$, permittivity $\epsilon_r$=$1.53$ and tan $\delta$=$0.0012$), commonly used in protective garments for rescue workers, is applied as substrate material. The flexible foam helps to protect the electronic circuitry against external factors, such as high temperatures and humidity.

The integrated electronic system is implemented in a $9$ $\mu$m copper layer on a copper-on-polyimide film, UPISEL$^{\textregistered}$-N by UBE, of $25$ $\mu$m thickness. The production

of the flexible substrate is performed by making use of an in-house photolithographic process [19] and by soldering the various components by means of reflow.

### 3.2.4 Flexible circuit and antenna design

For maximal user convenience, the flexible transceiver circuit is integrated with the textile antenna. The circuit is etched on a compact and very flexible polyimide substrate. To keep production costs low, this circuit topology is designed such that vias are avoided, as much as possible, and that only one side is used for component placement. Thereby, the bottom layer of the circuit substrate consists almost entirely of a copper ground plane, which is connected to the back side of the antenna patch, using a conductive adhesive.

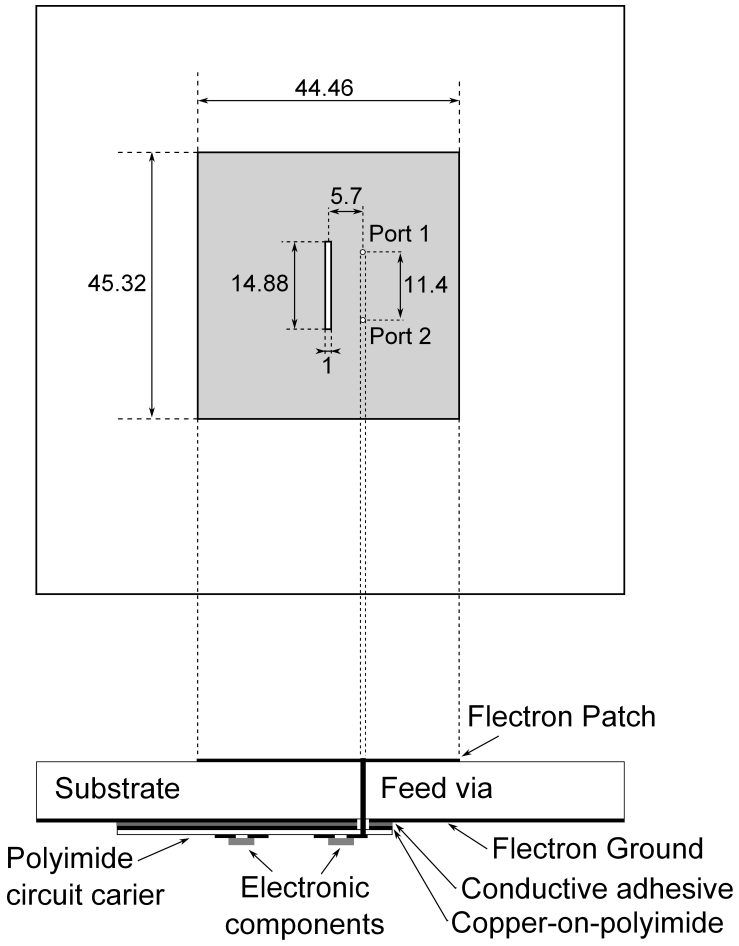


**Figure 3.3:** Antenna cross section (dimensions in mm).

The antenna is shown in Fig. 3.3, together with a cross section of the electronic system, integrated on the feed plane of the textile antenna. A dual-polarized antenna topology, with coaxial feeds implemented by means of vias, is adopted, since it only requires very short direct via connections between antenna patch and the transceiver's RF ports. This results in the shortest RF paths, compared to other potential feeding techniques, such as aperture-coupled feeds. Moreover, the apertures in an aperture-coupled feed topology may lead to significant radiation towards the human body. Conjugate matching is applied to connect both RF output ports of the ADF7242 transceiver to Johansson Technology 2450BM14E0007 baluns, specifically designed for this chip. Each balun is followed by a $400$ MHz wide bandpass-filter (Murata LFL182G50TC1B905), to protect the input from out-of-band signals. The outputs of the bandpass-filters are directly connected to the antenna feeds, ensuring the shortest possible length of the RF paths and reducing losses. The maximum output power of the transceiver, specified by Analog Devices, is $+4.8$ dBm. Taking into account the antenna gain and the insertion loss of the filter and balun, the maximum output power of the system is $8.9$ dBm effective isotopic radiated power (EIRP), which complies with the standard ($20$ dBm, ETSI EN 300 328 for wide band transmissions, such as in IEEE 802.15.4-2006 mode). To retain the required flexibility of the circuit, small integrated-circuit components are chosen. They are separated by a sufficiently large distance, to allow for a small bending radius. The largest rigid chip of the circuit has a footprint of $5 \times 6$ mm, thereby retaining a very flexible unit. To confirm its desired flexibility, the node is bent along a plastic tube with a curvature radius of $7.5$ cm, as shown on Fig. 3.4. This construction also allows the designer to perform reproducible measurements to evaluate the performance of the wireless nodes in bent condition.

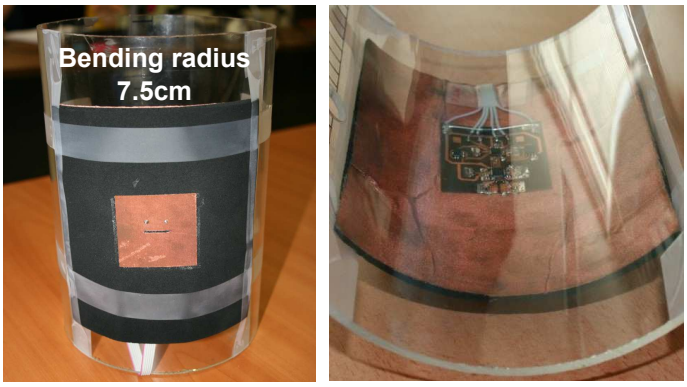


**Figure 3.4:** The integrated system, bent around a plastic tube with a radius of $7.5$ cm.

## 3.3 Measurements

The indoor environment, in which the body-worn system will be deployed, exhibits multipath signal propagation. A signal transmitted along a single polarization then results in multiple reflected signals that impinge onto the receive antenna at varying polarization angles. Reception of these signals, by an antenna system with dual orthogonal polarizations, yields significant diversity gain, when combining the outputs from the two decorrelated antenna feeds. Hence, the capability of the system to receive orthogonally polarized signals in a free-space setup, leading to sufficiently decorrelated signals in a multipath environment, is an important figure of merit for the diversity performance. Therefore, the operation of the newly designed wearable node in free-space conditions is validated, focusing on the discrimination of orthogonally polarized received signals, by measuring the Cross-Polar Discrimination (XPD).

Second, the polarization of signals, transmitted or received by a wearable antenna, is sensitive to bending of the antenna and to proximity of the human body. These effects render the polarization more elliptical, instead of linear [7]. For a multipath environment, this results in higher received signal correlation and reduced diversity gain. Hence, to carefully assess the performance under different conditions, the orthogonality of the two received signals in a free-space propagation environment is tested in planar, on-body, and bent conditions.

Third, measurements are performed in an indoor scenario, with a mobile user wearing the node integrated in his firefighter jacket. These experiments evaluate the node's diversity gain realized by polarization diversity using Selection Combining (SC) or Maximum Ratio Combining (MRC). Our previous measurements [8, 10] of the body-centric channel relied on a bulky wireless testbed, placed on a cart and connected by means of coaxial cables to the antennas worn by the mobile user. During the measurement campaign, the cart with the testbed was in close proximity of the mobile user, following his/her movements. Hence, cart, testbed, and coaxial cable connections may have an impact on the wireless channel. With the proposed system, body-centric channel characterization is performed in a more realistic way. Moreover, the channel measurements will be less time consuming and more accurate, thanks to the larger data throughput, being at least $100$ measurement points per second.

### 3.3.1 Free-space propagation: orthogonality of the antenna ports

To evaluate the orthogonality of the polarizations, the wearable node is first validated in the anechoic chamber. The measurements are performed for the stand-alone node, as well as for the node integrated into a firefighter jacket, worn by a person of size $1.85$ m and weight $80$ kg. A transmitter, connected to a Scientific Atlanta Model 12-1.7 Standard Gain Horn antenna, continuously broadcasts data packets, which are

received by the flexible node, at a distance of $4.436$ m from the transmitter. While the horn antenna is slowly rotating at a constant rotation speed of $2°$/s, as shown in Fig. 3.5, the received signal power of every packet on both polarizations is logged. The variation of the received power, as a function of the polarization angle, is shown in Fig. 3.6. The result illustrates the complementarity of both polarizations, for both the stand-alone antenna and the on-body setup, in anechoic propagation conditions.

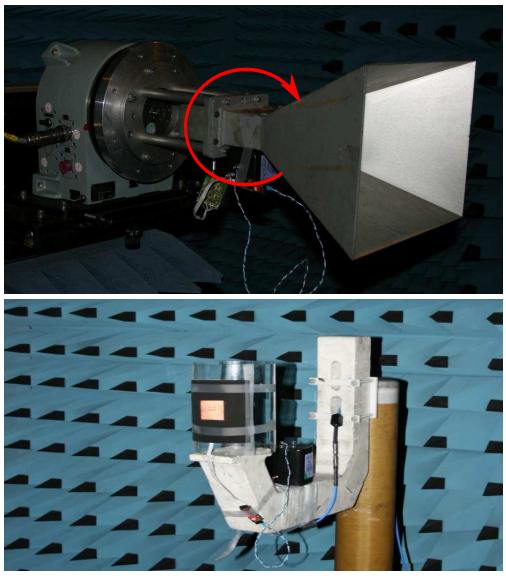

**Figure 3.5:** Measurement setup.

From this measurement, the XPD is calculated [20, 21], defined by

$$XPD_Y\,(dB) = 10\,log_{10}\left(\frac{|h_{YY}|^2}{|h_{XY}|^2}\right)$$

with $|h_{\bullet\bullet}|^2$ the squared channel amplitude factor for X=+$45°$, being the co-polar polarization, and Y=-$45°$, being the cross-polar polarization. The X and Y directions are tangential to the surface of the body torso, with the zero degrees reference corresponding to a vector pointing up towards the head. The average XPD of the integrated system equals $29.1$ dB for the stand-alone antenna and $27.1$ dB for the on-body measurement. This confirms that the system performance is not problematically degraded by the presence of the body and that sufficiently high RF isolation is maintained between the two polarizations of the dual-polarized textile patch antenna with both terminals connected to the transceiver. These are excellent values, illustrating the suitability of the patch antenna for polarization-diversity reception. Next, the measurement was repeated with the system bent, using the setup shown in Fig. 3.4. A bending radius

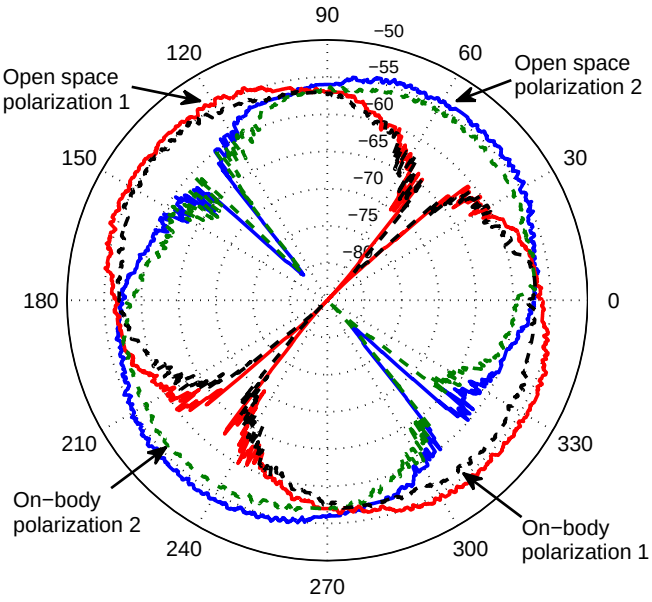


**Figure 3.6:** Received signals power [dBm] on both feeds, as a function of polarization angle of the TX antenna, for the patch antenna mounted as in Fig. 3.3, front view, for a stand-alone node and for the node integrated into a firefighter jacket, worn by a test person.

of 7.5 cm is realistic when deploying the textile node inside the sleeve of a garment, such that is positioned on the firefighter's arm. The variation of the received power, as a function of the radiation angle, is shown in Fig. 3.7. The curves now also illustrate the complementarity of both polarizations, when the wearable node is bent. Although bending slightly affects antenna impedance, port isolation, and resonance frequency [7], the average XPD is still 12.7 dB. This guarantees satisfactory system performance in bent conditions as well.

### 3.3.2 Multipath environment: channel measurement

To evaluate the node's performance in a multipath environment, a fire-fighter, walking in an indoor environment with the system integrated into his fire-fighter jacket, is considered. Fig. 3.8 shows part of the floor plan of the building with brick walls and reinforced concrete floors at Ghent University, where the measurements were carried out. The same transmitter as in the previous measurement is located in an office at position TX1 in Fig. 3.8, while the test person, wearing the garment, walks along the path A-B at about 1 m/s in the neighboring offices and corridors. While data packets are continuously being transmitted, the autonomous flexible system constantly mon-

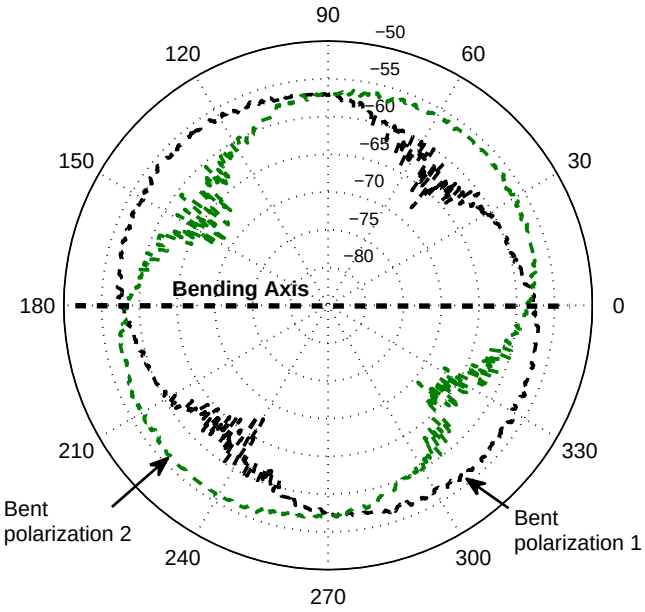


**Figure 3.7:** Received signals power [dBm] on both feeds as a function of polarization angle, for the bent patch antenna mounted as in Fig. 3.3, front view.

itors the signal strength on both polarizations. As the instantaneous time-varying received power varies partially independently at both ports, $2^{nd}$-order receive diversity, by means of SC, improves the performance of the wearable node, by selecting the polarization with the strongest signal for each received data packet, as shown in Fig. 3.9

### 3.3.3 Statistical analysis

The statistical distribution of the signal levels is determined, measured within region C of the floor plan, shown in Fig. 3.8, at a distance of 10m from the transmitter TX2. The analysis is performed on $32768$ recorded samples per polarization, at a sample rate of 50 samples/sec on each polarization.

The graph in Fig. 3.10 compares the Cumulative Distribution Function (CDF) curves obtained during the measurements with and without diversity to the theoretical Rayleigh fading CDF as well as to simulated characteristics for uncorrelated Rayleigh fading channels with SC and MRC.

Only the Non-Line-of-sight (NLoS) scenario was considered here, since this scenario is the most likely to occur in the rescue worker application under study. Moreover, similar conditions were also investigated in previous measurement campaigns, serving as a reference for the current results. NLoS propagation represents a worst-

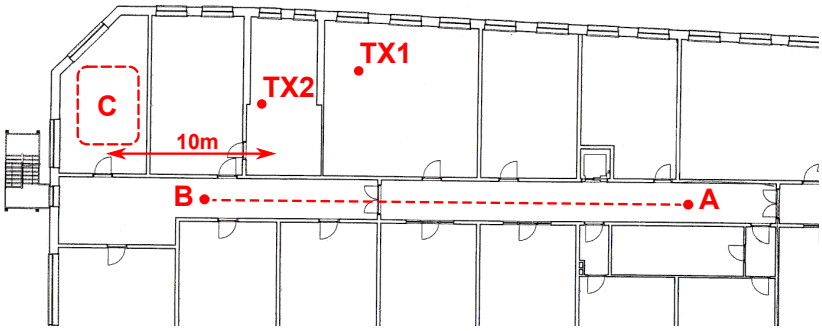


**Figure 3.8:** Floor plan of the indoor environment, in which the channel sounding experiment was performed.

case scenario, providing the most demanding conditions for the wireless off-body link.

The $10$ % outage probability of the dual polarized system with SC is then compared to a single-polarized system. These power levels define the $10^{\text{th}}$ percentile in the CDF, meaning that the power will be higher than these values $90$ % of the time. SC improves the $10$ % outage probability by $5.5$ dB, in comparison to a single polarization. Although MRC is not implemented in this transceiver, the MRC gain is calculated and drawn in Fig. 3.10. MRC increases the $10$ % outage probability by $7.5$ dB, compared to a single polarization. Considering the $1$ % outage probability, SC and MRC produce a gain of $9.5$ dB and $11.5$ dB, respectively, in comparison to a single polarization. The observed deviation from the Rayleigh characteristics below the $1$ % level is due to the limited number of recorded signals.

### 3.3.4 Power consumption

The power consumption is highly dependent on the operating mode of the node. In sleep mode, the total power consumption is less than $10$ $\mu$W. The measured power consumption for the wearable system, in full operation, equals $90$ mW ($27$ mA, $3.3$ V). Hence, even in continuous full operation, the system can be used during many hours, without recharging the battery. For the experiments, a low drop voltage regulator is mounted on top of the battery, causing an additional power dissipation of approximately 9mW. In addition, at the power input connector, an inversely polarized diode is placed for polarity protection.

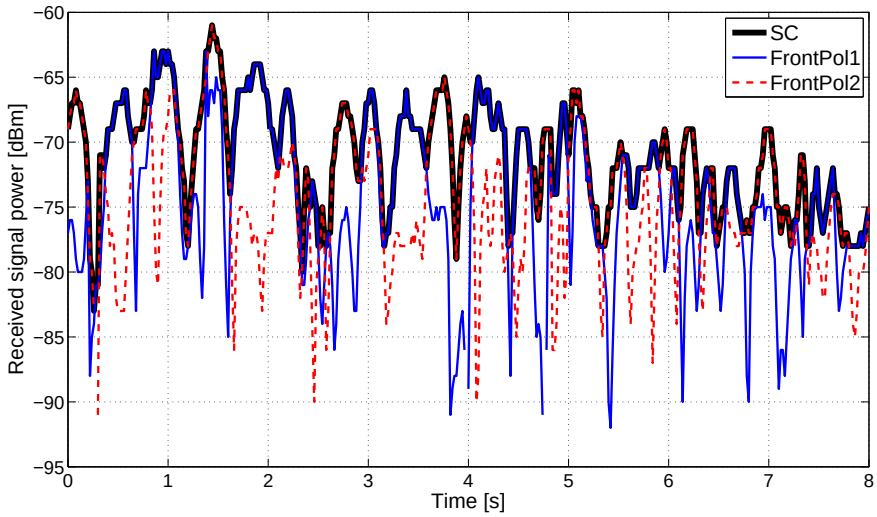


**Figure 3.9:** Signal power received along each polarization of the antenna, when integrated into a fire-fighter jacket.

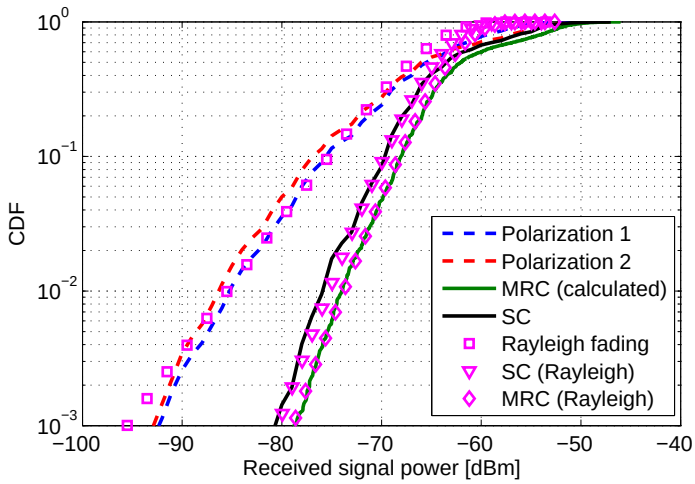


**Figure 3.10:** Cumulative Distribution Function (CDF), for the two single polarizations, compared to the CDF for Selection Combining, Maximum Ratio Combining and characteristics for uncorrelated Rayleigh fading channels.

## 3.4 Conclusions

The first autonomous textile wireless node, fully integrated onto a flexible dual-polarized textile patch antenna, was presented. This design is particularly suited to perform body-centric channel measurements with all the equipment integrated into clothing. The wearable node enables $2^{th}$-order receive diversity, by means of selection combining. Thanks to the integration of all the circuit components on the antenna feed plane, directly below the antenna patch and the ground plane, fragile and lossy interconnections are avoided. Moreover, the small size of the wearable node eliminates electromagnetic compatibility and signal integrity issues. This ultra-flexible and compact wireless transceiver/sensor node can be unobtrusively integrated into rescue worker garments, making it useful for a plethora of wearable applications. The flexible node exhibits a modular topology and is easily expandable to create a customizable textile module. Therefore, this new low-cost system is a step forward in designing comfortable commercial firefighter protective systems.

## Acknowledgement

This research was partially funded by the Inter-University Attraction Poles Program initiated by the Belgian Science Policy Office.

# Bibliography


[1] G. Magenes, D. Curone, L. Caldani, and E.L. Secco, "Fire fighters and rescuers monitoring through wearable sensors: The proetex project", in *Engineering in Medicine and Biology Society (EMBC), 2010 Annual International Conference of the IEEE*, 2010, pp. 3594–3597.

[2] IWT Belgium, the Flemish government agency for Innovation by Science and Technology, "Smart@fire, a groundbreaking european project (FP7) to encourage companies and researchers and provide them with financial means to develop innovative ICT solutions that better protect firefighters and help prevent accidents, and to integrate them into smart personal protective equipment (PPE).", June 2013.

[3] M.O. Munoz, R. Foster, and Yang Hao, "On-body channel measurement using wireless sensors", *Antennas and Propagation, IEEE Transactions on*, vol. 60, no. 7, pp. 3397–3406, July 2012.

[4] Lingfei Mo, Shaopeng Liu, R.X. Gao, D. John, J.W. Staudenmayer, and P.S. Freedson, "Wireless design of a multisensor system for physical activity monitoring", *Biomedical Engineering, IEEE Transactions on*, vol. 59, no. 11, pp. 3230–3237, 2012.

[5] Yao-Chiang Kan and Chun-Kai Chen, "A wearable inertial sensor node for body motion analysis", *Sensors Journal, IEEE*, vol. 12, no. 3, pp. 651–657, 2012.

[6] I. Khan, I. Ullah, and P.S. Hall, "Transmit-receive diversity for 2 x 2 multiple-input multiple-output channel in body area networks", *Microwaves, Antennas Propagation, IET*, vol. 5, no. 13, pp. 1589–1593, 2011.

[7] L. Vallozzi, H. Rogier, and C. Hertleer, "Dual Polarized Textile Patch Antenna for Integration into Protective Garments", *IEEE Antennas Wireless Prop. Lett.*, vol. 7, pp. 440–443, 2008.

[8] Patrick Van Torre, Luigi Vallozzi, Lennert Jacobs, Hendrik Rogier, Marc Moeneclaey, and Jo Verhaevert, "Characterization of measured indoor off-body MIMO channels with correlated fading, correlated shadowing and constant path loss", *Wireless Communications, IEEE Transactions on*, vol. 11, no. 2, pp. 712–721, 2012.

[9] P. S. Hall and Y. Hao, "Antennas and propagation for body centric communications", in *Antennas and Propagation, 2006. EuCAP 2006. First European Conference on*, 2006, pp. 1–7.

[10] L. Vallozzi, P. Van Torre, C. Hertleer, H. Rogier, M. Moeneclaey, and J. Verhaevert, "Wireless communication for firefighters using dual-polarized textile antennas integrated in their garment", *Antennas and Propagation, IEEE Transactions on*, vol. 58, no. 4, pp. 1357 –1368, April 2010.

[11] P. Vanveerdeghem, B. Jooris, P. Becue, P. Van Torre, H. Rogier, I. Moerman, and J. Knockaert, "Reducing power consumption in body-centric ZigBee communication links by means of wearable textile antennas", in *2nd International Workshop on Measurement-based Experimental Research, Methodology and Tools*, 2013.

[12] Maria Lucia Scarpello, Ilda Kazani, Carla Hertleer, Hendrik Rogier, and Dries Vande Ginste, "Stability and efficiency of screen-printed wearable and washable antennas", *Antennas and Wireless Propagation Letters, IEEE*, vol. 11, pp. 838–841, 2012.

[13] A. Alomainy, A. Sani, A. Rahman, J.G. Santas, and Yang Hao, "Transient characteristics of wearable antennas and radio propagation channels for ultrawideband body-centric wireless communications", *Antennas and Propagation, IEEE Transactions on*, vol. 57, no. 4, pp. 875–884, 2009.

[14] P.A. Catherwood and W.G. Scanlon, "Body-centric ultra-wideband multichannel characterisation and spatial diversity in the indoor environment", *Microwaves, Antennas Propagation, IET*, vol. 7, no. 1, pp. 61–70, 2013.

[15] Q.H. Abbasi, A. Sani, A. Alomainy, and Yang Hao, "On-body radio channel characterization and system-level modeling for multiband OFDM ultrawideband body-centric wireless network", *Microwave Theory and Techniques, IEEE Transactions on*, vol. 58, no. 12, pp. 3485–3492, 2010.

[16] Frederick Declercq and Hendrik Rogier, "Active integrated wearable textile antenna with optimized noise characteristics", *IEEE TRANSACTIONS ON ANTENNAS AND PROPAGATION*, vol. 58, no. 9, pp. 3050–3054, 2010.

[17] B. Huyghe, J. Vanfleteren, and J. Doutreloigne, "Design of flexible, low-power and wireless sensor nodes for human posture tracking aiding epileptic seizure detection", in *Sensors, 2009 IEEE*, 2009, pp. 1963–1966.

[18] H. MacLeod, C. Loadman, and Z. Chen, "Experimental studies of the 2.4-GHz ISM wireless indoor channel", in *Communication Networks and Services Research Conference, 2005. Proceedings of the 3rd Annual*, 2005, pp. 63–68.

[19] Jonathan Govaerts, Wim Christiaens, Erwin Bosman, and Jan Vanfleteren, "Fabrication processes for embedding thin chips in flat flexible substrates", *Advanced Packaging, IEEE Transactions on*, vol. 32, no. 1, pp. 77–83, 2009.

[20] F. Quitin, C. Oestges, F. Horlin, and P. De Doncker, "Polarization measurements and modeling in indoor NLOS environments", *Wireless Communications, IEEE Transactions on*, vol. 9, no. 1, pp. 21–25, 2010.

[21] L. Akhoondzadeh-asl, P.S. Hall, Y. Nechayev, and I. Khan, "Depolarization in on-body communication channels at 2.45 GHz", *Antennas and Propagation, IEEE Transactions on*, vol. 61, no. 2, pp. 882–889, 2013.

CHAPTER 4

# Synchronous Wearable Wireless Body Sensor Network Composed of Autonomous Textile Nodes

**Peter Vanveerdeghem, Patrick Van Torre, Christiaan Stevens, Jos Knockaert, and Hendrik Rogier**

Based on the article published in *MDPI sensors*, vol. 14, no.10, pp. 18583-18610, 2014.

★★★

*A novel, fully-autonomous, wearable, wireless sensor network is presented, where each flexible textile node performs cooperative synchronous acquisition and distributed event detection. Computationally efficient situational-awareness algorithms are implemented on the low-power microcontroller present on each flexible node. The detected events are wirelessly transmitted to a base station, directly, as well as forwarded by other on-body nodes. For each node, a dual-polarized textile patch antenna serves as a platform for the flexible electronic circuitry. Therefore, the system is particularly suitable for comfortable and unobtrusive integration into garments. In the meantime, polarization diversity can be exploited to improve the reliability and energy-efficiency of the wireless transmission. Extensive experiments in realistic conditions have demonstrated that this new autonomous, body-centric, textile-antenna, wireless sensor network is able to correctly detect different operating conditions of a firefighter during an intervention. By relying on four network nodes integrated into the protective garment, this functionality is implemented locally, on the body, and in real time. In addition, the received sensor data are reliably transferred to a central access point at the command post, for more detailed and more comprehensive real-time visualization. This information provides coordinators and commanders with situational awareness of the entire rescue operation. A statistical analysis of measured on-body node-to-node, as well as off-body person-to-person channels is included, confirming the reliability of the communication system.*

## 4.1 Introduction

Every year, more than 100 European firefighters lose their lives whilst saving others, as stated on the website of the Smart@Fire Seventh Framework Programme (FP7) project (2012–2015) [1]. Wireless sensor networks with on- and off-body wireless communication capabilities, detecting events by means of computationally efficient situational awareness algorithms, are very important to remotely monitor rescue workers and their environment. This functionality improves their safety and security, as well as the coordination of rescue operations, in general.

For critical applications, such as intervention by emergency services, novel fully-flexible and networked wearable systems must be developed, which can be unobtrusively and comfortably integrated into protective garments. A proof-of-concept of a smart textiles-based monitoring and coordinating system was developed earlier, with a special focus on firefighters, within the context of the ProeTEX FP7 project [2], whereas the ongoing Smart@Fire FP7 [1] project targets the further development of a realistic system. Electronic system integration on a flexible platform is essential, in order to design fully functional autonomous wearable sensing and communication networks, enabling automatic distributed event detection close to the sensors. Recent

developments in single-chip multifunctional wireless transceivers enable the development of very compact, versatile, low-cost and low-power sensor network nodes. The integration of such a sensor system into professional clothing or patient garments, by means of textile antennas, maximizes user convenience, without the need for user interaction. However, until today, no garment-integrated fully-operational system is available.

In this chapter, we present a novel, fully-autonomous, wearable, wireless sensor network. The network is composed of wirelessly interconnected flexible textile nodes that can quickly and unobtrusively be integrated inside the garments of a team of rescue workers. Each node autonomously performs cooperative synchronous acquisition and distributed event detection. Therefore, a low-power microcontroller on each flexible node implements computationally efficient situational-awareness algorithms that detect the events. In addition, sensor data and events are wirelessly transmitted to a base station and to the other on-body nodes. To set up reliable communication links, a dual-polarized textile patch antenna serves as a platform for the flexible electronic circuitry. A significant antenna gain [3, 4] and large radiation efficiency, as well as effective shielding of the body from the radio-frequency energy is provided, thanks to the ground-plane antenna topology.

Wireless transmission of sensor data in indoor environments is often compromised by multi-path radio propagation, causing severe signal fading. It is well known that antenna diversity mitigates the effects of signal fading. Spatial and pattern antenna diversity techniques are exploited by distributing nodes over the body, separating them physically from each other. Additionally, the nodes presented allow polarization diversity, thanks to the dual-polarized patch antenna combined with the two-port transceiver chip.

The wearable network node is based on the physical-layer communication unit, of which the wireless channel behavior is described in [5]. In the further research presented here, this node is applied as a building block of a complete, highly power-efficient wearable wireless sensor network. Therefore, dedicated embedded software was developed, implementing a highly robust wireless on-body network protocol, performing synchronous data acquisition on different sensor nodes. As each node is equipped with an integrated three-axis accelerometer, the system is highly relevant for fall-detection applications [6]. Sensor fusion can be exploited by designing additional sensors into the node circuit in a straightforward manner.

Every network node includes a situational awareness algorithm, to detect and classify events autonomously or in cooperation with other nodes. Measurements are preprocessed on each node and wirelessly transmitted to a central access point. The situational awareness algorithms are computationally optimized to be executed on a low-cost and low-power microcontroller. More computationally expensive tasks can be performed at the base station, if necessary. Measurements confirm efficient synchronous operation for a four-node on-body system, as well as for a three-node person-

to-person configuration. Synchronously acquired quadruple three-axis acceleration data are measured and transmitted, enabling detailed and real-time remote analysis of rescue-worker body orientation and movement.

In the literature, textile antenna research has mainly focused on dedicated antenna design and body-centric channel behavior, as well as on the performance of diversity textile antenna platforms [4, 7, 8]. In terms of complete on-body electronic systems, many rigid wearable nodes exist, often hindering the wearer's movements [9–12]. Many others also performed research on off-body antennas or body area radio propagation for sensor networks [13, 14]. Ongoing integrated circuit design, intended for body area networks in the $2.45$ GHz industrial, scientific and medical (ISM) radio band, is described in [15], indicating the relevance of this band for such applications. State-of-the-art, extremely low-power designs [16] leverage energy-harvesting sensor units for continuous long-term monitoring. A system relying on multiple wireless nodes, equipped with a number of sensors, fixed at several on-body locations, avoids false positive detections [17]. Network protocols and scheduling for body networks are discussed in [18–20]. Recent publications document wearable textile systems for biomedical monitoring [21]. However, in [21], the system does not provide network functionality, as no transmit function is available. On-body integration is impossible in that stage of development, as elaborate additional hardware is necessary for processing the received signal. Sampling of the unprocessed RF signal occurs via an external FPGA module, connected to a PC via USB. This system is suitable for lab experiments in a static setup only. Although the research presented in [22] is related, our system consists of fully wireless, flexible units, comfortably integrated into the rescue worker's garment. Signal-strength information is available for each data packet, providing valuable additional information for sensor localization [17] and body position recognition [23]. Processing of the measurements enables signal classification [24], with applications, such as gait analysis [25–27], kcal expenditure or physical rehab assessment [28]. The microcontroller in our proposed system executes a situational awareness algorithm on each on-body node, enabling automatic event detection and reporting by means of the wireless radio link.

We present a fully functional wearable sensor network employing a network protocol specifically developed for the difficult radio propagation environment encountered when performing indoor operations. To our knowledge, this is the first body-centric wireless wearable textile sensor network incorporating all of these features into a fully flexible garment-integrated system. Moreover, the system is fully tested in multiple measurement scenarios. The sensor data and their classification, as well as the radio propagation aspects are extensively documented in this chapter. In the literature, no such system, documented and validated to a similar extent, was found.

Section 4.2 provides an overview of the system at the network level, outlining the proposed transmission protocol for on- and off-body communication. A description of the hardware composing each wireless node, being the dual-polarized antenna and

key circuit components, as well as the proposed on-board computationally-efficient activity recognition algorithm, is given in Section 4.3. In Section 4.4, a measurement setup with a sensor-equipped test person is discussed, including a floor plan of the test environment and a graphical representation of the unprocessed measurement results. The relation between situational-awareness information, being the movements of the test person and his/her position in the floor plan and the sensor data, providing timestamps for the acceleration and received signal power data streams, is documented in Section 4.5. An evaluation of the on-body node-to-node link reliability is presented in Section 4.6, whereas an additional measurement assessing the performance of person-to-person communication in a three-person network is described in Section 4.7. A discussion follows in Section 4.8. The conclusions are summarized in Section 4.9.

## 4.2 System overview

Patients, healthcare professionals and rescue workers should be monitored by a distributed sensor network, in order to assist caregivers and intervention coordinators. In such a network, data processed near the sensors are transmitted to a central access point. The proposed wearable wireless body sensor network was designed, constructed and validated in order to fulfill these requirements.

The required functionality is provided by a dedicated network protocol embedded in each textile node's microprocessor, as well as in the central access point. The protocol is specifically designed for wireless communication between members and the coordinator of a small intervention team. In the typical scenario of a firefighting invention, for example, a group of two to three firefighters will penetrate a burning building, closely followed by a coordinator/commander outside the building. The envisaged network protocol shall ensure reliable communication and detect events within the team. Moreover, the protocol must be able to deliver this information to the command post, which may issue alerts, all without significant delay. We first outline this protocol, designed for an N-node body-worn network, involving multiple team members and the coordinator. In the next section, we proceed to a detailed description of the hardware components that compose each textile node of the body sensor network shown in Figure 4.1.

### 4.2.1 Network protocol for synchronous measurements

Synchronous sensor data acquisition, including a wireless communication link to a central access point, is implemented for an N-node body-worn network by means of the following protocol:

- Power-on cycle and node enumeration: During subsequent manual power-on of the nodes, the nodes detect each other's presence in the network and are automatically enumerated, acquiring their unique soft-ID's, which determine their

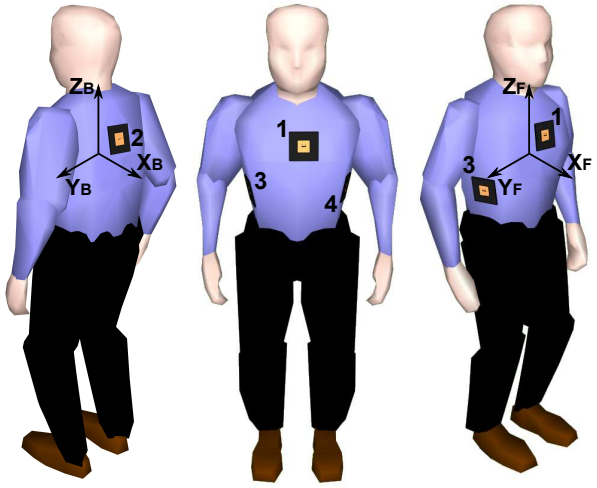


**Figure 4.1:** Wearable wireless body sensor network composed of four fully-autonomous and wireless textile nodes, synchronously capturing, preprocessing and relaying sensor data to a central access point.

time slots in the transmission cycle. Nodes have to be switched on sequentially, respecting at least one second in between the manual switch actions. Please note the proposed system is composed of battery-operated truly wireless sensor units, leading to a sequential power-on cycle due to the absence of a common power supply or any other wired connection between the nodes.

- When powered on, each node listens for packets from other nodes. If no packets are received within a one-second time-out period, this node is assigned soft-ID $= 1$ and autonomously starts transmitting sensor data, including this soft-ID number.
- After the last transmitted packet of the transmission cycle, an extra receive time slot is preserved to listen for other packets from new nodes that can join the network, as displayed in Figure 4.2.
- When a next node is powered-on, the new node first listens for data packets transmitted by other nodes, receiving data packets from all active nodes. The new node responds with its own sensor data and dynamically determined soft-ID number (being the highest soft-ID number in the network $+1$). This step is repeated for all N nodes in the body-centric network.
- Given the successful reception rate of more than $95\%$ observed in our measurements (as further documented in Section 4.6), the probability of missing all packets in the time-out period is extremely low, successfully avoiding an erroneous multiple assignment of the same soft-ID number.

In practice, the network activity and, hence, the enumeration process are also monitored and verified by the base station, confirming a correct initialization. The power-on cycle and enumeration process should be performed by all firefighters and the coordinator operating the base station well within each other's range, which is a realistic scenario, as firefighters always enter a building as a small team.

– Each node also transmits a unique and fixed hard-ID, allowing unambiguous identification by the base station, as well as avoiding re-enumeration of already active nodes in case of communication errors.
– When all nodes in the body-centric network are active, a time-slot is kept available to receive base station transmissions, as shown in Figure 4.2 for a four-node network. Base-station transmissions are recognized by a hard-ID $>127$ and do not lead to further network enumeration. In case of an emergency, the base station transmits a data packet containing an alert level. The alert level initiates different alarm conditions at the rescue worker's side. When an alert level is received by one or more of the wireless nodes, the alert level is forwarded by the wireless nodes themselves in their own transmit time slot together with the sensor data, to ensure all rescue workers receive the alert message. The alert level is stored on each wearable node. The initial alert level is zero; higher alert levels lead to audible alarm signals on the wearable nodes via a beeper, which has to be connected to a microcontroller output pin reserved for this purpose.

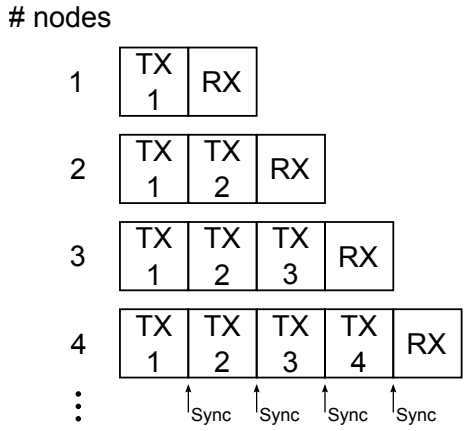


**Figure 4.2:** Power-on cycle and time-slot structure of the autonomous body-centric network.

- Data forwarding and measurement synchronization are possible thanks to the network nodes continuously monitoring each other's transmissions. At each time instant, the sensor data from the currently transmitting node are stored

in the memory of each receiving node, which will forward the collected data in its own transmit time slot. Thanks to the data forwarding, a redundancy leading to a performance increase comparable to $N^{th}$-order transmit diversity gain is obtained, providing a highly reliable cooperative data link towards the base station. The nodes synchronize their clocks using the time stamps of the received data packets from the other nodes. This enables fully-synchronous sensor data capturing on all nodes. The flowchart of the network protocol is shown in Figure 4.3.

- Data packet structure: The sensor data captured by the nodes are organized into a packet, as shown in Figure 4.4, transmitted by employing the IEEE $802.15.4$ mode supported by the transceiver chip, automatically adding an error-detecting code, ensuring the correctness of the received data. The node's hard-ID corresponds to a unique fixed serial number for each physical node, whereas the soft-ID number was assigned automatically during the network enumeration process.
- Scalability: The platform is highly versatile and can also operate in larger networks.
  - Up to $12$ nodes can actively forward packets from the base station or other users in the network. These nodes can be distributed over the members of an intervention team; three firefighters wearing four nodes or six firefighters wearing two nodes are efficient configurations. Two nodes per body provide enough information, but four nodes provide more accuracy and reliability thanks to the redundancy. Authorities in the firefighting world [1] state that teams of three firefighters are the maximum to be monitored by one commander.
  - Extra time slots can be provided in the transmission protocol to enable dual-polarized diversity reception, by sending all transmitted data packets twice and receiving odd and even packets alternatingly on different polarizations.
  - Parallel networks can be deployed at different frequencies; their data is then combined at the base station, using multiple low-cost receivers. In IEEE $802.15.4$ mode, the $2.45$ GHz ISM-band provides $16$ channels.

## 4.3 Wireless sensor node implementation

### 4.3.1 Hardware description

Figure 4.5(a),4.5(b) shows a prototype of an autonomous wireless sensor node completely integrated into a flexible garment-integrated patch and powered by a single battery. In Figure 4.5(a), the front side of the wireless sensor node is shown, where the patch antenna is visible with its dimensions. Figure 4.5(b) gives an overview of

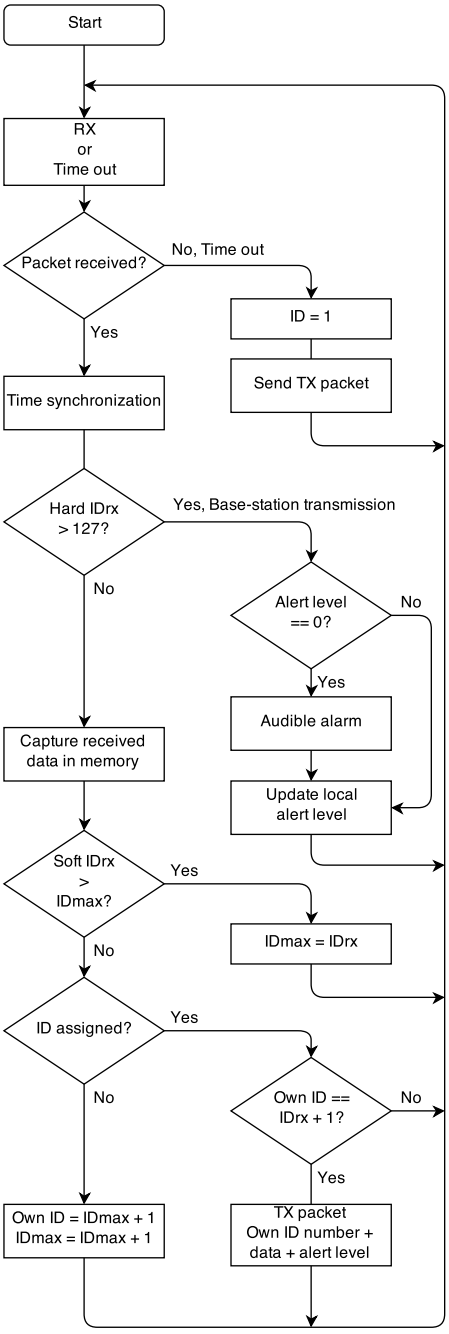


**Figure 4.3:** Simplified flowchart of the network protocol.

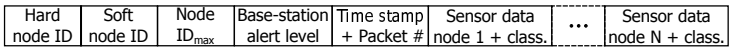


**Figure 4.4:** Data packet structure.

the backside of the wireless sensor node; this side includes all of the electronic components mounted on the flexible substrate. We now discuss the various components composing the block diagram of the node in Figure 4.6.

The basic platform for the wireless node is a dual-polarized textile patch antenna, as shown in Figure 4.7. Details about this antenna and its performance can be found in [4]. This compact wearable antenna is fully breathable, flexible and includes two feeds, enabling the excitation of two orthogonal linearly-polarized waves, with an antenna gain of $6$ dBi along the boresight and a better than $15$ dB isolation between the feed ports. The textile material makes the unit flexible and lightweight, without losing antenna performance, in comparison to rigid antennas. The antenna ground plane is constructed using FlecTron, a low-cost, conductive, electro-textile material with a thickness less than 0.25 mm and a surface resistivity less $0.1\Omega/$sq., minimizing the influence of the body in close proximity to the antenna. The substrate material is closed-cell, flexible, expanded-rubber protective foam, commonly used in protective garments for rescue workers (density = 187.3 kg/m$^3$, permittivity $\epsilon_r$ = $1.53$ and tan $\delta$ = $0.0012$) with a thickness of $5$ mm. The flexible foam will help to protect the electronic circuitry from external factors, such as humidity. As the networking-enabled wearable node designed here presents a further development of the wireless textile transceiver documented in [5], we refer the reader to this text for details about its fabrication, together with a validation of its physical-layer wireless communication performance, employing polarization diversity.

On the wireless node, a variety of analog and digital sensors can be incorporated. In this chapter, we discuss the integration of an Analog Devices ADXL $337$ three-axis accelerometer into our prototype. This sensor is very compact and provides accurate acceleration measurement data, which will be preprocessed, locally interpreted and transmitted to a central access point. The wireless sensor node measures acceleration with a specified full-scale range of $\pm 3$ g. Acceleration caused by gravity allows sensing of body orientation, whereas accelerations resulting from motion, shock or vibration produce information about the firefighter's actions. The accelerometer sensor is very robust as, according to the data sheet, $10,000$ *g* shock survival is guaranteed [29].

The microcontroller forms the heart of the system, providing the distributed network functionality. A highly compact and low-power advanced single-cycle microcontroller, the Silicon Laboratories C$8051$F$921$, is used. This processor collects sensor data and organizes it into packets for wireless transmission or storage into memory. Embedded software for this controller is developed in the C programming language and uploaded into the controller's nonvolatile code memory by the In-System Pro-

gramming interface via a USB cable [30].

On-board flash memory is available as nonvolatile storage space for measurement data. The memory unit is used as a buffer or as a data storage for processing and analysis. At a rate of 25 measurements per second, at least 11 h of continuous three-axis accelerometer data can be stored in the 4 MB flash installed on the prototype.

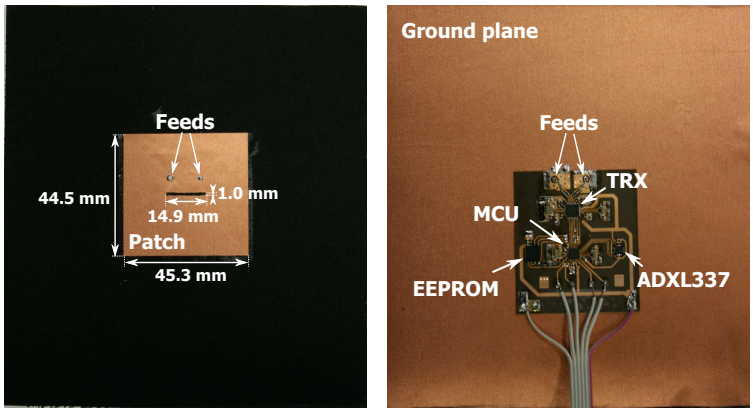


(a) (b)

**Figure 4.5:** (**a**) front side of the wireless sensor node; (**b**) back side of the wireless sensor node with the electronic components mounted on the flexible substrate.

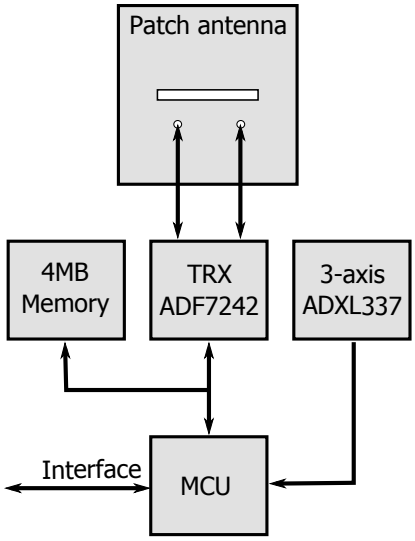


**Figure 4.6:** Block diagram of the wearable node, showing the MCU, flash memory, accelerometer and transceiver chip connected to the textile patch antenna.

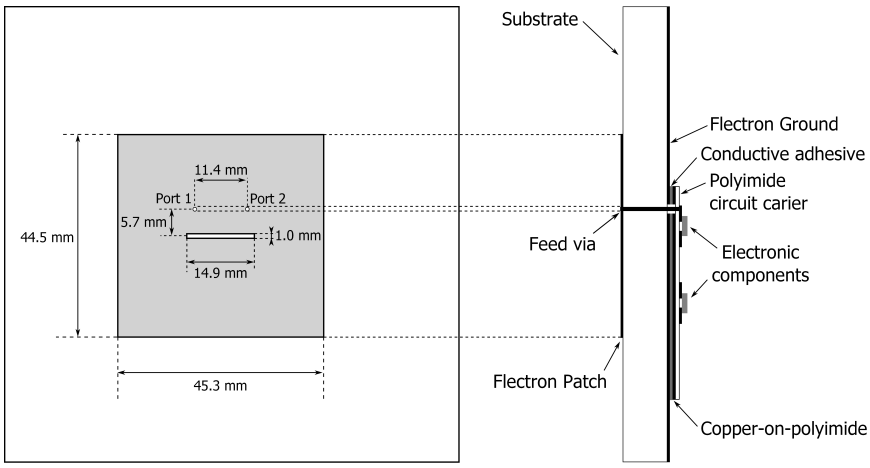


**Figure 4.7:** Cross-section of the dual-polarized textile antenna with electronic circuitry mounted onto the feed plane.

The state-of-the-art Analog Devices ADF7242 wireless $2.45$ GHz ISM-band transceiver is used to set up the wireless data link. This is the first single-chip $2.45$ GHz transceiver incorporating diversity, as well as IEEE $802.15.4$ and GFSK modulation. The maximum output power of the ADF $7242$ is limited to $+4.8$ dBm, which is well within the limits imposed by regulations ($20$ dBm, ETSI standard EN 300 328 [31] for wide band transmissions, such as in the IEEE 802.15.4-2006 mode). If desired, the range of the nodes can be significantly extended by increasing the transmit power up to the legal limit of $+20$ dBm. This option is discussed in the datasheet [32] of the ADF$7242$ transceiver chip and involves designing an integrated RF amplifier into the circuit.

### 4.3.2 Computationally simple classification

Each node includes a three-axis accelerometer, providing three independent sensor data streams. The sensor data can be used, independently or in cooperation with sensor data of the other nodes in the on-body network, to implement real-time activity recognition. An algorithm is proposed to detect and classify activities performed by firefighters during rescue operations, optimized for implementation on the microcontroller of each sensor node, with minimal processing power. Existing systems, as documented in [10], do not implement signal classification and event detection on the node itself. A flowchart of the computationally simple classification is given in Figure 4.8.

The most important situation that needs to be monitored in the rescue-worker application is lying down [2], as this potentially corresponds to an emergency situation

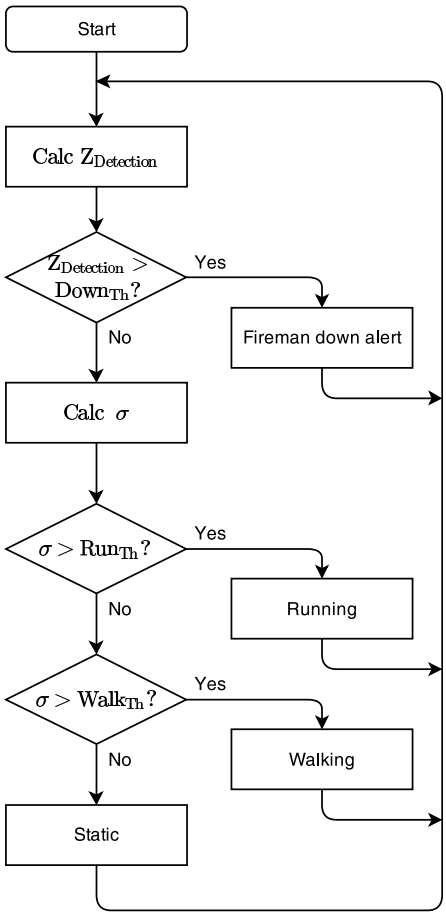


**Figure 4.8:** Flowchart of the computationally simple classification.

where the rescue worker's life is at risk. When the person is walking or standing, the measured gravity vector value will always be approximately $-1$ $g$ along the z-axis. When lying down, the measured gravity vectors for all axes reorient, and no repetitive accelerations are detected. Lying flat on the ground, the gravity vector for the z-axis will be approximately $0$ $g$. By combining the measurements along the z-axis from all nodes, averaged over one second of sensor acquisition, lying down is readily detected. The decision rule for lying down is given by:

$$\langle Z_{detection} \rangle = \frac{\sum_{n=1}^{N} \sum_{m=1}^{M} Z_{n,m}}{N \cdot M} > \text{Down}_{\text{Th}} \rightarrow \text{Lying down} \tag{4.1}$$

with $n$ the node number, $N$ the total number of nodes, $m$ the measurement sample number and $M = f_s.\Delta t =$ Sample rate.$1s$ the number of measurements per node during a one-second time window. The threshold is set to $\text{Down}_{\text{Th}} = -0.5\ g$, which corresponds to the firefighter lying down, with an angle of $30°$ or less (straight up = $90°$) with respect to the ground.

A detection algorithm is proposed for walking or running, based on the repetitive accelerations observed in [27, 33]. Running generates larger and higher-frequency accelerations, resulting in a larger standard deviation of the accelerometer data, compared to walking [25–27]. Therefore, the standard deviation $\sigma$ of the accelerometer sensor data is observed over a one-second time frame, given by:

$$\sigma = \sqrt{\frac{\sum_{m=1}^{M} \left(\overline{Z} - z_m\right)^2}{M}} \tag{4.2}$$

with $M = f_s$, being the sample rate, and $\overline{Z}$ the average over a one-second time window.

The decision rules for walking and running are given by the following thresholds:

$$\text{Run}_{\text{Th}} \geq \sigma > \text{Walk}_{\text{Th}} \rightarrow \text{Walking} \tag{4.3}$$

$$\sigma > \text{Run}_{\text{Th}} \rightarrow \text{Running} \tag{4.4}$$

When $\sigma$ exceeds a preselected threshold level, the corresponding activity is in progress. The threshold values for the activity algorithm are empirically selected:

$$0.4\ g \geq \sigma > 0.08\ g \rightarrow \text{Walking} \tag{4.5}$$

$$\sigma > 0.4\ g \rightarrow \text{Running} \tag{4.6}$$

When an alarm situation occurs, the status of the activity recognition algorithm is transported in the wireless data packet to the base station, directly or with priority, and forwarded by other nodes in the network, providing a fast and very reliable information link from the rescue worker to the base station.

## 4.4 Measurements for four on-body nodes

The performance of the wireless sensor network is assessed for a realistic application, where the wearable system is deployed in a protective garment, worn by a rescue worker performing a number of movements and postures at different locations. A number of real-world situations are studied in an indoor office environment, as well as in an outdoor scenario.

### 4.4.1 Measurement setup

Four wireless nodes are integrated into a firefighter garment, deployed on the front, back, left and right sides of the body. The antennas radiate away from the body in different directions, providing spatial, as well as pattern diversity. The setup is illustrated in Figure 4.1. For clarity, only the front $(1)$ and rear $(2)$ nodes are initially taken into consideration. Given the relative orientation of the two nodes, the vectors of the x- and y-axes of both nodes will be opposite. The gravity vectors provide information about the orientation of the body of the rescue worker. The central access point is represented by a receiving node that relies on similar hardware as the mobile nodes, but now with two omni-directional monopole antennas connected to the inputs.

In the indoor office environment, the base station node is located at a height of $2$ m above the office floor (RX1) and connected to a computer performing real-time data processing. The office at Ghent University is located on the first floor, consisting of solid brick floors and reinforced concrete walls. The floor plan of the office and its surroundings is given in Figure 4.9. Next to the building, there is a inclined street with its down-hill direction to the left, reaching the ground floor level at the right, surrounded by other buildings. In the outdoor environment, the receive node is placed outside the office building (RX2), along the inclined street, as illustrated on the floor plan in Figure 4.9.

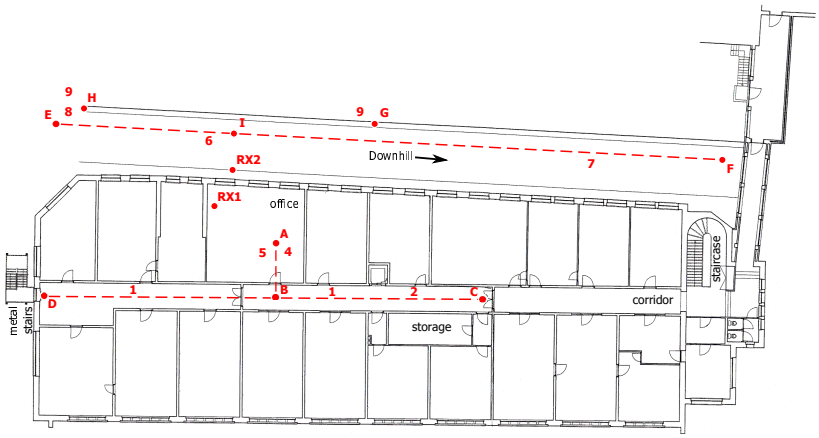


**Figure 4.9:** Floor plan of the office environment at Ghent University.

### 4.4.2 Data reliability

In the course of an indoor measurement, where the firefighter walks in the office floor along the path A–B–D–B–C–B–A in the floor plan, as shown in Figure 4.9, a total of $16$ packets out of the full set of 1,900 packets transmitted to RX1 was lost for

four nodes. However, as the sensor data pertaining to the nodes from which packets were missing at the base station were repeated by the other three on-body nodes, all sensor data were recovered. In an indoor environment, the signals from $N$ different nodes are influenced by decorrelated fading, leading to an $N^{th}$-order diversity gain. This clearly demonstrates the vast improvement in transmit reliability of the body-centric network. An overview of the packet loss and recovery is shown in Table 4.1.

**Table 4.1:** Overview of the packet loss and recovery during the measurement campaign.

| Parameter or Variable | Value |
|---|---|
| Number of active nodes | 4 |
| Total transmission time | 76 s |
| Number of packets per second | 25 |
| Total number of packets transmitted | 1900 |
| Number of packets received directly | 1884 |
| Number of packets recovered by Node 1 | 7 |
| Number of packets recovered by Node 2 | 1 |
| Number of packets recovered by Node 3 | 3 |
| Number of packets recovered by Node 4 | 5 |
| Total number of packets recovered through forwarding | 16 |
| Total number of lost packets | 0 |

### 4.4.3 Synchronization of four nodes

In Figure 4.10, the sensor data, acquired along the vertical accelerometer axes during a jump, are illustrated, in order to demonstrate the synchronicity of the measurements on all four nodes. Traces for the other axes are also synchronized, but have been omitted for the sake of graph clarity.

### 4.4.4 Accelerometer measurement

Plots of the measurements in both indoor and outdoor environments are displayed in Figures 4.11 and 4.12, respectively. Features visible in the graph are caused by specific movements and postures of the rescue worker. They are linked to his position in the floor plan, as shown in Figure 4.9. For clarity of the graphs, the sensor data for only two nodes are shown. The on-body network provides reliable connectivity over the full trajectory covered by the test person. Further analysis of the sensor data follows in Section 4.5.

### 4.4.5 Signal strength measurements

While the test person walks along the outdoor path E–F, the receive node RX2 at the base station observes the signal power of the received packets from the front and

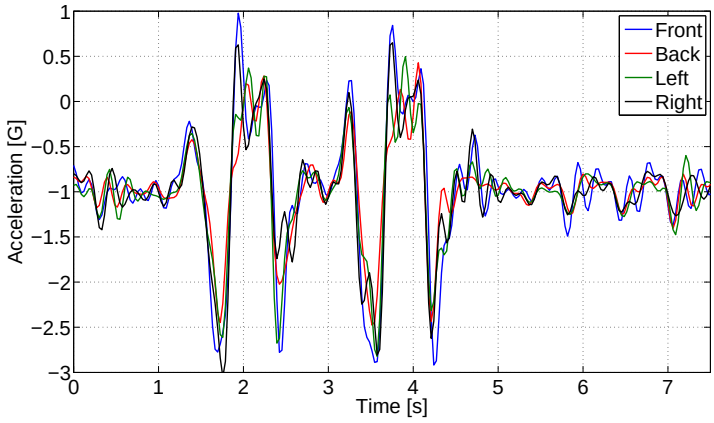


**Figure 4.10:** Synchronization of the sensor data related to the vertical z-axis of the wireless nodes, when the test-person is jumping.

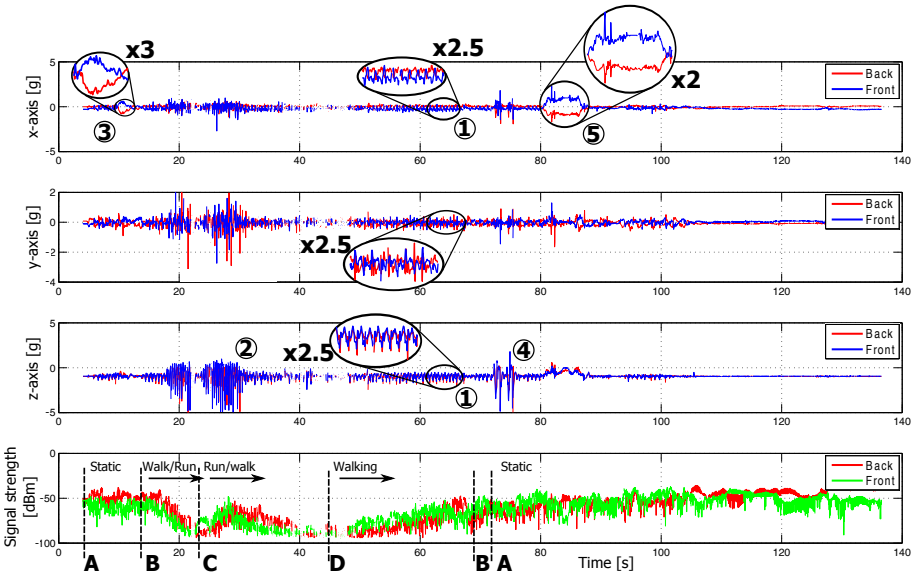


**Figure 4.11:** Measurement results along the indoor path A–B–C–D–B–A, followed by some activities performed in the neighborhood of A (x,y,z-axes + signal strength).

back node. At the beginning of the path (E, marked on Figure 4.12), the front node is in Line of Sight (LoS) with the receiver node, providing a large signal strength on the receiving node. When the test person passes by the fixed node at Position I, the signal strength of both nodes are equal. After this point, the back node is in LoS with the fixed node, providing a large signal strength in comparison with the front

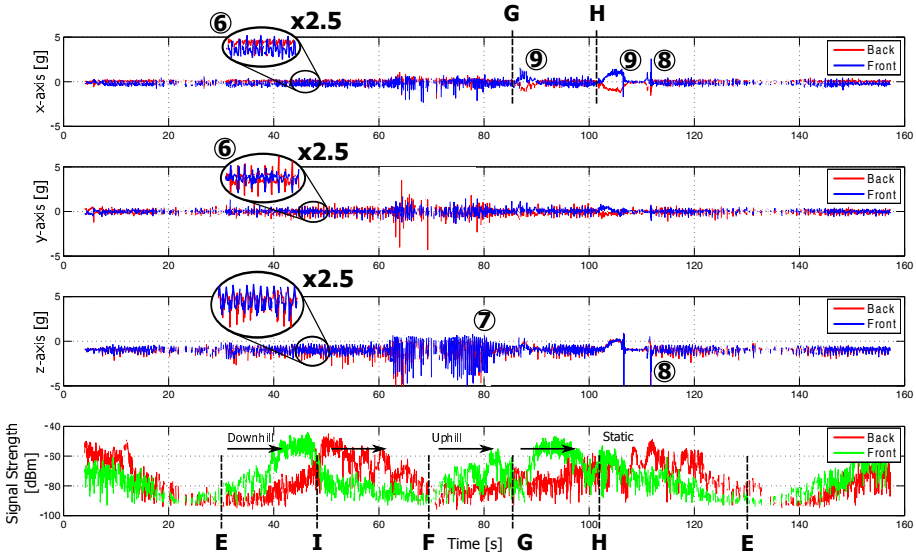


**Figure 4.12:** Measurement results along the outdoor path, starting with random walk moving to location E, followed by the path E–I–F–G–H, ending with some activities performed in the neighborhood of H and random walk around location E (x,y,z-axes + signal strength).

node. Differences in signal strength up to 35 dB occur between the two nodes. The configuration of a front/back sensor node system has clear advantages compared to a single sensor system. The total coverage area of the sensor system increases thanks to the transmit diversity gain and the multi-hop wireless network topology.

### 4.4.6 Power consumption

The wireless node is powered by a small (5 mm $\times$ 25 mm $\times$ 35 mm) one-cell Lithium polymer (Li-po) battery of 400 mAh and a low-drop linear voltage regulator. From the technical data sheet of the various integrated components of the wireless sensor, an estimation of the power consumption can be made. The microcontroller will consume an average current of 4 mA at 3.3 V and at a clock frequency 24.576 MHz. In sleep mode, the current consumption can be lowered to 600 nA. The accelerometer used on the wireless sensor only consumes 0.3 mA during operation at 3.3 V. The flash memory consumes on average 12 mA at 3.3 V while operating (reading or writing); in standby mode, the current consumption is lowered to 25 µA or to 5 µA in deep power-down mode. The most power consuming device on the wireless sensor is the transceiver chip. At the the highest output power, a maximum current of 25 mA is used at 3.3 V. In receiving mode, the maximum current consumption is 19 mA. While the transceiver is not transmitting data packets, it will be configured in the receiving mode. In idle mode, the power consumption is lowered to 300 nA. An overview of the

current consumption is summarized in Table 4.2.

**Table 4.2:** Current consumption of the wireless node.

| Component | Power Mode | Current Consumption |
|---|---|---|
| Microcontroller | Idle | 2.5 mA |
| | Sleep | 0.1 μA |
| | Normal | 4 mA |
| Transceiver | Idle | 1.8 mA |
| | Sleep | 0.3 μA |
| | Transmit, ($P_{out}$ = +4 dBm) | 25 mA |
| | Receive | 19 mA |
| Memory | Stand by | 25 μA |
| | Deep Power-down | 5 μA |
| | Read/Write | 12 mA |
| Accelerometer | Power on | 300 μA |

The maximum current consumption is estimated at 29.4 mA at 3.3 V, taking into account the maximum power consumption while transmitting and no operation of the flash memory is performed. Due to the circuit topology, it is not possible to read or write data into the flash memory while transmitting a data packet.

In full operation, the measured average power consumption of one node of the wearable sensor network equals 90 mW (27 mA current consumption, at 3.3 V supply voltage) with negligible variation when operating in transmit or receive mode. This enables the sensor network to operate for many hours, without the need for charging the battery. Furthermore, the power consumption can further be minimized by employing the sleep mode of the system when there is no need to operate continuously at high speed. In this mode, the total power consumption is less than 10 mW. The system can be activated at regular intervals based on the hardware wake-up timer integrated in the microcontroller, to check the activity by the base station or other on-body nodes.

## 4.5 Spectrogram and classification of accelerometer measurements

The sensor data from the four-node on-body experiment is now analyzed employing classification algorithms. Activity recognition is illustrated at the base station, as well as locally at each wearable node.

### 4.5.1 Classification of the accelerometer data

The following actions are clearly detectable based on the accelerometer measurements. The markers refer to floorplan in Figure 4.9, for the location of the firefighter and Figure 4.11 or 4.12 for the corresponding sensor data.

- Walking (1, 6): A firefighter walks at moderate speed. This movement introduces significant repetitive accelerations measured by both wireless nodes. The accelerations are clearly visible along all of the axes of the sensors, as shown in Figures 4.11 and 4.12. The walking speed is determined based on the repetition frequency of the accelerations, allowing step counting.
- Running (2, 7) introduces stronger accelerations on both wireless nodes. These accelerations are clearly visible in Figures 4.11 and 4.12 and are easily detected based on the acceleration values and main frequency component.
- Bending (3) of the rescue worker introduces reorientation of the measured gravity vector caused by the movement of the upper body. Thanks to the opposite direction of the nodes on the body, the signs of the accelerations measured on the front and back are opposite, allowing easy detection of bending. This movement is performed at Point A in the office and is clearly detectable in the measurement data in Figure 4.11. A difference of the opposite gravity vectors (larger than $0.5\ g$) indicates bending.
- Jumping (4, 8) causes large accelerations along all axes of the accelerometers, especially along the z-axis of the test person, as seen in Figures 4.11 and 4.12. The test person climbs onto a wall and jumps down at Point H. In the indoor environment, the test person jumps up and down at Point B.
- Lying down (5): When a person is lying on the ground, the accelerometer will determine the direction of the gravity vector, providing body orientation data. In the measurement, the test person lies face-down at Point A in Figure 4.11, causing both sensor nodes to provide oppositely oriented gravity vectors along the x-axis, with a maximum difference of the opposite gravity vectors of $2\ g$. The gravity vectors for both nodes along the z-axis will approximate $0\ g$. When a position occurs in between frontal and sideways lying, the difference of the opposite gravity vectors is still detectable along both the x- or y-axes. A continuous difference of at least $1.4\ g$ along the x- or y-axes is observed, clearly indicating this lying position.

- Climbing (9) on top of objects also introduces a reorientation of the measured gravity vector. This movement consists of lateral (along the y-axis) and forward (along the x-axis) bending of the body, together with a reorientation of the gravity vector along the z-axis. The test person climbs onto a wall of approximately $1.5$ m and $1$ m height at Point G and Point H, respectively.

### 4.5.2 Spectrogram

In Figure 4.13, the rectangular windowed fast Fourier transform (FFT) of the accelerometer data is plotted for Node 1, as a spectrogram with a time window of $256$ samples, clearly indicating different movements of the test person. This spectrogram is normalized to the amplitude of the largest frequency component.

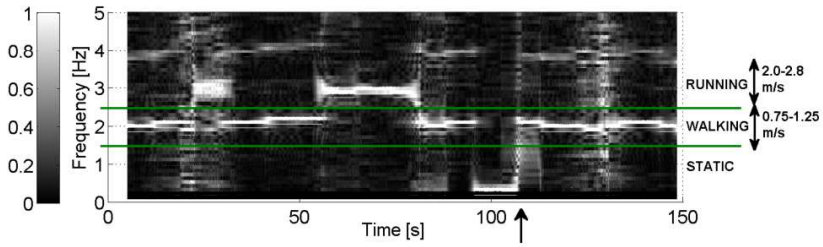


**Figure 4.13:** Spectrogram for the frequency components of the accelerometers in the outdoor measurement (normalized amplitude).

At a normal walking speed, a main frequency component of $2$ Hz is observed, whereas $3$ Hz is obtained when running. A person who is running takes larger steps, which explains why an approximately double speed results in an increase of the main frequency component by only a factor of $1.5$. However, running is easily detected, because both the frequency and amplitude of the main spectral component significantly increase compared to walking. In a stationary position, a frequency component of $0$ Hz (DC), is observed. This is clearly shown when the test person has climbed on the wall in the outdoor measurement. Accelerations for step counting are easily detected in the spectrogram. After the test person climbs the wall, the increasing main frequency component in the time needed to achieve normal walking speed is indicated by an arrow in Figure 4.13, illustrating the accuracy obtained by the sensor network.

### 4.5.3 Activity recognition results

In Figure 4.14, the measurement data from two nodes are displayed (for clarity reasons), while several activities are performed during a time frame of approximately $3$ min. Below the acceleration data from the two sensor nodes, the status of the activity recognition algorithm is shown. The implementation of the algorithm allows easy

recognition of the current activity of the rescue worker. Four levels are used in the graph to indicate the status of the activity recognition algorithm.

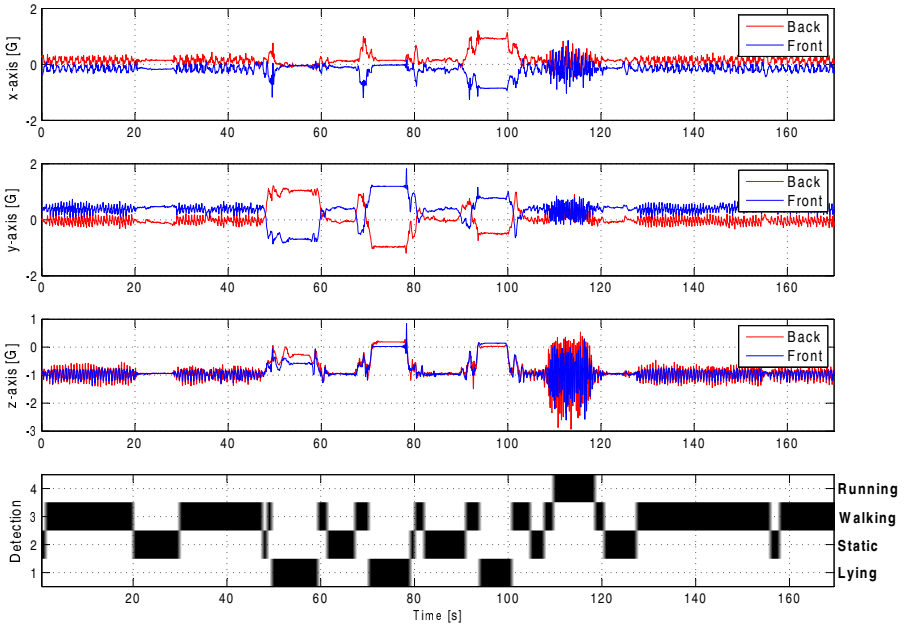


**Figure 4.14:** Activity recognition results for walking, running and lying down in different positions.

As can easily be verified in the unprocessed measurement in Figure 4.14, the classification algorithm successfully determines the user state in a computationally efficient way. Although detection on one on-body node is already remarkably accurate, the combination of data from all sensors in the on-body network further increases the reliability as a classification system for user actions.

## 4.6 Evaluation of on-body node-to-node link reliability

An important aspect in the functionality of the body-worn system is that off-body transmissions are employed for the node-to-node communication on the same body, relying on reflections in the environment. As this issue raises questions about link reliability, especially between front and back nodes, an experiment is performed illustrating the received signal levels, as well as the packet loss for the node-to-node links.

A person equipped with four nodes is performing a random walking behavior in an indoor environment, including maneuvers, such as jumping and lying down. The

nodes numbered 1 to 4 are located in the front, back, left and right of the body, in that order. The base station is placed within line of sight of the walking person. The total number of 5940 received packets corresponds to 4 min of walking and allows accurate statistics of the link behavior.

The cumulative distribution function of the received signal powers for the 12 node-to-node links is displayed in Figure 4.15. These curves illustrate that the signal level is at least 15 dB above the ADF7242 transceiver's specified receiving threshold of −95 dBm for 98% of the received packets.

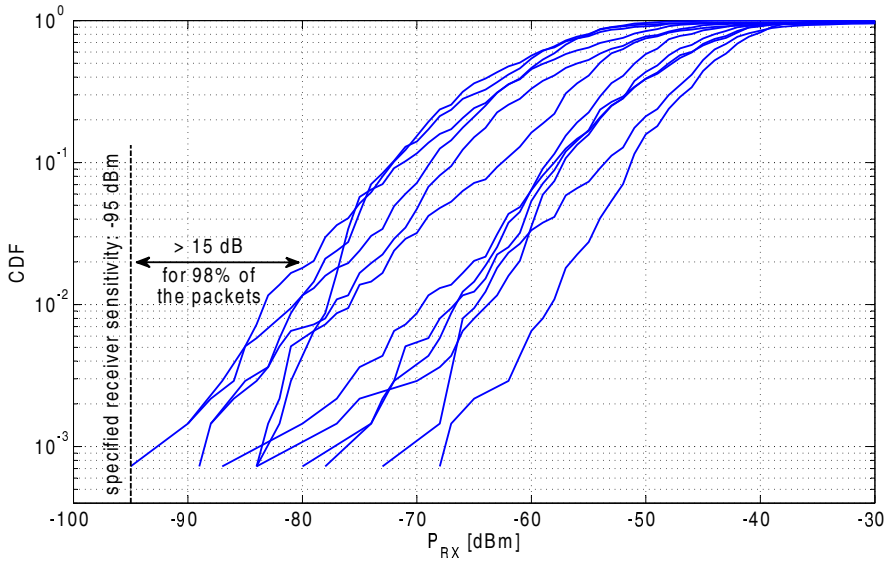


**Figure 4.15:** Cumulative distribution function of the received signal levels for the 12 on-body node-to-node links in a front, back, left and right configuration.

In total, 12 node-to-node links exist in a four-node network. The nodes corresponding to each link are listed in Table 4.3, including the median received power and packet loss for each link. The maximum number of subsequently lost packets on each link is included, as this is valuable information to acknowledge the reliability of the network enumeration protocol explained in Section 4.2.1.

The maximum number of subsequently lost packets on any node-to-node link is three, corresponding to a maximum link interruption of 120 ms, whereas the timeout for the enumeration process is 1 s. Note that packets are always received at a 25 Hz rate, independent of the number of active nodes, as transmissions by all active nodes are received, making the probability of an enumeration fault extremely low. In the unlikely case that such an error does occur, this will be immediately detected by the base station.

**Table 4.3:** Median received power and packet loss for the on-body node-to-node links. Node numbers correspond to the following locations: 1, front; 2, back; 3, left; 4, right.

| TX Node | RX Node | Median $P_{RX}$ | Packet Loss (%) | Max # Subsequently Lost Packets |
|---|---|---|---|---|
| 1 | 2 | −59 | 0.43541 | 1 |
| 1 | 3 | −55 | 3.4833 | 1 |
| 1 | 4 | −48 | 4.4993 | 3 |
| 2 | 1 | −60 | 3.7736 | 1 |
| 2 | 3 | −45 | 3.701 | 2 |
| 2 | 4 | −54 | 3.7736 | 1 |
| 3 | 1 | −50 | 3.3382 | 1 |
| 3 | 2 | −47 | 0.21771 | 1 |
| 3 | 4 | −61 | 3.701 | 2 |
| 4 | 1 | −47.5 | 3.5559 | 1 |
| 4 | 2 | −44 | 0.072569 | 1 |
| 4 | 3 | −58 | 3.4833 | 1 |

## 4.7 Performance analysis for a three-person network

As a further assessment of the reliability of the wireless network and classification in the case of multiple persons, a measurement is performed employing three persons, each wearing one network node on the chest. The three persons are performing independent random walks within the same area, separated by varying distances of up to 20 m. The persons are all randomly switching between actions, such as walking, running, standing still, laying down and jumping, clearly illustrating the presence of separate persons. The computationally simple classification method is performed on the sensor data of the three persons, confirming its reliability for different test persons. Both the sensor data and the classification results are shown in Figure 4.16. The markers on the graphs refer to the actions, as described in Section 4.5. Although only one node is used for each person to measure accelerations and perform automatic classification, the computationally simple algorithm still performs very well.

Additionally, the experiment proves the following important communication properties of the system:

- Node-to-node communication is also very reliable between nodes mounted on different persons operating in a team.
- Thanks to the forwarding of packets, not a single measurement is lost, even when only one unit installed on each body.

The Cumulative Distribution Function (CDF) of the received signal powers for the six node-to-node links is displayed in Figure 4.17. These curves illustrate that the signal level is at least 20 dB above the ADF7242 transceiver's specified receiving threshold of −95 dBm for 98% of the received packets. In comparison, the node-to-node

communication is even more reliable between nodes on different bodies, compared to the link between nodes on the same body. This behavior is as expected, as when the nodes are mounted on different persons of a team a line-of-sight link often exists between these nodes.

Interestingly, the median received power is in the same range for the person-to-person links compared to on-body node-to-node links. The persons are constantly reorienting during the random walk and located at varying distances from each other, resulting in a constantly changing path loss. However, the spread between different CDF curves is much more limited for the person-to-person links. The reason for this behavior is that for the full measurement, the propagation conditions are similar for each pair of nodes, with each node worn on the front of a person performing a random walk over a $4$-min time span. In comparison, for the on-body node-to-node communication, the nodes are in fixed locations on the same body, causing systematic differences in the CDF curves due to the specific set of fixed body locations corresponding to each pair of communicating nodes. The packet loss values, as shown in Table 4.4, are also significantly lower for the person-to-person links, confirming the results observed in the CDF characteristics.

**Table 4.4:** Median received power and packet loss for the person-to-person links.

| TX Person | RX Person | Median $P_{RX}$ | Packet Loss (%) | Max # Subsequently Lost Packets |
|---|---|---|---|---|
| 1 | 2 | $-51$ | 0.55866 | 1 |
| 1 | 3 | $-54$ | 0.8126 | 1 |
| 2 | 1 | $-52$ | 0.76181 | 1 |
| 2 | 3 | $-54$ | 0.8126 | 1 |
| 3 | 1 | $-51$ | 0.71102 | 1 |
| 3 | 2 | $-51$ | 0.25394 | 1 |

We conclude that distributing the nodes over several persons does not compromise the wireless communication between nodes or the network functionality in any way. Node-to-node links on the same body, as well as person-to-person links are always very reliable, thanks to the low packet loss for each link, combined with the redundancy introduced by forwarding packets, leading to a reliability increase of the communication system comparable to $\mathrm{N}^{\mathrm{th}}$-order transmit diversity for an $N$-node network [34].

## 4.8 Discussion

The flexible wearable wireless network system successfully measured three-axis accelerations and transmitted these measurements and a classification thereof to the base station without a single missing sensor measurement in all experiments performed.

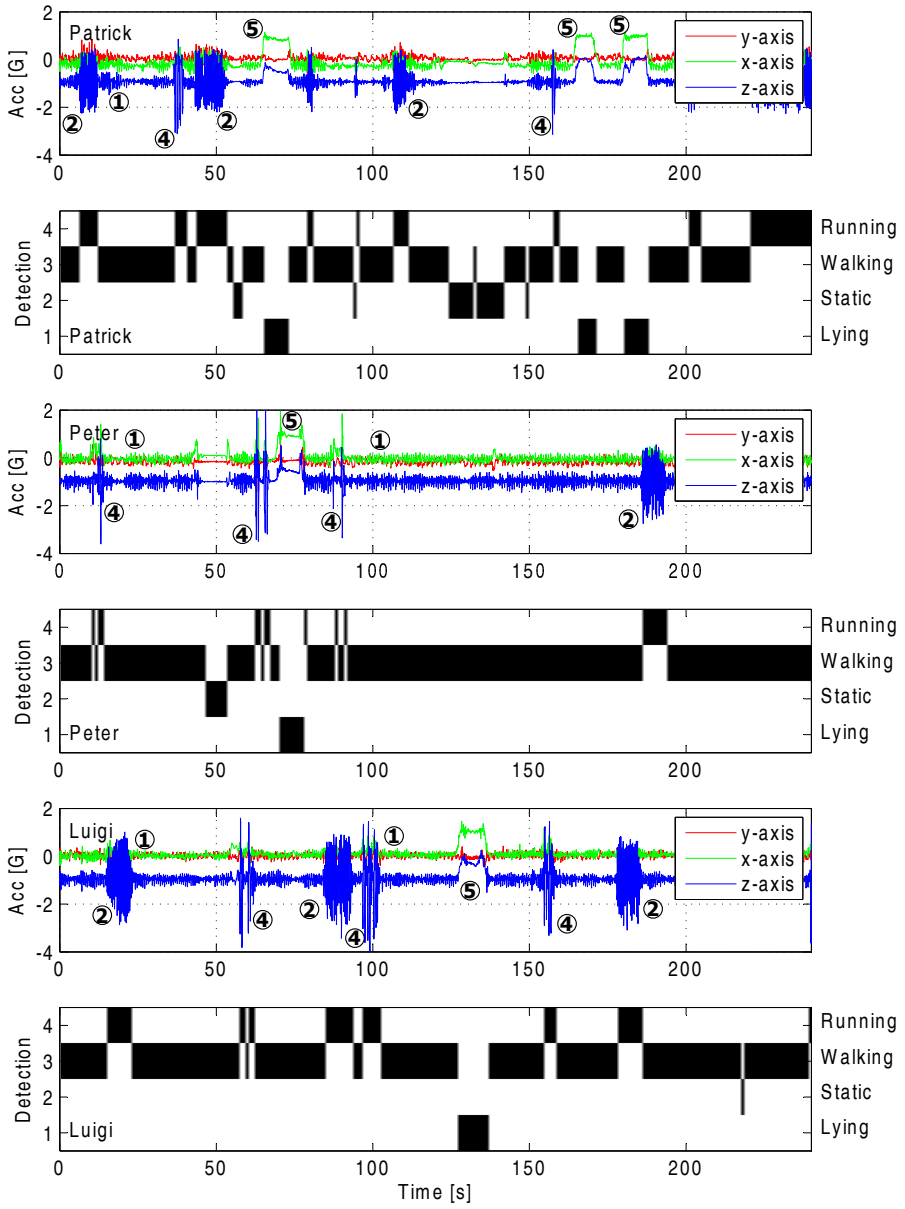


**Figure 4.16:** Accelerometer data and classification results for three persons in the wireless sensor network.

Additionally, this performance was achieved with very low delays, even when data was received via forwarding.

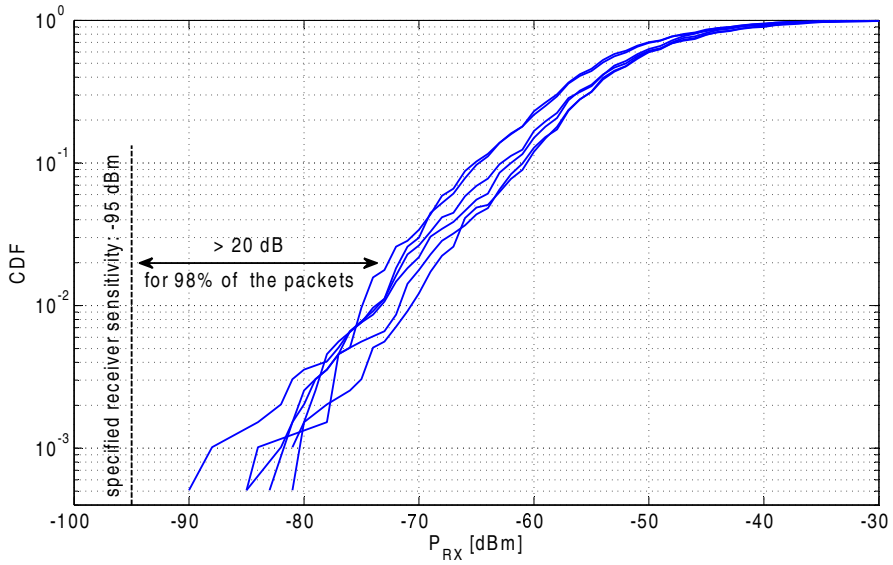


**Figure 4.17:** Cumulative distribution function of the received signal levels for the six off-body person-to-person links.

An important advantage of the node is surely the textile patch antenna, which offers more antenna gain than the popular inverted-F antenna seen in many other publications. Both the circuit and the antenna are very flexible, providing a great advantage for garment integration of the system. The dedicated network protocol and embedded classification algorithm are important extra features increasing the reliability.

Although a minor degree of packet loss, varying between $0.2\%$ and $4.5\%$, does occur on the individual links between nodes, or between a node and the base station, a dedicated network protocol improves connectivity by means of data forwarding. In this network protocol, specifically designed for the difficult radio propagation conditions experienced by moving persons in an indoor environment, all data transmitted by each network node are forwarded by all of the other nodes. Data forwarding creates redundancy, resulting in a very reliable data transmission towards the base station, which results in a performance increase comparable to $N^{th}$-order selection combining diversity for an N-node network, as shown earlier in [34]. This approach leads to a very significant increase in data reliability and/or communication range.

The proposed protocol is an important feature of the system. Thanks to its simplicity and the data redundancy introduced, it is very suitable for the typical scenario of moving persons in an indoor environment, experiencing dramatically varying radio propagation between each set of nodes or between each node and the base station. Established network protocols, such as ZigBee, used in many publications, are more suitable for networks with nodes in static positions. Problems arise when channels are

rapidly changing, for each transmitted packet, due to the higher complexity of the protocol. Additionally, the proposed protocol allows quasi delay-free operation, thanks to the immediate forwarding of data. For a 12-node network, the delay would maximally augment to $0.5$ s in the worst-case propagation conditions.

The network does require a power-on sequence to initialize. Nodes should be switched on subsequently with all persons wearing nodes well within each other's range and respecting a one-second interval in between switch actions. This disadvantage does not cause a problem in realistic interventions where the members of a small team start their actions together. Note that the protocol offers extreme reliability in return, after correct initialization. Many problems occurring with more complex protocols are avoided. Suddenly missing nodes, appearing again later, rejoin the network immediately, as if nothing happened. Of course, the proposed protocol is only suitable for low data-rate communication and is focusing on data integrity in exchange for data throughput. However, in realistic firefighting conditions, only low date-rate information is available, as high data-rate sources, such as video cameras, are unusable, due to smoke causing zero visibility.

Specific validation of on-body node-to-node links, as well as off-body person-to-person links was performed, resulting in the very important conclusion that either form of communication is very reliable. More than $98\%$ of the transmitted packets were received at a power level that was at least $15$ dB and $20$ dB higher than the specified receiving threshold for the transceiver chip, for node-to-node and person-to-person links, respectively.

A classification algorithm was also programmed on the microcontroller on each node and validated in realistic conditions. The three-person measurement demonstrated the reliable operation of this computationally simple algorithm for persons of different body sizes. Despite the simplicity of the embedded classification, the algorithm combined with the forwarding of the classification results has the potential to provide information about the user state to the base station in extremely bad radio propagation conditions, where the base station is not receiving all of the raw measurement data anymore.

## 4.9 Conclusions

A novel autonomous wearable cooperative wireless sensor node network was developed, synchronously measuring and interpreting accelerometer data on multiple nodes and transmitting the data to a base station. Event detection is performed close to the sensors, by means of the on-node low-energy microcontroller, running a computationally-efficient algorithm. The system operates very reliably in various radio-propagation environments. The received signal strength can be used as a valuable additional parameter, providing ranging and orientation information. On-body node-to-node communication is exploited to synchronize measurements on multiple autonomous nodes,

at different body locations, and to share sensor data between these nodes. $N^{th}$-order transmit diversity performance is approached, by repeating the sensor data from the other on-body nodes, drastically enhancing communication reliability by eliminating packet loss. The system is highly valuable for rescue workers and law-enforcement officers, as well as for a wide range of military and civilian applications. Network functionality can readily be enhanced, by extending the software on the embedded microcontroller. Besides increasing the number of nodes on the body of one person, several persons can join the sensor network, share each other's sensor data and forward each other's data packets. Sensor fusion can be enabled by integrating multiple sensors, such as temperature, moisture and gas sensors, on a single wireless node. The small-size and low-cost sensor nodes, easily and comfortably integrated into clothing, also implement a real-time situational awareness system.

## Acknowledgement

This research was partially funded by the Inter-University Attraction Poles Program initiated by the Belgian Science Policy Office.

# Bibliography


[1] IWT Belgium, the Flemish government agency for Innovation by Science and Technology, "Smart@Fire, a groundbreaking european project (FP7) to encourage companies and researchers and provide them with financial means to develop innovative ICT solutions that better protect firefighters and help prevent accidents, and to integrate them into smart Personal Protective Equipment (PPE).", June 2013.

[2] D. Curone, E.L. Secco, A. Tognetti, G. Loriga, G. Dudnik, M. Risatti, R. Whyte, A. Bonfiglio, and G. Magenes, "Smart garments for emergency operators: The ProeTEX project", *Information Technology in Biomedicine, IEEE Transactions on*, vol. 14, no. 3, pp. 694 –701, May 2010.

[3] L. Vallozzi, P. Van Torre, C. Hertleer, H. Rogier, M. Moeneclaey, and J. Verhaevert, "Wireless communication for firefighters using dual-polarized textile antennas integrated in their garment", *Antennas and Propagation, IEEE Transactions on*, vol. 58, no. 4, pp. 1357–1368, 2010.

[4] L. Vallozzi, H. Rogier, and C. Hertleer, "Dual polarized textile patch antenna for integration into protective garments", *Antennas and Wireless Propagation Letters, IEEE*, vol. 7, pp. 440–443, 2008.

[5] Peter Vanveerdeghem, Patrick Van Torre, Christiaan Stevens, Jos Knockaert, and Hendrik Rogier, "Dual-diversity wearable wireless node integrated on a dual-polarized textile patch antenna", *Science, Measurement Technology, IET*, vol. 8, no. 6, pp. 452-458, 2014..

[6] Lina Tong, Quanjun Song, Yunjian Ge, and Ming Liu, "HMM-based human fall detection and prediction method using tri-axial accelerometer", *Sensors Journal, IEEE*, vol. 13, no. 5, pp. 1849–1856, 2013.

[7] L. Vallozzi, P. Van Torre, C. Hertleer, H. Rogier, M. Moeneclaey, and J. Verhaevert, "Wireless communication for firefighters using dual-polarized textile antennas integrated in their garment", *Antennas and Propagation, IEEE Transactions on*, vol. 58, no. 4, pp. 1357 –1368, April 2010.

[8] P. Van Torre, L. Vallozzi, C. Hertleer, H. Rogier, M. Moeneclaey, and J. Verhaevert, "Indoor off-body wireless MIMO communication with dual polarized textile

antennas", *Antennas and Propagation, IEEE Transactions on*, vol. 59, no. 2, pp. 631 –642, feb. 2011.

[9] M.O. Munoz, R. Foster, and Yang Hao, "On-body channel measurement using wireless sensors", *Antennas and Propagation, IEEE Transactions on*, vol. 60, no. 7, pp. 3397–3406, July 2012.

[10] Yao-Chiang Kan and Chun-Kai Chen, "A wearable inertial sensor node for body motion analysis", *Sensors Journal, IEEE*, vol. 12, no. 3, pp. 651–657, 2012.

[11] Lara González-Villanueva, Stefano Cagnoni, and Luca Ascari, "Design of a wearable sensing system for human motion monitoring in physical rehabilitation", *Sensors*, vol. 13, no. 6, pp. 7735–7755, 2013.

[12] Daniel Rodríguez-Martín, Carlos Pérez-López, Albert Samà, Joan Cabestany, and Andreu Català, "A wearable inertial measurement unit for long-term monitoring in the dependency care area", *Sensors*, vol. 13, no. 10, pp. 14079–14104, 2013.

[13] D.L. Paul, H. Giddens, M.G. Paterson, G.S. Hilton, and J.P. McGeehan, "Impact of body and clothing on a wearable textile dual band antenna at digital television and wireless communications bands", *Antennas and Propagation, IEEE Transactions on*, vol. 61, no. 4, pp. 2188–2194, 2013.

[14] S. Van Roy, F. Quitin, LingFeng Liu, C. Oestges, F. Horlin, J. Dricot, and P. De Doncker, "Dynamic channel modeling for multi-sensor body area networks", *Antennas and Propagation, IEEE Transactions on*, vol. 61, no. 4, pp. 2200–2208, 2013.

[15] A.C.W. Wong, M. Dawkins, G. Devita, N. Kasparidis, A. Katsiamis, O. King, F. Lauria, J. Schiff, and A.J. Burdett, "A 1 V 5 mA multimode IEEE 802.15.6/bluetooth low-energy WBAN transceiver for biotelemetry applications", *Solid-State Circuits, IEEE Journal of*, vol. 48, no. 1, pp. 186–198, 2013.

[16] Yanqing Zhang, Fan Zhang, Y. Shakhsheer, J.D. Silver, A. Klinefelter, M. Nagaraju, J. Boley, J. Pandey, A. Shrivastava, E.J. Carlson, A. Wood, B.H. Calhoun, and B.P. Otis, "A batteryless 19 $\mu$W MICS/ISM-band energy harvesting body sensor node SoC for ExG applications", *Solid-State Circuits, IEEE Journal of*, vol. 48, no. 1, pp. 199–213, 2013.

[17] G. Lo, S. Gonzalez-Valenzuela, and V.C.M. Leung, "Wireless body area network node localization using small-scale spatial information", *Biomedical and Health Informatics, IEEE Journal of*, vol. 17, no. 3, pp. 715–726, 2013.

[18] D. He, C. Chen, S. Chan, J. Bu, and P. Zhang, "Secure and lightweight network admission and transmission protocol for body sensor networks", *Biomedical and Health Informatics, IEEE Journal of*, vol. 17, no. 3, pp. 664–674, 2013.

[19] Shih Heng Cheng and Ching Yao Huang, "Coloring-based inter-WBAN scheduling for mobile wireless body area networks", *Parallel and Distributed Systems, IEEE Transactions on*, vol. 24, no. 2, pp. 250–259, 2013.

[20] A. Boulis, D. Smith, D. Miniutti, L. Libman, and Y. Tselishchev, "Challenges in body area networks for healthcare: the MAC", *Communications Magazine, IEEE*, vol. 50, no. 5, pp. 100–106, 2012.

[21] P.J. Soh, B. Van den Bergh, Hantao Xu, H. Aliakbarian, S. Farsi, P. Samal, G.A.E. Vandenbosch, D.M.M. Schreurs, and B.K.J.C. Nauwelaers, "A smart wearable textile array system for biomedical telemetry applications", *Microwave Theory and Techniques, IEEE Transactions on*, vol. 61, no. 5, pp. 2253–2261, 2013.

[22] Rui Zhang, F. Hoflinger, and L. Reindl, "Inertial sensor based indoor localization and monitoring system for emergency responders", *Sensors Journal, IEEE*, vol. 13, no. 2, pp. 838–848, 2013.

[23] P. Barsocchi, "Position recognition to support bedsores prevention", *Biomedical and Health Informatics, IEEE Journal of*, vol. 17, no. 1, pp. 53–59, 2013.

[24] H. Ghasemzadeh, S. Ostadabbas, E. Guenterberg, and A. Pantelopoulos, "Wireless medical-embedded systems: A review of signal-processing techniques for classification", *Sensors Journal, IEEE*, vol. 13, no. 2, pp. 423–437, 2013.

[25] E. Sejdic, K.A Lowry, J. Bellanca, M.S. Redfern, and J.S. Brach, "A comprehensive assessment of gait accelerometry signals in time, frequency and time-frequency domains", *Neural Systems and Rehabilitation Engineering, IEEE Transactions on*, vol. 22, no. 3, pp. 603–612, May 2014.

[26] Kristin A. Lowry, Ann L. Smiley-Oyen, Andrew J. Carrel, and John P. Kerr, "Walking stability using harmonic ratios in parkinson's disease", *Movement Disorders*, vol. 24, no. 2, pp. 261–267, 2009.

[27] D. Jarchi, C. Wong, R.M. Kwasnicki, B. Heller, G.A Tew, and Guang-Zhong Yang, "Gait parameter estimation from a miniaturized ear-worn sensor using singular spectrum analysis and longest common subsequence", *Biomedical Engineering, IEEE Transactions on*, vol. 61, no. 4, pp. 1261–1273, April 2014.

[28] G. Fortino, R. Giannantonio, R. Gravina, P. Kuryloski, and R. Jafari, "Enabling effective programming and flexible management of efficient body sensor network applications", *Human-Machine Systems, IEEE Transactions on*, vol. 43, no. 1, pp. 115–133, 2013.

[29] Analog Devices, "ADXL337 datasheet", Tech. Rep., Analog Devices, One Technology Way, P.O. Box 9106, Norwood, MA 02062-9106, USA, 2010.

[30] Silicon Laboratories, "AN127: Flash programming via the C2 interface", Tech. Rep., Silicon Laboratories , 400 West Cesar Chavez, Austin, TX 78701, USA, 2012.

[31] European Telecommunications Standards Institute, "Etsi en 300 328 harmonized european standard", Tech. Rep., European Telecommunications Standards Institute, Route desLucioles; ETSI: Sophia-Antipolis Cedex, FR, 2012.

[32] Analog Devices, "ADF7242 datasheet", Tech. Rep., Analog Devices, One Technology Way, P.O. Box 9106, Norwood, MA 02062-9106, USA, 2010.

[33] M. Yoneyama, Y. Kurihara, K. Watanabe, and H. Mitoma, "Accelerometry-based gait analysis and its application to parkinson's disease assessment - part 2 : A new measure for quantifying walking behavior", *Neural Systems and Rehabilitation Engineering, IEEE Transactions on*, vol. 21, no. 6, pp. 999–1005, Nov 2013.

[34] P. Van Torre, P. Vanveerdeghem, and H. Rogier, "Correlated shadowing and fading characterization of MIMO off-body channels by means of multiple autonomous on-body nodes", in *Antennas and Propagation (EUCAP), 2014 8th European Conference on*, April 2014.

CHAPTER 5

# Compact Personal Distributed Wearable Exposimeter for the GSM-900 downlink band

**Peter Vanveerdeghem, Patrick Van Torre, Arno Thielens, Jos Knockaert, Wout Joseph, and Hendrik Rogier**

Based on the article submitted to *IEEE Sensors*

★★★

*A compact wearable Personal Distributed Exposimeter is proposed, sensing the power density of incident radio-frequency (RF) fields on the body of a human. In contrast to current commercial exposimeters, our Personal Distributed Exposimeter, being composed of multiple compact personal wearable RF exposimeter sensor modules, minimizes uncertainties caused by the proximity of the body, the specific antenna used and the exact position of the exposimeter. For unobtrusive deployment inside a jacket, each individual exposimeter sensor module is specifically implemented on the feedplane of a textile patch antenna. The new wearable sensor modules high-resolution logarithmic detector logs RF signal levels. Next, on-board flash memory records minimum, maximum and average exposure data over a time span of more than two weeks, at a one-second sample period. Sample-level synchronization of each individual exposimeter sensor module enables combining of measurements collected by different nodes. The system is first calibrated in an anechoic chamber, and then compared to a commercially available single-unit exposimeter. Next, the Personal Distributed Exposimeter is validated in realistic conditions, by measuring the average RF power density on a human during a walk in an urban environment and comparing the results to spectrum analyzer measurements with a calibrated antenna.*

## 5.1 Introduction

National legislation and the international Commission on Non-Ionizing Radiation Protection (ICNIRP) [1] impose limits in terms of whole-body averaged SAR (SARwb) [2]. Since these SARwb levels can only be evaluated by numerical simulations [3], equivalent reference levels, which can be measured and compared to the international guidelines issued by INCIRP, have been defined on the incident power density. Such exposure measurements are currently performed with commercially available Personal ExposiMeters (PEMs) [2, 4–7].

These measurements are compromised by large measurement uncertainties, due to shadowing by the test person's body [8, 9], dependence on polarization [10] and out-of-band detection. Furthermore, conventional PEMs cannot be unobtrusively deployed on the human body, whereas a fully integrated wearable on-body PEM enables continuous monitoring of long-term RF exposure, without hindering the test person's daily activities. Moreover, an on-body Personal Distributed Exposimeter (PDE), composed of multiple PEMs, increases the measurement accuracy [11].

We present a fully autonomous on-body PDE, composed of multiple independent RF-exposure modules, each integrated on a textile antenna feed plane. Thanks to their ground plane [12], the applied patch antennas minimize capacitive antenna loading by the body. Without loss of generality, we specifically configure the exposimeter for the Global System for Mobile Communications (GSM) worldwide downlink [925 MHz -

960 MHz] frequency band [13]. Each wearable exposimeter module makes use of a state-of-the-art logarithmic-detector to pair accuracy with a dynamic range of 80 dB. The on-board flash memory logs for over two weeks of measurement data, thereby eliminating a permanent Personal Computer (PC) connection. A similar on-body device was documented in [11], yet without data logging or unobtrusive integration potential. To the authors knowledge, this is the first fully tested wearable PDE.

In Section 5.2, the wearable PDE system is described, followed by its validation on a human body in Section 5.3. The calibration procedure is explained in Section 5.4. A real life measurement is outlined in Section 5.5. Conclusions are listed in Section 5.6.

## 5.2 System overview

The PDE is composed of multiple newly designed wearable exposimeter modules, of which the construction is described below.

### 5.2.1 Antenna

Due to the large wavelength of the frequency of the GSM downlink band, an aperture-coupled shorted patch antenna is selected, as displayed in Fig. 5.1. The antenna features a compact size and excellent antenna performance in proximity of the human body, while avoiding fragile probe feed connections [14, 15]. Therefore, this antenna is more suitable for garment integration than conventional antennas. Further improvement of the coupling between the antenna and the exposimeter module is obtained by employing an H-shaped coupling slot, thereby also minimizing the backward radiation into the human body [16]. The textile material is flexible and lightweight, without sacrificing antenna performance, in comparison to rigid antennas. A flexible polyurethane protective foam (thickness = 11 mm permittivity $\epsilon_r$ = 1.16 and tan $\delta$ = 0.010), commonly used in protective garments for rescue workers is applied as a substrate material, protecting the electronic circuitry from external factors, such as heat and humidity. A low-cost, conductive, electro-textile material, called Flectron, is used to construct the ground plane and radiating element. The material has a thickness less than 0.25 mm and surface resistivity less than 0.1 $\Omega$/sq., minimizing conductor losses. The influence of the body, which is in close proximity to the antenna, is limited, thanks to the ground plane structure. This feature will also make the PDE's performance nearly independent from the test person's body morphology. The feed substrate is constructed using two stacked Aramid textile layers, a material which is frequently used as outer layer in firefighter jackets (thickness = 0.95 mm, permittivity $\epsilon_r$ = 1.97 and tan $\delta$ = 0.02). The feed line is realized by means of copper foil. The antenna covers the complete GSM 935 MHz to 960 MHz downlink band. The 3 dB beam width of the antenna approximately equals 110°, with an antenna gain of 2.9 dBi and an antenna efficiency of 76.6%. The top view of the antenna and its

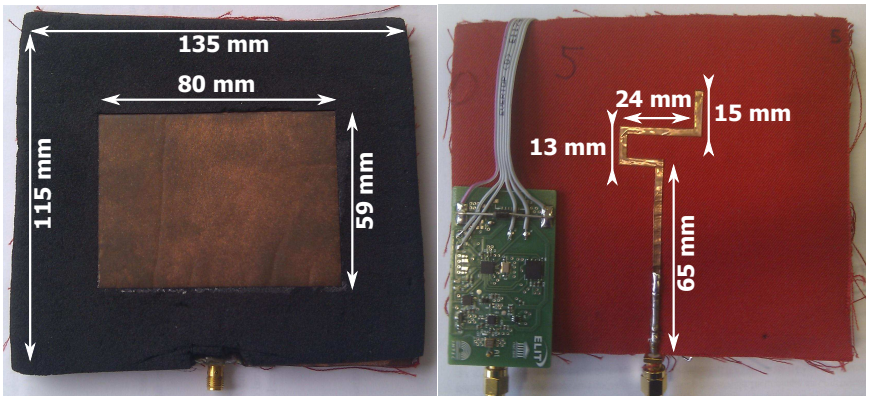


**Figure 5.1:** Top- and bottom-view of the patch antenna. On the bottom view, the exposimeter electonics and antenna are shown separately. In the actual implementation, the exposimeter's electronics are mounted onto the feed plane of the antenna.

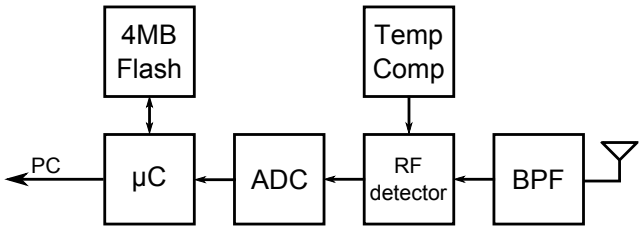


**Figure 5.2:** Bock diagram of single autonomous exposimeter module, with integrated bandpass filter (BPF), logarithmic RF detector and temperature compensation (Temp Comp). The PC connection is only used to configure the microcontroller (uC) and to download logged data from the 4 MB on-board flash memory.

dimensions are shown in Fig. 5.1, with the electronic circuitry integrated onto the feed plane of the antenna.

By placing the electronics on the feed plane of the patch antenna, each very compact module may be unobtrusively integrated into garments or clothing [17]. In addition, each unit can be encapsulated together with the textile antenna into a breathable Thermoplastic PolyUrethane coating (TPU), implementing a washable system [18].

### 5.2.2 System design

The block diagram of the proposed exposimeter module, integrated on the antenna feed-plane is presented in Fig. 5.2. The selection of the key components is motivated as follows.

The RF-signal received by the antenna is filtered by a Surface Acoustic Wave (SAW) Bandpass filter (BPF), to remove undesired out-of-band signals. In this con-

figuration for the GSM downlink, the TriQuint 856528 SAW filter is chosen, with a bandwidth of $35$ MHz and passband insertion loss of $2.5$ dB. Outside the passband, an attenuation of $35$ dB is quickly achieved. Thanks to the filter architecture, no additional impedance matching network is required, helping to reduce the physical size of the circuit. The filtered signal is measured by an Analog Devices ADL5513 [19] Logarithmic RF Detector, providing an output voltage proportional to the input RF level in dBm over a very large dynamic range. The output voltage of the RF detector is measured by a $16$ bit Analog-to-Digital Converter (ADC) and transported on the PDE board to the C8051F921 microcontroller ($\mu$C), by Silicon Labs, through the high speed Serial Peripheral Interface (SPI) data bus. To correct the small temperature-dependent variation of the output level of the Logarithmic RF Detector, an automatic frequency-dependent temperature compensation is implemented by a Digital-to-analog-converter (DAC) connected to the on-board microcontroller and its built-in temperature sensor. The micro controller is programmed in C. The software is uploaded to its memory through the In-Circuit-Programming interface.

The digitized measurement data are further processed by the on-board software at a data rate of $1000$ samples/sec. The minimum, maximum, as well as arithmetic- and geometric averages of the received RF signal power, over a one-second time slot, are stored into the on-board flash memory. The $4$ MB flash memory provides up to two weeks of non-volatile storage space. To guarantee the data integrity, at each time slot, a check sum of the measurement data is calculated and stored into the memory together with the measured data.

Besides the storage of the averaged measurement data at a one-second rate, the system may store raw sampled data at a full sample rate of $1000$ samples per second for analysis of high-speed measurements in post processing. The maximum sample rate of the exposimeter is $250$ ksps, as determined by the ADC specifications.

After the logging period, the measurement data are easily transferred to the personal computer (PC) over the USB-link for data-analysis.

Owing to the flexible and lightweight design of the system, the PDE is comfortably wearable by the test persons without restricting their movements. A top-view of the exposimeter circuit is shown in Fig. 5.3. Its planar circuit board's size of $35$ mm by $55$ mm is smaller than the antenna, allowing easy integration onto its feed-plane. An overview of the technical specifications is shown in Table 5.1.

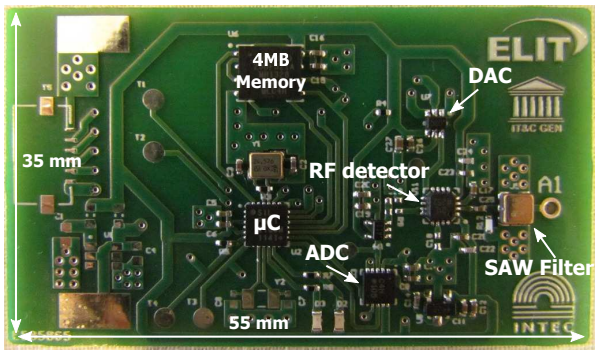


**Figure 5.3:** Top view of the system [57 mm $\times$ 33 mm]

**Table 5.1:** Specifications of the single PEM node

| Specification | Value |
|---|---|
| Dynamic Range | 80 dB |
| Minimum Input Power | $-70$ dBm |
| Maximum Input Power | 10 dBm |
| Operating supply voltage | 3.5 - 12 V |
| Size antenna | 100 mm x 125 mm |
| Size PCB | 35 mm x 55 mm |
| Frequency range | 1 MHz - 4 GHz |

### 5.2.3 Frequency selection of the personal exposimeter

The measured frequency band is selected by the bandpass Surface Acoustic Wave (SAW) filter. For each desired frequency band, a filter with the appropriate response may be inserted, without needing to adjust the circuit design. In this application, the full GSM $900$ frequency band is measured, without further adjustments to the circuit or antenna, allowing to measure the incident power density in this particular frequency band.

### 5.2.4 Calibration

The digitized output voltage of the logarithmic-detector is a function of the corresponding RF input power. This function is accurately determined by means of calibration.

The calibration of the RF input level of the exposimeter without antenna is performed in an anechoic chamber. Calibration datasets are constructed for each unit separately and stored into its flash memory for use during the actual exposure measurements. Logarithmic detection results in an accurate measurement over a large dynamic range, stored in a limited number of bits per measurement value. The Logarithmic RF Detector exhibits $80$ dB dynamic range, with a minimum RF input level of $-70$ dBm. By employing the calibration data, a $1$ dB resolution is achieved. To compensate the temperature-dependent offset, the output voltage of the DAC (Analog Devices AD5641 [20]) is automatically adjusted [19] as a function of the operating temperature.

### 5.2.5 Exposimeter synchronization

In the proposed PDE setup, where more than one exposimeter node is employed on the human test person, synchronization of all the exposimeter nodes is required to achieve an exposure measurement with accurate timestamps. All the exposimeter nodes are equipped with the same $24.576$ MHz crystal with a frequency stability of $10$ PPM. The sample period is directly derived from this main on-board clock, thereby minimizing the influence of frequency instability over a long time. Synchronization is achieved by connecting each individual exposimeter node to the PC. The PC will initialize the timing registers of the microcontroller for deriving the sample period. In addition, a time stamp is placed into the flash memory based on the PC clock. This ensures that all modules composing the exposimeter will sample at the same time instant within the defined sample period, with only a minimal deviation. After synchronization, each individual exposimeter immediately starts capturing exposure data. When the measurement campaign is terminated by the user, the data are transferred to the PC, including the time stamps in the flash memory. Based on the timestamps, the processing software aligns the data samples and starts further data processing.

**Table 5.2:** Current consumption of the main components of the exposimeter node

| Component | Power Mode | Current Consumption | Power @ 3V3 |
|---|---|---|---|
| Microcontroller | Idle | 2.5 mA | 8.25 mW |
| | Sleep | 0.1 μA | 0.33 μW |
| | Normal | 4 mA | 13.2 mW |
| RF detector | Power on | 31 mA | 102.3 mW |
| | Power Down | $< 200$ μA | $< 660$ μW |
| Memory | Stand by | 25 μA | 82.5 μW |
| | Deep Power-down | 5 μA | 16.5 μW |
| | Read/Write | 12 mA | 39.6 mW |
| ADC | Power on at 100 ksps | 550 μA | 1.82 mW |
| | Stand by | 1 nA | 3.3 nW |
| Temp comp. | Normal mode | 60 μA | 198 μW |
| | Power down | 500 nA | 1.65 μW |

### 5.2.6 Power consumption

The exposimeter is powered by a 1-cell Lithium polymer (Li-po) battery and a low-drop linear voltage regulator. From the technical data sheets of the integrated components, an estimation of the power consumption is made. An overview of that current consumption is given in Table 5.2.

The microcontroller will consume an average current of $4$ mA at $3.3$ V and at a clock frequency $24.576$ MHz. In sleep mode, the current consumption can be reduced to $600$ nA. The flash memory consumes on average $12$ mA at $3.3$ V while operating (reading or writing), whereas in standby mode, the current consumption is reduced to $25$ $\mu$A, or to $5$ $\mu$A in deep power-down mode.

The most current-consuming device on the exposimeter node is the RF detector, consuming $31$ mA in full operation. In power down mode, its current consumption is lowered to less than $200$ $\mu$A. The current consumption of the ADC and temperature compensation circuits is $550$ $\mu$A and $60$ $\mu$A, respectively.

The average current consumption is estimated to be $40$ mA at $3.3$ V, taking into account that the detector is always in power on mode, while the memory is accessed only once every second.

In full operation, the measured average power consumption of one exposimeter node equals $131$ mW ($39.6$ mA current consumption, at $3.3$ V supply voltage). This enables the sensor network to operate for many hours, without the need for charging the battery. The power consumption can further be reduced by employing the sleep mode of the system when there is no need to continuously operate at high speed.

## 5.3 Validation

### 5.3.1 Free-space performance

To measure the frequency response at the input of the exposimeter, the complete sensor (including vertically polarized antenna) is placed in an anechoic chamber at $4.34$ m from the radiating antenna. The TX standard gain horn (NSI-RF-SG975, with a gain of $14$ dBi at $942.5$ MHz), connected to a signal source with an output power of $10$ dBm (cable losses = $3.75$ dB), swept over a frequency range from $840$ MHz to $1040$ MHz, is radiating along both horizontal and vertical TX polarizations. The response is shown in Fig. 5.4, indicating a large attenuation for out-of-band signals. Clearly, the attenuation is very steep on the bottom side of the GSM downlink band, resulting in a rejection by at least $35$ dB of $880$-$915$ MHz GSM-900 uplink signals. For frequencies slightly above the GSM-900 downlink band, a better than $23$ dB attenuation is also sufficient, considering that, according to the band planning, no strong signals are expected adjacent to the upper end of the GSM downlink band.

Since the measured received power on the exposimeter in this anechoic measurement is significantly larger than the signals that will actually be measured during a real-world measurement, out-of-band signals will be below the noise floor of the exposimeter thanks to the band-pass filtering characteristics. They will not affect the actual measurements in the desired frequency band.

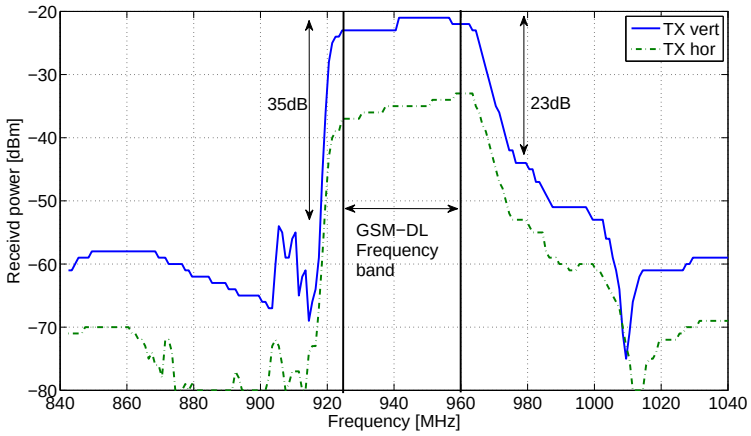


**Figure 5.4:** Free-space frequency response of the vertically polarized exposimeter

The clearly visible difference of approximately $12$ dB between both TX polarizations is due to the vertically polarized receive antenna of the node. An ideal exposimeter has no dependence of the polarization. In order to minimize the influence of the received polarizations, several exposimeters are placed onto the body, oriented along

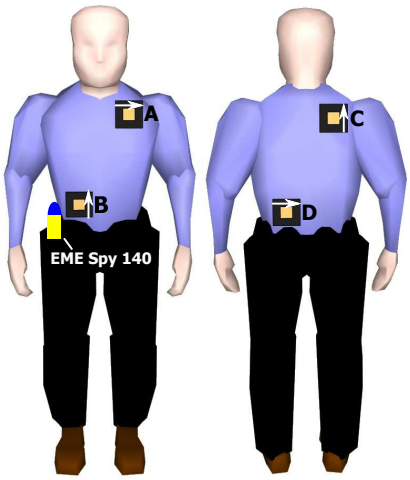


**Figure 5.5:** Positions of the four Personal ExposiMeter (PEM) modules composing the Personal Distributed Exposimeter (PDE), shown together with the position of the EME Spy 140 onto the body of the test-person

orthogonal polarizations, as further described and evaluated.

While the transmitted signal of the base station is vertically polarized, the received polarization will vary due to the angle of arrival on the nodes and the different paths followed by the signal in the environment. By orienting the nodes along both polarizations, all signals received from the base station can be captured. Furthermore, these linearly polarized antennas are easier to construct, in comparison to textile patch antennas with a circular polarization, thereby reducing the cost and the size of the nodes.

### 5.3.2 On-body performance

The PDE is configured for the GSM-900 downlink frequency band, which is present in most environments. Four separate nodes of the PDE are distributed at optimal positions over the front and rear sections of the torso of a 1.85 m large test person having a weight of 80 kg, as shown in Fig. 5.5. The polarizations of the individual nodes are also chosen for complementarity.

The person with the four nodes distributed over the body stands on the rotor inside the anechoic chamber, in the far-field of the standard gain horn, radiating at $942.5$ MHz, being the center frequency of the GSM-900 downlink band, connected to a signal generator with a transmit power of $10$ dBm (cable losses = $3.75$ dB). The person wearing the PDE is rotated in the azimuth plane over an azimuth angle of $360°$. These measurements are repeated for Horizontal (H) and Vertical (V) TX polarizations. During these measurements, a commercially available secondary exposimeter

(EME Spy 140) is worn at waist-height. The distance from the middle of the human test subject to the aperture of the horn antenna is $4.34$ m.

These measurements are plotted in a logarithmic scale, shown in Figs. 5.6 and 5.7, for TX Vertical and Horizontal polarizations, respectively. Besides the field strength on each single node, the averaged field strength over the four nodes is calculated in the azimuth plane for each azimuth angle $\varphi$, for both horizontal and vertical polarizations. The average field strength of the proposed PDE, calculated for each angle in the azimuth plane, is approximately constant, making the exposimeter output independent of the transmit polarization.

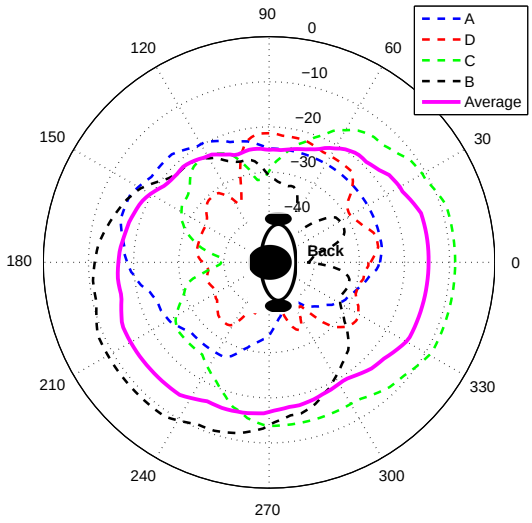


**Figure 5.6:** Electric field strength [dB] on all $4$ nodes in the azimuth plane, worn on-body as shown in Fig. 5.5. $180^\circ$ = front side of the body, vertically polarized TX antenna

In order to determine the dependence on the polarization when worn on-body, the standard deviation $\sigma_{pol}$ is calculated based on the difference in the received field strength of both polarizations. It is determined for both the "EME Spy 140" and for the PDE, by averaging the logarithmic field strength over the four nodes. This results in

$$\sigma_{\text{PDE diff H/V}} = 2.32\ dB$$
$$\sigma_{\text{EME Spy 140 diff H/V}} = 3.73\ dB$$

This allows us to conclude that the PDE is less polarization dependent than the "EME Spy 140". To compare the PDE and the "EME Spy 140" in an on-body sce-

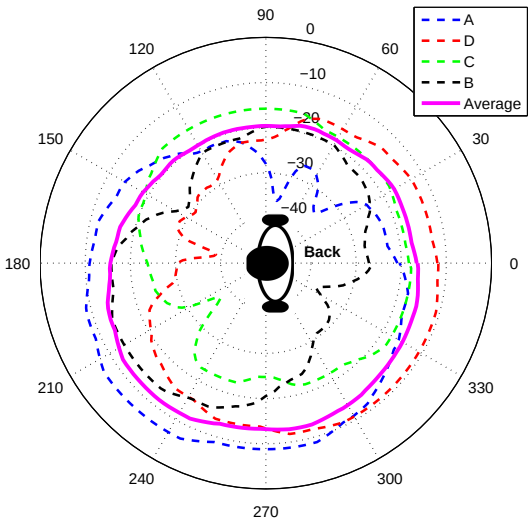


**Figure 5.7:** Electric field strength [dB] on all $4$ nodes in the azimuth plane, worn on-body as shown in Fig. 5.5. $180^{\circ}$ = front side of the body, horizontally polarized TX antenna

nario, the standard deviation $\sigma$ of the field strength over different azimuth angles is calculated for both horizontal as well as vertical polarization. $\sigma$ indicates how circular the pattern is in azimuth angle. A pattern that is perfectly omnidirectional results in a standard deviation of $0$ dB. $\sigma_{\phi}$ is derived from the (Logarithmic) field strength on the four nodes, resulting in

$$\begin{aligned} \sigma_{\text{PDE Hor}} &= 2.70\ dB \\ \sigma_{\text{PDE Vert}} &= 3.35\ dB \\ \sigma_{\text{EME Spy 140 Hor}} &= 6.94\ dB \\ \sigma_{\text{EME Spy 140 Vert}} &= 9.13\ dB \end{aligned}$$

We clearly obtain a better performance for the PDE in comparison to the commercial exposimeter. In Figs. 5.8 and 5.9, the normalized field strengths, for both the PDE and the ”EME Spy 140”, are plotted for a vertically and horizontally polarized transmitted signal, respectively. This visually verifies the above results. The PDE clearly achieves a more uniform distribution of the field strength over the azimuth plane.

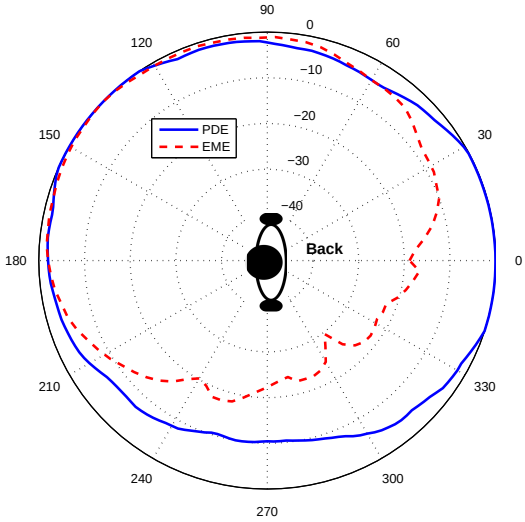


**Figure 5.8:** Normalized electric field strength [dB] on the PDE and "EME spy 140". $180^{\circ}$ = front side of the body, TX vertical polarization

## 5.4 Calibration

As discussed above, the power received by the PDE is almost constant, independent of polarization or azimuth angle for a given transmit power. To obtain an accurate measurement result of the actual RF field strength at the location of the human body in a real environment, the PDE requires calibration, which is performed in an anechoic chamber. The calibration eliminates the influence of the body on the PDE measurement.

The measurements in the anechoic chamber for both horizontal and vertical TX polarizations, used earlier to validate the exposimeters, are now employed to calibrate the PDE when performing on-body measurements. $P^{H}_{geom}(\varphi)$ and $P^{V}_{geom}(\varphi)$ are the geometric average received powers for the horizontally and vertically transmit polarization as a function of the azimuth angle, respectively. Furthermore, the free-space incident powers $S^{H}_{inc}$ and $S^{V}_{inc}$ are measured using the NBM-550 broadband probe, for both polarizations at the TX horn antenna, as described in section 5.3.2 for the PDE, but now with the broadband probe at exactly the same location.

From the calibration measurements, the geometric average Antenna Aperture ($AA_{geom}$) of the total PDE is determined, given by

$$AA_{geom}(\varphi,\psi) = \frac{P^{H}_{geom}(\varphi)}{S^{H}_{inc}} cos^{2}(\psi) + \frac{P^{V}_{geom}(\varphi)}{S^{V}_{inc}} sin^{2}(\psi)$$

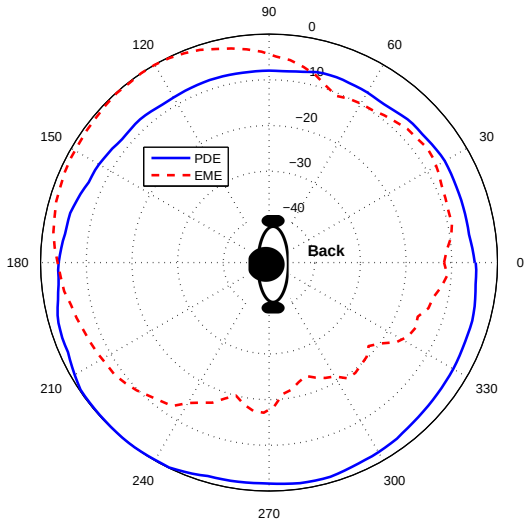


**Figure 5.9:** Normalized electric field strength [dB] on the PDE and "EME spy 140". $180^{\circ}$ = front side of the body, TX horizontal polarization

where $S_{inc}^{V}$ =0.541 $mW/m^2$ and $S_{inc}^{H}$ =0.394 $mW/m^2$, and with $\psi$ the polarization of an incident electric field. $AA_{geom}(\varphi, \psi)$ is calculated for $10^3$ $\psi$-samples, located in the interval [0-2$\pi$] radians. The $\psi$-samples are drawn from a Gaussian distribution in an "Urban Macro cell" scenario [3, 21], in order to take into account a realistic polarization of the incident electric field. This scenario provides the best correspondence to earlier measurements performed in the city of Ghent [6].

The set of values resulting from this procedure provides the distribution of $AA_{geom}$ for realistic angles of arrival. From this distribution, the median is chosen as the value of the Antenna Aperture ($AA_{geom}$) of the total PDE. In addition, the full calibration procedure is repeated 100 times, and the results are averaged in order to improve accuracy. Based on this calibration process, the average value of $AA_{geom}$ is found to be $6.58\ cm^2$

Once the value of $AA_{geom}$ is determined, a real world measurement can start. After this measurement, the incident power received on the body of the test person can be determined by

$$S_{inc} = \frac{P_{geom}}{AA_{geom}}, \tag{5.1}$$

where $P_{geom}$ is the geometric average received power on the four nodes of the PDE, observed during the real world measurement.

## 5.5 Real-world measurement

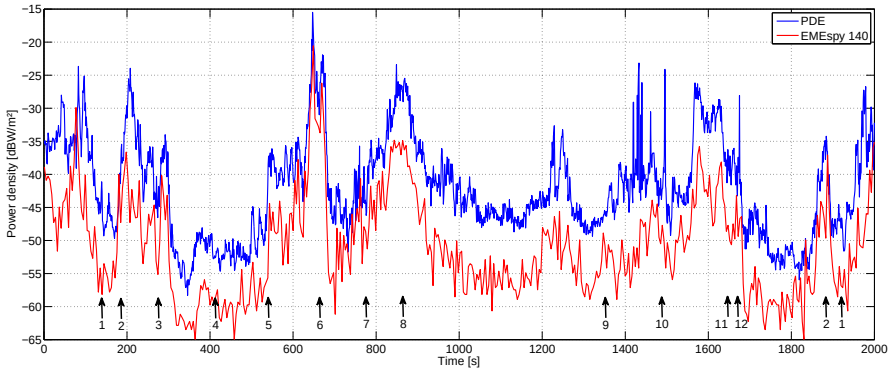


**Figure 5.10:** Received power density $[dBW/m^2]$ on the body of the test person, measured with the active nodes of the PDE versus the commercially available exposimeter. The position markers corresponding to the numbers in Fig. 5.11

To perform a real-world measurement, the same test person as in previous measurements, equipped with the PDE and the "EME spy 140", walks along a predefined path in the city-center of Ghent (Belgium). During this walk, the received power is recorded on all the exposimeter nodes as well as on the "EME spy 140", in a time interval of 1 second. Fig. 5.10 shows the total power density received by the test person with the calibrated PDE during the complete walk, as well as the power density on the "EME spy 140". In Fig. 5.11, the 2.6 km outdoor trajectory through Ghent, followed by the test person, is shown. On this map, the position markers corresponding to the numbers in Fig. 5.10, as well as the position of the nearby GSM-900 base-stations [22], are shown.

The total power density, received during the walk, is determined based on the active exposimeter nodes of the PDE, after applying the calibration procedure described in Section 5.4. The power density of the "EME spy 140" is extracted from the measurement logging file. The measurement results clearly show that the received powers of both measurement devices exhibit the same trend, but with short-term differences in power density levels. The shadowing by the body has a significant influence on the measurement results by the commercial "EME spy 140". As stated earlier in Section 5.3, the signals received on the "EME spy 140" are dependent on the angle of arrival of the signals in the azimuth plane. The omnidirectional receive pattern, which is obtained with the PDE, ensures a more accurate estimation of the power density levels in comparison to a non-distributed device such as the "EME spy 140".

The maximum instantaneous power density measured by the PDE during the experiment is $28\ mW/m^2$. As a result, the average power density levels over a 6-minute

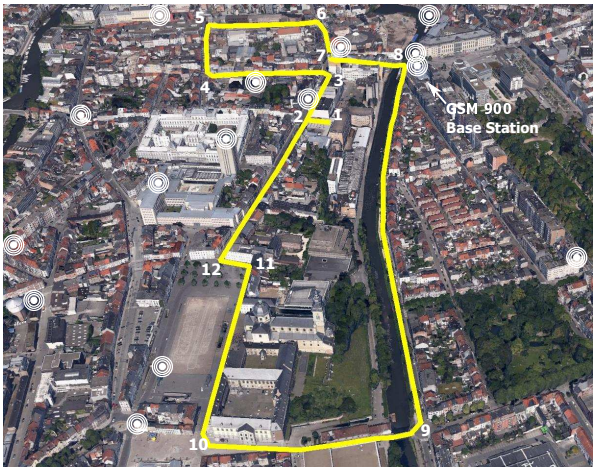


**Figure 5.11:** Map of Ghent with the path walked by the test person, with numbered position markers and GSM-900 basestation symbols, (source: Google Earth)

time frame are well below the ICNIRP reference level of $4.8\ W/m^2$ [1]. Furthermore, from these measurements, the SARwb can be determined, as described in [23, 24].

## 5.6 Conclusion

A compact wearable Personal Distributed Exposimeter is proposed, which increases the measurement accuracy in comparison to conventional Personal Exposimeters, including the dependency on the polarization and the angle in the azimuth plane. The Personal Distributed Exposimeter is composed of several newly designed on-body exposimeter modules, which are integrated onto the feed plane of a textile antenna. The different modules apply synchronous exposure data sampling, while being unobtrusively integrated inside a garment and being distributed over the body of the test person. Therefore, this new compact exposimeter is a step forward towards user-friendly Personal Distributed Exposimeters in multiple frequency bands, integrated into a single garment for measuring exposure data in a convenient way. Validation of the Personal Distributed Exposimeter shows that the system exhibits less dependence of the received polarization or the angle of the azimuth plane, compared to commercial available exposimeters. A fast and accurate calibration process is proposed, to eliminate the influence of the body onto the PDE. To validate the measurements performed by the Personal Distributed Exposimeter, a real world exposure measurement was carried out for the GSM-900 downlink band. The measurement is performed in the city center of Ghent, whose propagation characteristics correspond to an Urban Macro Cell. The measurement was also carried out employing an ”EME spy 140”

commercial exposimeter. This experiment clearly illustrates that the PDE provides a more accurate estimation of the power density levels on the human body. The commercial, non-calibrated exposimeter deployed on the body influences the measurement results due to shadowing by proximity of the body, leading to an underestimation of the power density levels on the human body. The maximum instantaneous power density measured by the PDE during the experiment equals $28\ mW/m^2$, which is well below the ICNIRP reference level of $4.8\ W/m^2$ for an average power density level in a $6$-minute time frame. Based on these measurement data, the whole-body SAR may readily determined. Besides for verifying compliance of RF field exposure with ICNIRP reference levels, the proposed modules can also serve as sensor nodes to evaluate the potential of RF energy harvesting [25–28] and wireless power transfer [29].

# Bibliography


[1] International Commission on Non-Ionizing Radiation Protection, "Guidelines for limiting exposure to time-varying electric, magnetic, and eletromagnetic fields (up to 300GHz)", *Health Physics*, vol. 74, pp. 494–552, 1998.

[2] Wout Joseph, Günter Vermeeren, Leen Verloock, and Luc Martens, "Estimation of whole-body SAR from electromagnetic fields using personal exposure meters", *Bioelectromagnetics*, vol. 31, no. 4, pp. 286–295, 2010.

[3] Günter Vermeeren, Wout Joseph, Christof Olivier, and Luc Martens, "Statistical multipath exposure of a human in a realistic electromagnetic environment", *Health Physics*, vol. 94, no. 4, pp. 345–354, 2008.

[4] Damiano Urbinello, Anke Huss, Johan Beekhuizen, Roel Vermeulen, and Martin Röösli, "Use of portable exposure meters for comparing mobile phone base station radiation in different types of areas in the cities of Basel and Amsterdam", *Science of The Total Environment*, vol. 468469, pp. 1028 – 1033, 2014.

[5] György Thuróczy, Ferenc Molnár, Gábor Jánossy, Noémi Nagy, Györgyi Kubinyi, József Bakos, and Judit Szabó, "Personal RF exposimetry in urban area", *Annals of telecommunications - Annales des télécommunications*, vol. 63, no. 1-2, pp. 87–96, 2008.

[6] Wout Joseph, Günter Vermeeren, Leen Verloock, Mauricio Masache Heredia, and Luc Martens, "Characterization of personal RF electromagnetic field exposure and actual absorption for the general public", *Health Physics*, vol. 95, no. 3, pp. 317–330, 2008.

[7] Arno Thielens, Sam Agneessens, Leen Verloock, Emmeric Tanghe, Hendrik Rogier, Luc Martens, and Wout Joseph, "On-body calibration and processing for a combination of two radio-frequency personal exposimeters", *Radiation Protection Dosimetry*, in press.

[8] S. Iskra, R. McKenzie, and I. Cosic, "Factors influencing uncertainty in measurement of electric fields close to the body in personal RF dosimetry", *Radiation Protection Dosimetry*, 2010.

[9] John F.B. Bolte, Gerard van der Zande, and Jos Kamer, "Calibration and uncertainties in personal exposure measurements of radiofrequency electromagnetic fields", *Bioelectromagnetics*, vol. 32, no. 8, pp. 652–663, 2011.

[10] John F.B. Bolte and Tessa Eikelboom, "Personal radiofrequency electromagnetic field measurements in the Netherlands: Exposure level and variability for everyday activities, times of day and types of area", *Environment International*, vol. 48, pp. 133 – 142, 2012.

[11] Arno Thielens, Hans De Clercq, Sam Agneessens, Jeroen Lecoutere, Leen Verloock, Frederick Declercq, Günter Vermeeren, Emmeric Tanghe, Hendrik Rogier, Robert Puers, Luc Martens, and Wout Joseph, "Personal distributed exposimeter for radio frequency exposure assessment in real environments", *Bioelectromagnetics*, vol. 34, no. 7, pp. 563–567, 2013.

[12] P. Salonen, L. Sydanheimo, M. Keskilammi, and M. Kivikoski, "A small planar inverted-F antenna for wearable applications", in *Wearable Computers, 1999. Digest of Papers. The Third International Symposium on*, Oct 1999, pp. 95–100.

[13] Wout Joseph, Günter Vermeeren, Leen Verloock, and Luc Martens, "Estimation of whole-body SAR from electromagnetic fields using personal exposure meters", *Bioelectromagnetics*, vol. 31, no. 4, pp. 286–295, 2010.

[14] Frederick Declercq, A. Georgiadis, and Hendrik Rogier, "Wearable aperture-coupled shorted solar patch antenna for remote tracking and monitoring applications", in *Proceedings of the 5th European conference on Antennas and propagation EUCAP*. 2011, pp. 2992–2996, IEEE.

[15] C. Hertleer, A. Tronquo, H. Rogier, L. Vallozzi, and L. Van Langenhove, "Aperture-coupled patch antenna for integration into wearable textile systems", *Antennas and Wireless Propagation Letters, IEEE*, vol. 6, pp. 392–395, 2007.

[16] V. Rathi, G. Kumar, and K. P. Ray, "Improved coupling for aperture coupled microstrip antennas", *Antennas and Propagation, IEEE Transactions on*, vol. 44, no. 8, pp. 1196–1198, Aug 1996.

[17] Peter Vanveerdeghem, Patrick Van Torre, Christiaan Stevens, Jos Knockaert, and Hendrik Rogier, "Flexible dual-diversity wearable wireless node integrated on a dual-polarised textile patch antenna", *IET Science, Measurement & Technology*, vol. 8, no. 6, pp. 452-458, 2014.

[18] M.L. Scarpello, I. Kazani, C. Hertleer, H. Rogier, and D. Vande Ginste, "Stability and Efficiency of Screen-Printed Wearable and Washable Antennas", *Antennas and Wireless Propagation Letters, IEEE*, vol. 11, pp. 838–841, 2012.

[19] Analog Devices, "ADL5513 datasheet rev 0", Tech. Rep., Analog Devices, One Technology Way, P.O. Box 9106, Norwood, MA 02062-9106, U.S.A., 2008.

[20] Analog Devices, "AD5641 datasheet rev d", Tech. Rep., Analog Devices, One Technology Way, P.O. Box 9106, Norwood, MA 02062-9106, U.S.A., 2008.

[21] Arno Thielens, Günter Vermeeren, Wout Joseph, and Luc Martens, "Stochastic method for determination of the organ-specific averaged SAR in realistic environments at 950 MHz", *Bioelectromagnetics*, vol. 34, no. 7, pp. 549–562, 2013.

[22] Belgian Institute for Postal services and Telecommunications, "Antenna site register", 2014.

[23] Arno Thielens, Peter Vanveerdeghem, Sam Agneessens, Patrick Van Torre, Günter Vermeeren, Hendrik Rogier, Luc Martens, and Wout Joseph, "Whole-body averaged SAR assessment using a personal, distributed exposimeter", in *Proceedings of BioEM2014*. 2014, p. 6, The Bioelectromagnetics Society (BEMS).

[24] Arno Thielens, Peter Vanveerdeghem, Sam Agneessens, Patrick Van Torre, Günter Vermeeren, Hendrik Rogier, Luc Martens, and Wout Joseph, "Whole-Body Averaged Specific Absorption Rate Estimation using a Personal, Distributed Exposimeter", Accepted for publication in *Antennas and Wireless Propagation Letters, IEEE*, 2014.

[25] T. Le, K. Mayaram, and T. Fiez, "Efficient far-field radio frequency energy harvesting for passively powered sensor networks", *Solid-State Circuits, IEEE Journal of*, vol. 43, no. 5, pp. 1287–1302, May 2008.

[26] J. Zbitou, M. Latrach, and Serge Toutain, "Hybrid rectenna and monolithic integrated zero-bias microwave rectifier", *Microwave Theory and Techniques, IEEE Transactions on*, vol. 54, no. 1, pp. 147–152, Jan 2006.

[27] G. Andia Vera, A. Georgiadis, A. Collado, and S. Via, "Design of a 2.45 GHz rectenna for electromagnetic (EM) energy scavenging", in *Radio and Wireless Symposium (RWS), 2010 IEEE*, Jan 2010, pp. 61–64.

[28] Antwi Nimo, Dario Grgi, and Leonhard M. Reindl, "Optimization of passive low power wireless electromagnetic energy harvesters", *Sensors*, vol. 12, no. 10, pp. 13636–13663, 2012.

[29] N. Carvalho, A. Georgiadis, A. Costanzo, H. Rogier, A. Collado, J. A. García, S. Lucyszyn, P. Mezzanotte, J. Kracek, D. Masotti, A. Boaventura, M. Nieves Ruíz, M. Pinuela, D. Yates, P. Mitcheson, M. Mazanek, and V. Pankrac, "Wireless Power Transmission: R&D Activities within Europe", *IEEE Trans. Microwave Theory Tech., vol. 62, no. 4, pp. 1031–1045, Apr. 2014.*

CHAPTER 6

# Conclusions and future work

## 6.1 Conclusions

The research presented in this work, focused on the integration of electronic systems on wearable textile antenna platforms. The integration of electronics onto a textile antenna has proven its added value, by reducing power consumption, increasing the antenna efficiency, improving the link quality, etc. Several prototypes were developed and evaluated for rescue worker applications. Besides the rescue worker applications, a consumer application was also considered.

First, a textile wearable wireless node, for operation in the $2.45$ GHz ISM band, was designed. The electronic system was integrated onto the feed plane of the textile antenna, complete with a transceiver implementing receive diversity. Fragile and lossy interconnections were eliminated. They were replaced by very short radio-frequency signal paths in the antenna feed plane, reducing electromagnetic compatibility and signal integrity problems. The resulting textile wireless node was validated, both in flat and bent state, in the anechoic chamber, by assessing the characteristics of the integrated system in free-space conditions. Moreover, performance was verified in various real-world conditions, integrated into a firefighter garment, and used as an autonomous body-centric measurement device. Furthermore, these textile wearable wireless nodes were used to deploy a fully-autonomous, wearable, wireless sensor network, where each flexible textile node performed cooperative synchronous acquisition and distributed event detection. The results of the computationally efficient situational-awareness algorithms, which are implemented on these wearable wireless nodes, are wirelessly transmitted to a base station, directly, as well as forwarded by other on-body nodes. By repeating the sensor data from the other on-body nodes, the communication reliability is drastically enhancing by exploiting diversity to eliminate packet loss. Extensive experiments in realistic conditions have demonstrated that this new autonomous, body-centric, textile-antenna, wireless sensor network is able to correctly detect different operating conditions of a firefighter during an intervention.

Besides increasing the number of nodes on the body of one person, several persons can join the sensor network, share each other's sensor data and forward each other data packets.

Second, a compact wearable Personal Distributed Exposimeter was designed, composed of several newly designed compact personal wearable RF exposimeter modules. Each individual exposimeter module is integrated onto the feed plane of a wearable textile patch antenna, allowing unobtrusive garment integration. The design allows sample-level synchronization of each individual exposimeter module to enable combining of measurement data collected by different nodes. Validation of the Personal Distributed Exposimeter shows that the system exhibits less dependence of the received polarization or the angle in the azimuth plane, compared to commercial available exposimeters. A fast and accurate calibration process is proposed, to eliminate the influence of the body onto the PDE. To illustrate the Personal Distributed Exposimeter, a real world exposure measurement was carried out for the GSM-900 downlink band. The measurement is performed in the city center of Ghent, which is characterized as an Urban Macro Cell environment.

## 6.2 Future developments

### 6.2.1 General improvements

The electronic systems are implemented on a copper-on-polyimide film. This technique provides a good overall flexibility for the textile antenna system. The size of the copper-on-polyimide circuit can be further reduced, by removing the non-copper plated polyimide film from the circuit, providing extra flexibility of the wearable system. Furthermore, stretchable textiles have the potential to further enhance the flexibility and breathability of the textile system. By enhancing the system with the proposed techniques, mechanical stress can be minimized or eliminated, increasing the robustness of the total wearable system.

The designed integrated wearable textile systems can be further improved with other functionalities, such as an advanced power management system. Such power management system can consist of different components, such as flexible batteries, providing energy to the system without hindering the user, as well as a solar panel, providing continuously energy to the system.

More flexibility of the textile system can be obtained by miniaturizing the electronic system, which is integrated onto the textile antenna. The presented prototypes are constructed using several discrete components (transceiver chip, microcontroller, memory, filters, etc.). To minimize the size, these components can be integrated into a single chip, specifically designed for these applications, ensuring a flexible integrated system. Furthermore, this chip can be integrated into a versatile printed circuit board, by thinning the silicon chip itself, which enhances a flexibility of the circuit. Practical

experience in thinning silicon chips exists at Ghent University.

### 6.2.2 Large scale production

During this research, working prototypes were developed. These prototypes, both the flectron antenna patch and ground plane, as well as the substrate of the textile antenna were handmade or cut by means of a laser. Making these textile antennas requires good practice, and knowledge, which is no problem for prototyping or small-scale production. When moving towards large scale production for integration into rescue worker garments, the fabrication process needs to be optimized.

The textile antenna fabrication process needs to be optimized for convenient integration into rescue worker garments. The substrates of the textile antennas presented in this work, are made out of the same material as applied for garments of rescue workers, allowing to integrate the assembly of the textile antennas during the production of the garments. The fabrication of the antennas is critical in terms of size of the antenna patch and alignment of the patch with respect to its feed structure. To optimize the production in terms of the accurate size of the patch, several options can be studied. An option already applied during this work, is to make use of a laser cutter. The used laser cutter has an accuracy of approximately $0.1$ mm, which is suitable for this application. The construction by laser cutter needs further research in terms of integrating the laser in production process of garments. Besides a laser cutter, a cutting plotter is a second cheaper option to cut the textile material. Besides the accuracy of the size of the different parts of the antenna, the alignment of the several antenna components is critical. In aperture-coupled antenna designs, the antenna feed needs to be accurately aligned with the antenna patch. To attach the conductive textile material onto the flexible foam, thermal glue is used, which is activated by applying heat onto the surface of the antenna. This technique of activating the adhesive is also a disadvantage. When the fabricated antenna is exposed to excessive heat, the thermal glue may loosen, such that the antenna patch detaches from the substrate material. Further research is required to find a way to attach the different textile components to each other without compromising flexibility, performance and safety. An option that has already been investigated, is the use of chemical activated adhesives.

Furthermore, research on automatic assembly of integrated systems is required. Automatic production and assembly of rigid Printed Circuit Boards is common nowadays, but less common for the production and assembly of flexible printed circuits boards. The fabrication process of integrating the electronics onto the textile antenna, needs to be further evaluated to achieve an automatic fabrication process.

APPENDIX A

# Schematics wireless sensor

The schematic of the electronic circuit which is integrated onto the feed plane of the dual-polarized antenna, described in Chapters 3 and 4 is shown in Fig. A.1.

The heart of the system is the ADF7242 transceiver from Analog Devices together with the Silicon Laboratories C8051F921 microcontroller. The transceiver supports the IEEE 802.15.4-2006 $2.4$ GHz PHY requirements, as well as proprietary GFSK/FSK/GMSK/MSK modulation schemes, selected according to the desired application. The transceiver features a dual-port RF interface, enabling diversity reception. Two Johansson Technology 2450BM14E0007 baluns are used to conjugate match RF output ports of the ADF7242 transceiver to the $400$ MHz wide bandpass-filter (Murata LFL182G50TC1B905), to protect the input from out-of-band signals. Embedded software for the microcontroller is developed in the C programming language and uploaded into the controller's nonvolatile code memory by the In-System Programming interface via a USB cable. The $4$ MB on-board flash memory can be used as a buffer or as a data storage for processing and analysis. The transceiver, microcontroller and memory are connected through a Serial Peripheral Interface (SPI) bus. For the rescue-worker application, a $3$-axis accelerometer is integrated, the ADXL337 from Analog Devices. This accelerometer is directly connected to the microcontroller's analog-to-digital converter (ADC).

Fig. A.2 shows the composite drawing of the top- and bottom- layer of PCB layout of the wireless node circuit. The circuit is implemented in a $9$ $\mu$m copper layer on a copper-on-polyimide film, UPISEL®-N by UBE, of $25$ $\mu$m thickness.

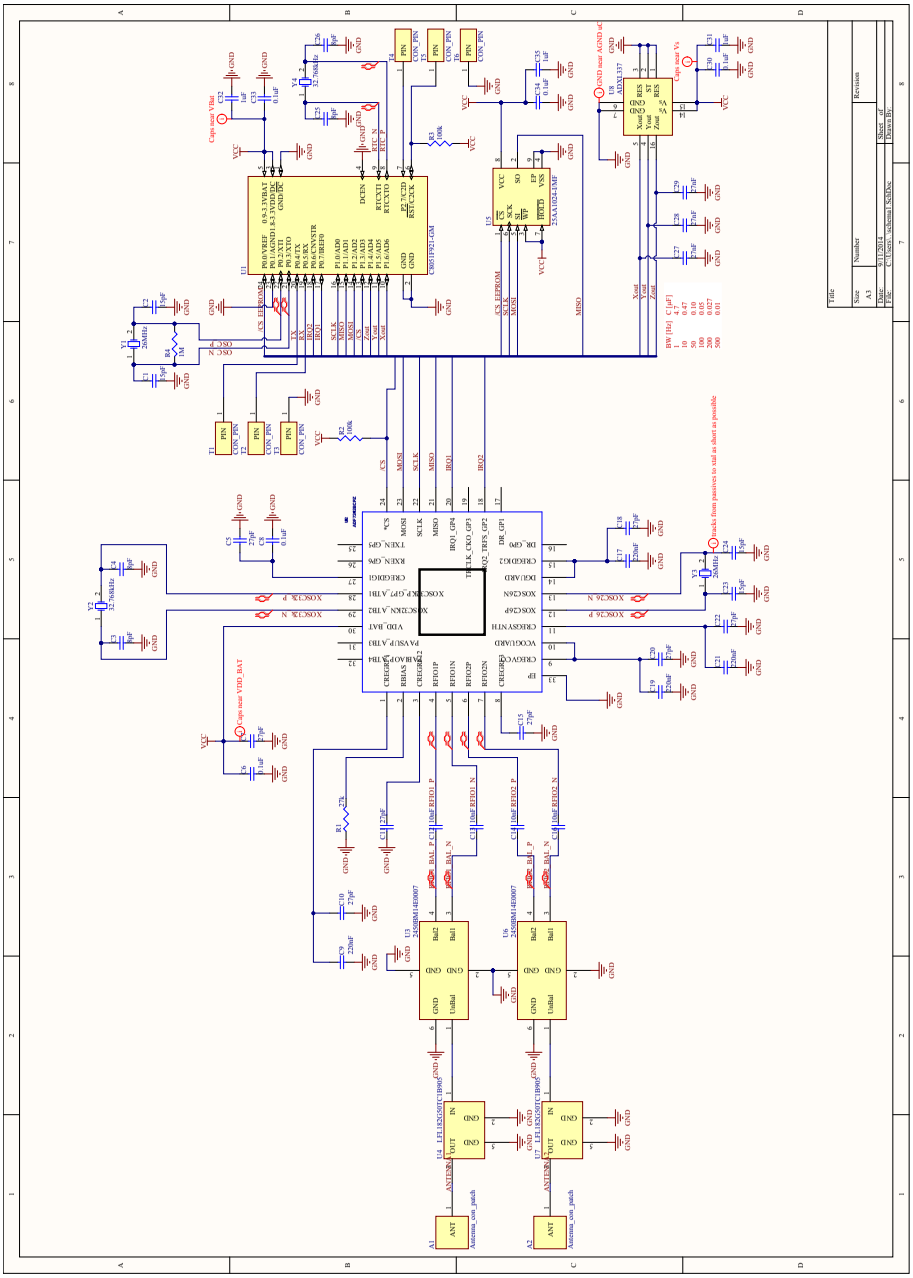

**Figure A.1:** Schematic Wireless node

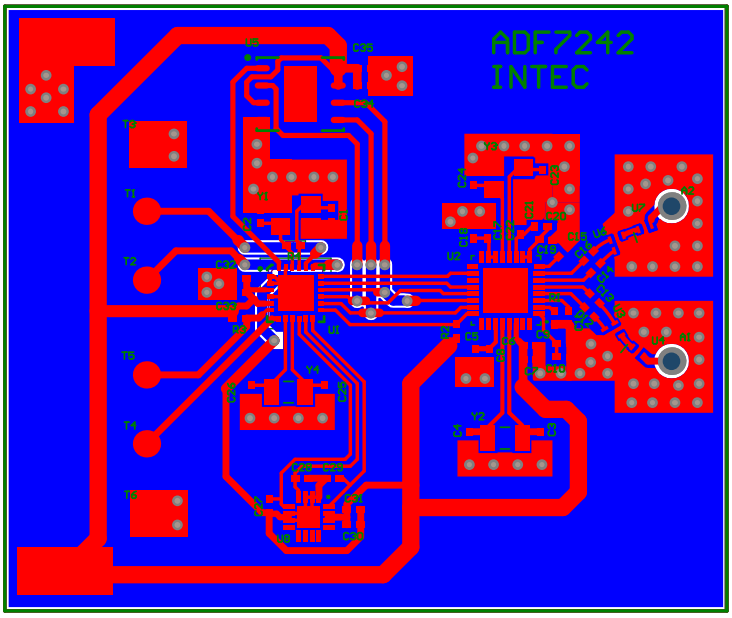


**Figure A.2:** PCB layout of the Wireless node

# APPENDIX B

# Exposimeter

The schematic of the exposimeter which is used in the Personal Distributed Exposimeter (PDE), described in Chapter 5 is shown in Fig. B.1.

The RF signal captured by the antenna is filtered by a Surface Acoustic Wave (SAW) Bandpass filter (BPF), for the desired frequency band. The RF signal, after the BPF is measured by a Logarithmic RF Detector (ADL5513, Analog devices), providing an output voltage which is proportional to the input RF level in dBm over a large dynamic range.

The output voltage of the detector is measured by means of a 16 bit wide Analog-to-Digital Converter (ADC) and transported to the C8051F921 microcontroller ($\mu$C), by Silicon Laboratories, through the Serial Peripheral Interface (SPI) data bus. Small temperature-dependent variations of the output level of the Logarithmic RF Detector are corrected by an automatic frequency-dependent temperature compensation, implemented by means of a Digital-to-analog-converter (DAC) connected to the on-board microcontroller and its built-in temperature sensor. The embedded software on the micro controller is programmed in C and uploaded to its memory through the In-Circuit-Programming interface. The 4 MB on-board flash memory can be used as a buffer or as a data storage for processing and analysis.

Fig. A.2 shows the composite drawing of the top- and bottom- layer of PCB layout of the wireless node circuit.

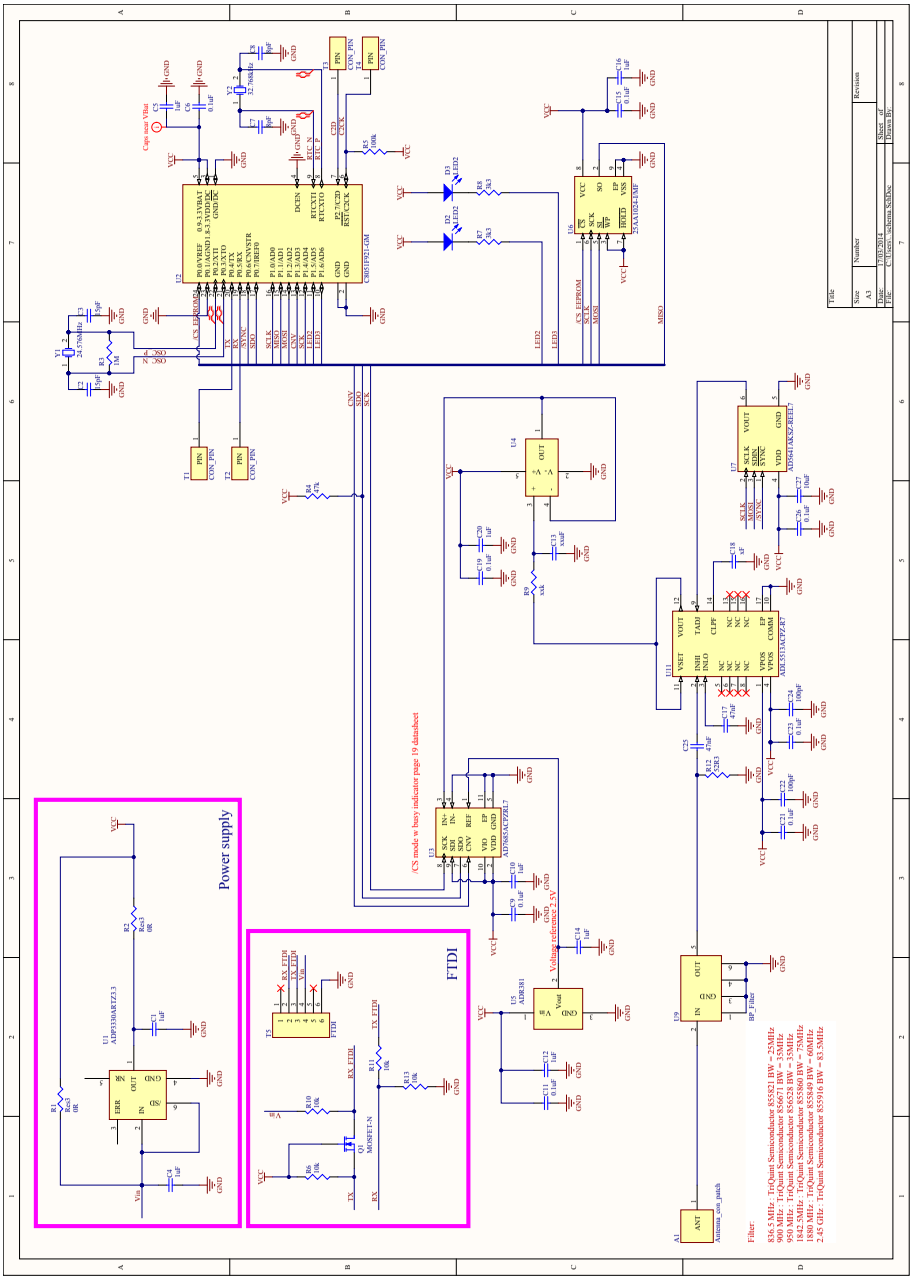


**Figure B.1:** Schematic Exposimeter

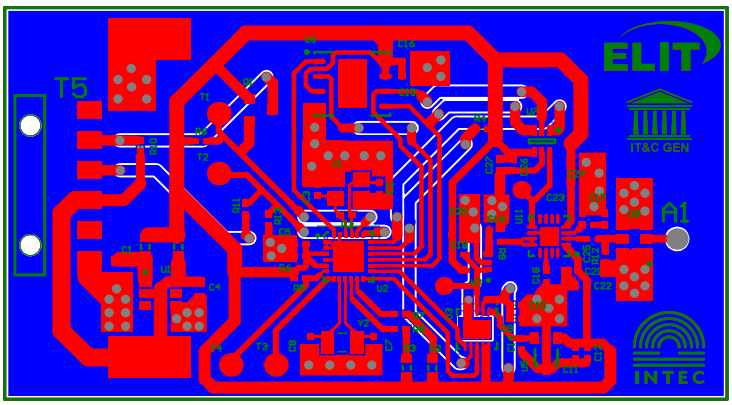


**Figure B.2:** PCB layout of the Exposimeter module